UNIVERSITY OF TORONTO

Weld Design for Rectangular HSS Overlapped K-Connections

Kyle Tousignant

and

Jeffrey A. Packer

Department of Civil Engineering, University of Toronto

Final Report to the American Institute of Steel Construction on the Research Project "Weld Design for Rectangular HSS: T / Cross- Connections under Branch Bending and Overlapped K-Connections"

October 2014

ABSTRACT

A laboratory-based test program was conducted to assess the performance and evaluate the design of welds in rectangular hollow structural section (HSS) overlapped K-connections. A large-scale 33-ft. span, simply-supported, rectangular HSS Warren truss comprised of weld-critical overlapped K-connections was designed and fabricated. Connections were deliberately intended to be weld-critical and varied three key parameters that are known to influence the strength of welds to rectangular HSS: branch member overlap, chord wall slenderness, and branch-to-chord width ratio. By means of a quasi-static point load applied to strategic truss panel points, sequential failure of nine test welds to the overlapping branch members was obtained. Strain distributions adjacent to the weld and branch loads at rupture were measured. By using mechanical and geometrical properties of the welds and HSS members, and the measured weld fracture loads, the structural reliability (or safety index) of the existing AISC specification formulas was determined. The existing AISC 360-10 provisions for weld effective lengths in overlapped rectangular HSS K-connections were found to be conservative and hence more liberal (but still safe) recommendations are proposed.

TABLE OF CONTENTS

SYMBOLS AND ABBREVIATIONS

A_b	Cross-sectional area of the rectangular HSS branch member, in.^{2}
A_g	Gross cross-sectional area of the rectangular HSS member, in.^{2}; complement of the outside HSS corner, in. ^{2}
A_h	Enclosed area of the rectangular HSS, in. ^{2}
AISC	American Institute of Steel Construction
ASD	Allowable stress design method (AISC, 2010)
A_w	Effective throat area of the weld, in. ^{2}
AWS	American Welding Society
A_ε	Complement of the inside HSS corner, in. ^{2}
B	Overall width of rectangular HSS chord member, measured normal to the plane of the connection, in.
B_b	Overall width of rectangular HSS branch member, measured normal to the plane of the connection, in.
B_{bi}	Overall width of the overlapping branch, in.
B_{bj}	Overall width of the overlapped branch, in.
C	HSS torsional constant
CIDECT	Comité International pour le Développement et l'Etude de la Construction Tubulaire
CISC	Canadian Institute of Steel Construction
COV	Coefficient of variation
CSA	Canadian Standards Association
E	Weld effective throat according to AWS (2010), in.; Young's modulus of elasticity, taken as 29 x 10^3 ksi
F_{EXX}	Electrode classification number, ksi
F_{nw}	Nominal strength of the weld metal per unit area, ksi
FOS	Factor of Safety, taken as the ratio (capacity / demand)
F_u	Ultimate tensile strength of rectangular HSS chord, ksi
F_{ub}	Ultimate tensile strength of rectangular HSS branch, ksi
F_y	Specified minimum yield stress of rectangular HSS chord, ksi
F_{yb}	Specified minimum yield stress of rectangular HSS branch, ksi
F_{ybi}	Specified minimum yield stress of the overlapping branch, ksi
F_{ybj}	Specified minimum yield stress of the overlapped branch, ksi

H	Overall height of rectangular HSS chord member, measured in the plane of the connection, in.
H_b	Overall height of rectangular HSS branch member, measured in the plane of the connection, in.
H_{bi}	Overall depth of the overlapping branch, in.
H_{bj}	Overall depth of the overlapped branch, in.
HSS	Hollow structural section
I	Moment of inertia about the axis of bending, in.^{4}
I_g	Moment of inertia of the outside HSS corner regions, in.^{4}
I_ε	Moment of inertia of the inside HSS corner regions, in.^{4}
J	Torsional stiffness constant
K	Effective length factor
L	Distance between chord panel points, in.; distance between points of lateral support for the chord, in.; panel point to panel point length of a member, in.
L_H	Horizontal weld leg size measured from the root to the toe, in.
LRFD	Load and resistance factor design method (AISC, 2010)
L_V	Vertical weld leg size measured from the root to the toe, in.
LVDT	Linearly varying differential transformer
M_D	Bending moment due to dead load, kip-in.
ME	Macroetch Examination
M_n	Nominal flexural strength, kip-in.
M_L	Bending moment due to live load, kip-in.
M_{n-b}	Nominal flexural strength of the branch, kip-in.
M_{n-ip}	Nominal flexural strength of weld for in-plane bending (AISC, 2010), kip-in.
M_{n-op}	Nominal flexural strength of weld for out-of-plane bending (AISC, 2010), kip-in.
M_p	Plastic bending moment, kip-in.
NIST	National Institute of Standards and Technology
O_v	Overlap connection coefficient
P	Axial force, kips
P_D	Axial force due to dead load, kips
P_L	Axial force due to live load, kips
$P_{n,i}$	Nominal axial strength of the overlapping branch, kips
$P_{n,j}$	Nominal axial strength of the overlapped branch, kips
$P_{ultimate}$	Actual axial strength of welded joint (ultimate load), kips
PP	Panel point

Q_f	Chord-stress interaction parameter, equal to 1.0 for chord connecting surface in tension
R_c	Mean corner radius, in.
R_n	Nominal strength of rectangular HSS member, kips; nominal strength of weld, kips
R_{nw}	Nominal strength of welded joint, ksi
S	Elastic section modulus of the rectangular HSS member, in.^{3}
SG	Strain gage
TC	Tensile coupon
WPS	Welding procedure specification
Z	Plastic section modulus of the rectangular HSS member, in.^{3}
a	Weld effective throat according to Packer et al. (2009), in.
b	Clear distance between the webs less the inside corner radius on each side, in.
b_0	Overall width of rectangular HSS chord member according to Packer et al. (2009), in.
b_1	Overall width of rectangular HSS branch member according to Packer et al. (2009), in.
b_{eoi}	Effective width of the branch face welded to the chord, in.; effective length of the weld to the chord, in.
b_{eov}	Effective width of the branch face welded to the overlapped branch, in.; effective length of the weld to the chord, in.
d	Greatest perpendicular dimension measured from a line flush to the base metal surface to the weld surface, in.
e	Eccentricity in a truss connection, positive being away from the branches, in.
h	Clear distance between the flanges less the inside corner radius on each side, in.; mid-contour length, in.
h_g	Length of the outside HSS corner radius contour, in.
h_ε	Length of the inside HSS corner radius contour, in.
i	Subscript/ term used to identify the overlapping branch member; Subscript/ term used to identify weld elements
j	Subscript/ term used to identify the overlapped branch member
l_e	Effective length of groove and fillet welds for rectangular HSS, in.
l_{ei}	Effective length of an element in a weld group, in.
m_R	Mean of the ratio (actual element strength / nominal element strength)
p	Projected length of the overlapping branch on the connecting face of the chord, in.

q	Overlap length, measured along the connecting face of the chord beneath the region of overlap of the branches, in.
r	Governing radius of gyration in.
r_i	Inside HSS corner radius, in.
r_o	Outside HSS corner radius, in.
t	Wall thickness of rectangular HSS chord member, in.
t_0	Wall thickness of rectangular HSS chord member according to Packer et al. (2009), in.
t_1	Wall thickness of rectangular HSS branch member according to Packer et al. (2009), in.
t_b	Wall thickness of rectangular HSS branch member, in.
t_{bi}	Wall thickness of the overlapping branch member, in.
t_{bj}	Wall thickness of the overlapped branch member, in.
t_w	Weld effective throat, in.
t_{wi}	Weld effective throat of an element in a weld group, in.
α	Coefficient of separation (taken to be 0.55)
β	Width ratio; the ratio of overall branch width to chord width for rectangular HSS
β^+	Safety index
$\bar{\varepsilon}$	Average strain, in./in.
ε_1, ε_2	Measured strain at the extreme fibre of the HSS, in./in.
ε_y	Strain at material yield point, in./in.
ε_{rup}	Elongation at rupture, in./in.
λ_p	Limiting slenderness parameter for compact element (AISC, 2010)
λ_r	Limiting slenderness parameter for non-compact element (AISC, 2010)
$\emptyset$	Resistance factor (associated with the load and resistance factor design method)
θ	Included angle between the branch and chord, degrees; Angle of loading measured from the weld longitudinal axis, degrees
φ	Curvature of the HSS section, rad/in.

Chapter 1: Introduction

(a) Retractable stadium roof at the Rogers Center in Toronto, Canada

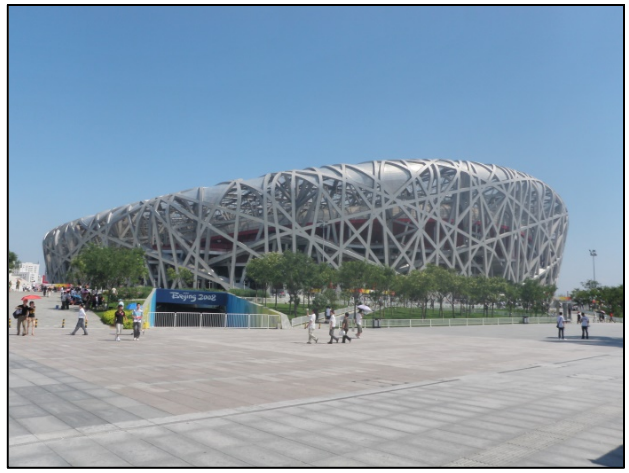

(b) Beijing National Stadium (or "Bird's Nest") in Beijing, China

Figure 1-1 Global applications of HSS in exposed steel structures

The use of tubes in the design of steel structures has become increasingly popular since production of hollow structural sections (HSS) began in 1952 in Corby, England. Today in North America, HSS for building applications are produced domestically by a significant number of manufacturers. During the popular "continuous cold-forming" manufacturing process, flat steel plate is gradually formed by rollers into a round hollow section. The edges are then welded together to produce what is referred to as the "mother tube". The mother tube goes through a series of progressive shaping stands, which transform the round HSS into the final square or rectangular shape.

HSS are used in a wide variety of structural applications including traffic and pedestrian bridges, stadia roofs, and roller coasters, and are preferred in buildings that have exposed architectural steel work because of their smooth visual appeal. Notable examples of HSS use in the global market are the retractable stadium roof at the Rogers Center in Toronto, Canada, and the Beijing National Stadium (or "Bird's Nest") in Beijing, China (see Figures 1-1(a) and Figure 1-1(b), respectively). In addition to providing aesthetic value, HSS offer design advantages that include a high strength-to-weight ratio, torsional rigidity, and less surface area compared to equivalent wide flange ("W"-) sections. These advantages can lead to savings in structural weight, transportation, fabrication, erection, and finishing.

Over the last 60 years, HSS research programs, many of which were sponsored by the International Committee for the Development and Study of Tubular Construction (CIDECT), have investigated member stability, fire protection, composite construction, and connection static and fatigue behavior. The results of these programs are today incorporated into national and international codes, standards and guidelines including The American Institute of Steel Construction (AISC) Specification for Structural Steel Buildings (2010), Canadian Institute of Steel Construction (CISC) guide (Packer & Henderson, 1997) and Eurocode 3: Design of steel structures (CEN, 2005). HSS research continues to look at topics of blast resistance, robustness, manufacturing, dynamic behavior, and welding.

1.1. HSS Trusses and Connections

Trusses are used in a broad range of buildings, mainly where there are requirements for long, unsupported, spans such as bridges, aircraft hangers, and sports stadia roofs. Traditional trusses like Warren (“K”-joint) and Pratt (“N”-joint) trusses are comprised of triangulated web (or “branch”) members that carry predominantly axial forces, and are pin-jointed at their ultimate limit state. HSS are an aesthetic and functional complement to traditional trusses, which allow their efficiency as compression elements to be exploited.

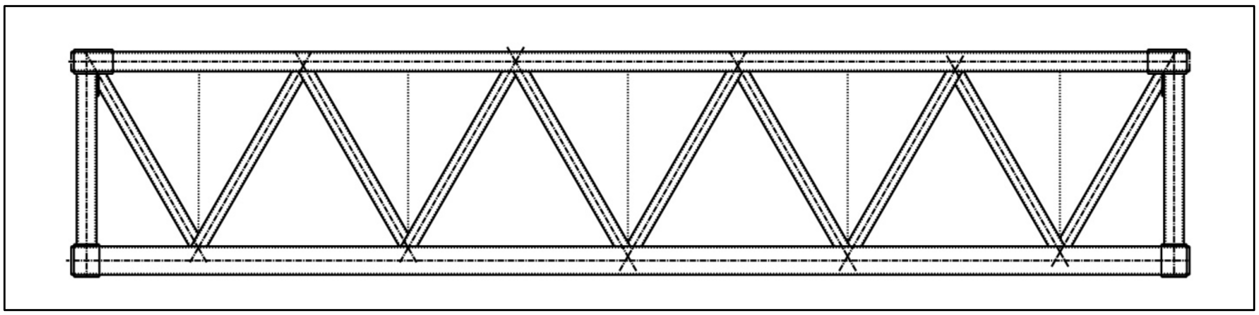

Figure 1-2 Warren truss arrangement (modified Warren truss with verticals)

A Warren-truss (or “K-”) connection is formed at the intersection of two web members with the chord of the truss and may be either gapped or overlapped depending on the design requirements. An overlapped K-connection is formed by intersecting web members above the chord, and is generally stronger and more rigid than a gapped K-connection. They are, however, more difficult to fabricate, and cost accordingly. The Warren truss arrangement, patented in 1848 by designers James Warren and Willoughby Theobald Monzani, is shown in Figure 1-2.

A substantial amount of testing has been performed on isolated rectangular HSS K-connections since the 1960s and on full-scale rectangular HSS trusses since the 1970s. The latter tests were conducted, among other things, to establish a correlation between the behavior of isolated and in-situ joints, thus allowing design recommendations to be made for HSS truss-type connections.

1.2. Design of HSS Truss-Type Connections

Differences in the relative flexibility across HSS chord walls can result in a highly non-uniform stress distribution in the connected elements. Research has observed that both the strength and rigidity of HSS connections decrease as the branch-to-chord width ratio (β) decreases and as the chord wall slenderness value (B/t) increases (Packer & Henderson, 1997). This affects the requirements for the design of such connections, including both the members and the welds.

1.2.1. Design Methods for Welds

The design criteria for welds to HSS have continually evolved as more data becomes available through testing and experimental research. At present, there are two design methods available for proportioning the welds (Packer et al., 2010):

(i) The welds may be proportioned to develop the yield strength of the connected branch wall at all locations around the branch perimeter.
(ii) The welds may be designed as “fit-for-purpose”, and proportioned to resist the applied forces in the branch.

The former design method has been historically used, and thus welds to HSS are found routinely oversized – especially in HSS branches that have low axial loads, for any number of possible reasons. In such situations, a “fit-for-purpose” design method is ideal. When following this approach, it is necessary to make use of effective weld properties in order to account for the non-uniform loading of the weld perimeter due to the relative flexibility of the connecting chord face. These effective weld properties are the focus of this report.

1.3. Experimental Program Overview

An experimental program was developed at the University of Toronto to evaluate the performance of large-scale rectangular HSS overlapped K-connections subject to axial tension acting in the overlapping branch member. A large-scale 33-ft. span, simply-supported, rectangular HSS Warren truss comprised of weld-critical overlapped K-connections was designed and fabricated. Connections were deliberately intended to be weld-critical and varied three key parameters that are known to influence the strength of welds to rectangular HSS: branch member overlap, chord wall slenderness, and branch-to-chord width ratio. By means of a quasi-static point load applied to strategic truss panel points, sequential failure of nine test welds to the overlapping branch members was obtained. Strain distributions adjacent to the weld and branch loads at rupture were measured. By using mechanical and geometrical properties of the welds and HSS members, and the measured weld fracture loads, the structural reliability (or safety index) of the existing AISC specification formulas was determined.

The following chapters summarize previous research into the strength and behavior of isolated rectangular HSS connections and full-scale rectangular HSS trusses, the incorporation of that research into current design criteria, the experimental program conducted to evaluate the performance of large-scale rectangular HSS overlapped K-connections, the results from these tests, a detailed analysis, and the conclusions made.

Chapter 2: Relevant Research and Current Design Criteria

This chapter provides an overview of the information that is currently available for the design of welded rectangular HSS overlapped K-connections and rectangular HSS trusses. The behavior, strength, and flexibility of HSS connections are discussed first, in order to introduce the basis of the current design methods that are available for welds in rectangular HSS connections. A history of the full-scale tests performed on weld-critical rectangular HSS gapped K-, T-,Y- and X- (or “Cross”-) connections is discussed, and the findings from this research are shown incorporated into the existing AISC 360 specification formulas (AISC, 2010) for the effective length of welds in rectangular HSS connections. The analysis and design of planar HSS trusses is then reviewed with emphasis on the analytical methods used to establish axial force and bending moment distributions as well as truss deflections for design.

2.1. Introduction to Rectangular HSS K-Connections

According to the governing steel design code in the United States, ANSI/AISC 360 (2010), the classification of rectangular HSS truss-type connections is based on the method of force transfer in the connection, not on the physical appearance of the connection. To qualify as a K- (or “N-”) connection, a joint must substantially equilibrate the branch member punching load from one member, $P\sin\theta$ (where θ is the included angle between the branch and chord), by the similar load in another branch member on the same side of the chord. The primary mechanism of force transfer is thus required to not occur through the chord.

Such connections can occur with branch members either spaced apart or overlapping, a consideration that depends on the design requirements in terms of branch loads and aesthetics. In most cases, a noding eccentricity, e, is inherent, which produces bending moments in the chord that need to be accounted for during design. The terminology for gapped and overlapped rectangular HSS K-connections according to ANSI/AISC 360 (2010) is shown in Figure 2-1 where, in order to identify the overlapping and overlapped (or “thru-”) members, the terms i and j have been used, respectively. The same terminology is adopted throughout this report.

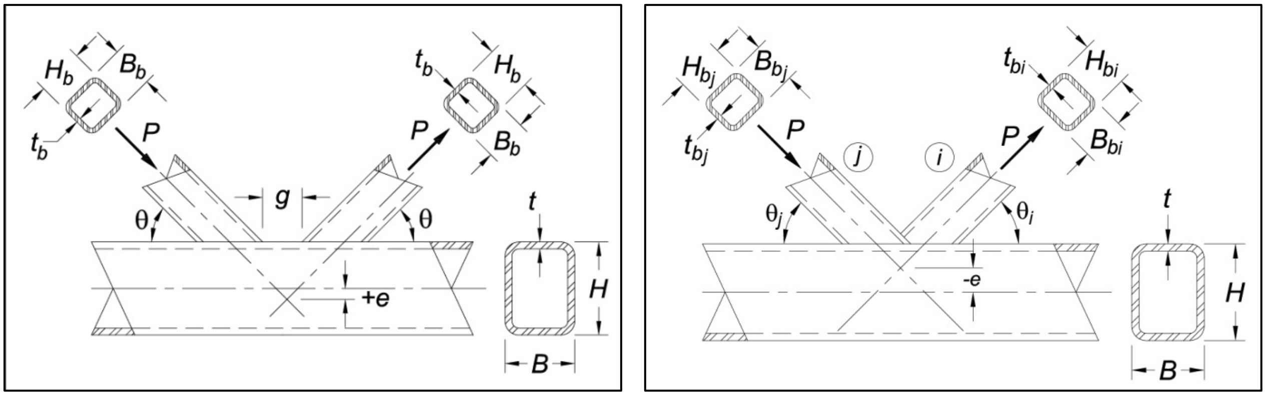

(a) Gapped K-connection (b) Overlapped K-connection

Figure 2-1 Standard terminology for gapped and overlapped rectangular HSS K-connections (AISC, 2010)

Several different failure modes can occur in rectangular HSS connections depending on the joint classification as a K-, Y-, or X- (Cross-) connection, the geometric parameters, and the loading conditions. Experimental research has shown that for such connections, there are seven basic failure modes (IIW, 2012; ISO, 2013):

1. Chord face failure or chord plastification
2. Chord punching shear
3. Local yielding of tension brace
4. Local yielding of the compression brace
5. Chord shear
6. Local chord member yielding
7. Chord side wall failure (or chord web failure)

Figure 2-2 shows the possible failure modes for rectangular HSS K-connections. In the current design codes and guidelines, limits are placed on various connection parameters in order to simplify the design of HSS connections and, as a result, it is possible to predict the strength of a connection using only one or two of the basic failure modes (or "decisive limit states").

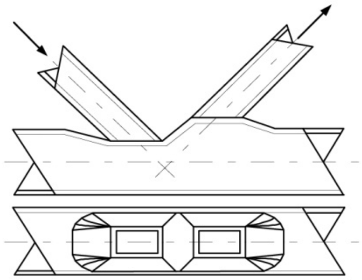

(a) Chord face plastification

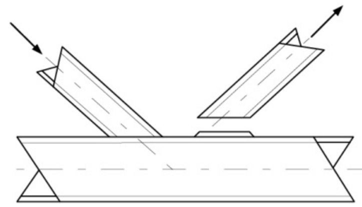

(b) Punching shear failure of the chord

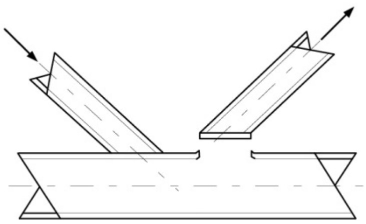

(c) Uneven load distribution in the tension brace

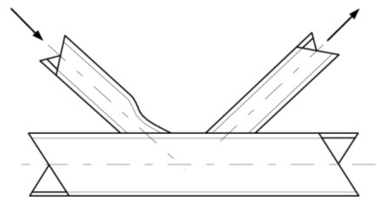

(d) Uneven load distribution in the compression brace

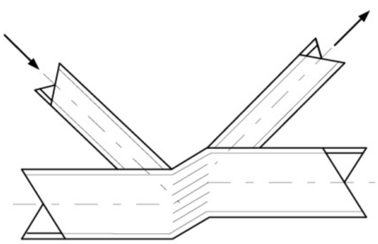

(e) Shear yielding of the chord in the gap

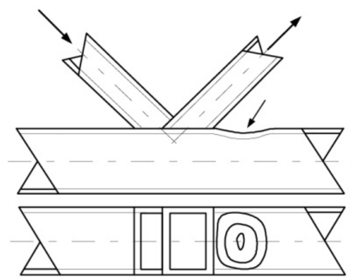

(f) Local buckling of the chord face

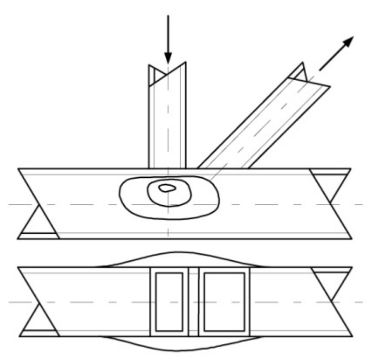

(g) Chord side wall failure

Figure 2-2 Possible failure modes for rectangular HSS gapped and overlapped K-connections (Packer et al., 2009)

2.1.1. Strength and Behavior

In this section, emphasis is placed on the strength and behavior of rectangular HSS overlapped (as opposed to gapped) K-connections, since the former are the topic of this report. The strength of rectangular HSS overlapped K-connections is addressed in Section K3 of AISC 360 (2010) and is based on only one decisive limit state. It is thus acceptable to design or analyze such a connection by checking only the limit state of local yielding in the branch members due to uneven load distribution, which may be manifested by either local buckling of the compression branch member or premature yield failure of the tension branch member. According to the load and resistance factor design (LRFD) method, the strength of a rectangular HSS overlapped K-connection is initially determined by the available axial force in the overlapping branch member ($P_{n,i}$) according to the following equations:

When $25\% \leq O_v < 50\%$:

$$P_{n,i} = F_{ybi} t_{bi} \left[\frac{O_v}{50} (2H_{bi} - 4t_{bi}) + b_{eoi} + b_{eov} \right] \quad \textbf{2-1}$$

When $50\% \leq O_v < 80\%$:

$$P_{n,i} = F_{ybi} t_{bi} (2H_{bi} - 4t_{bi} + b_{eoi} + b_{eov}) \quad \textbf{2-2}$$

When $80\% \leq O_v \leq 100\%$:

$$P_{n,i} = F_{ybi} t_{bi} (2H_{bi} - 4t_{bi} + B_{bi} + b_{eov}) \quad \textbf{2-3}$$

where:

$$b_{eoi} = \frac{10}{B/t} \left(\frac{F_y t}{F_{ybi} t_{bi}} \right) B_{bi} \leq B_{bi} \quad \textbf{2-4}$$

$$b_{eov} = \frac{10}{B_{bj}/t_{bj}} \left(\frac{F_{ybj} t_{bj}}{F_{ybi} t_{bi}} \right) B_{bi} \leq B_{bi} \quad \textbf{2-5}$$

$P_{n,i}$ is then used to determine the available axial force in the overlapped branch member ($P_{n,j}$) by virtue of Equation 2-6:

$$P_{n,j} = P_{n,i} \left(\frac{F_{ybj} A_{bj}}{F_{ybi} A_{bi}} \right) \quad \textbf{2-6}$$

An LRFD resistance factor of $\emptyset = 0.95$ is then applied to the connection available axial strength ($P_{n,i}$ and $P_{n,j}$) to determine the factored resistance. These equations are based on the load-carrying contributions of the four side walls of the branch member and are only valid within the Limits of Applicability of Section K2.3, which are summarized in Table 2-1.

In Table 2-1, F_{yb} is the branch member yield stress, and B_b, H_b, and t_b are the width, height, and thickness of the branch member, respectively. It may also be useful to note that the amount of overlap, O_v, is the percent value determined by dividing the overlap length measured along the connecting face of the chord beneath the region of overlap of the branches, q, by the projected length of the overlapping branch, p, as illustrated in Figure 2-3.

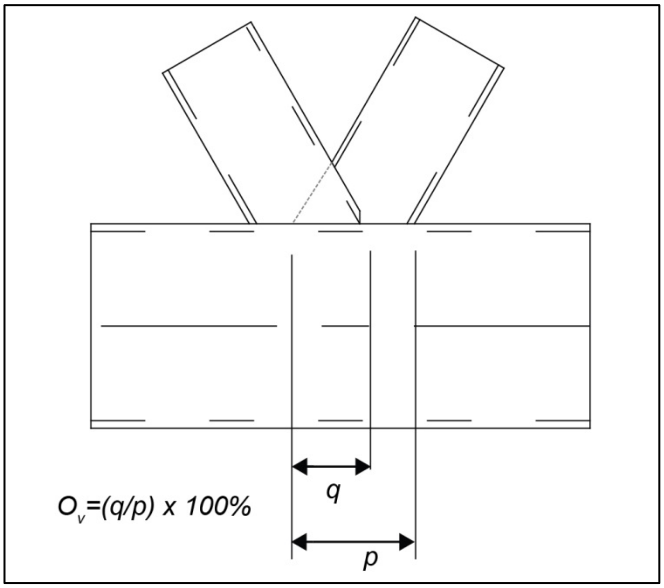

Figure 2-3 Definition of overlap

In addition to the connection available strength, the overall strength of the HSS members must be checked in accordance with Sections D, E and F of AISC 360 (2010) and the welds must be proportioned either to develop the branch yield strength or to resist the applied loads. Effective length factors for compressive buckling can be determined, when necessary, in accordance with CIDECT Design Guide No. 3 (Packer et al., 2009) or the CISC guide (Packer & Henderson, 1997).

Table 2-1 Limits of validity for the design axial resistance of uniplanar overlapped K-connections with rectangular HSS

Criteria	Limit(s)	Rationale according to IIW (1989)
Joint eccentricity	$-0.55H \leq e \leq 0.25H$	
Branch angle	$\theta \geq 30°$	to prevent excessive difficulties welding the heel
Chord wall slenderness	B/t and $H/t \leq 30$	to prevent excessively large connection deformations (inadequate for serviceability)
Branch wall slenderness	B_b/t_b and $H_b/t_b \leq 35$ (tension branch) B_b/t_b and $H_b/t_b \leq 1.1\sqrt{\frac{E}{F_{yb}}}$ (compression branch)	
Width ratio	B_b/B and $H_b/B \geq 0.25$	
Aspect ratio	$0.5 \leq H_b/B_b$ and $H/B \leq 2.0$	
Overlap	$25\% \leq O_v \leq 100\%$	to enable effective shear transfer from one branch to the other
Branch width ratio	$B_{bi}/B_{bj} \geq 0.75$	
Branch thickness ratio	$t_{bi}/t_{bj} \leq 1.0$	to prevent a stronger member from bearing on a weaker member
Material strength	F_y and $F_{yb} \leq 52\ ksi$	
Ductility	F_y/F_u and $F_{yb}/F_{ub} \leq 0.80$	to ensure ductility is adequate to redistribute stress

2.2. Welds in Rectangular HSS Connections

Design criteria for welds have evolved over the years as more data has become available through testing and experimental research. The way in which a weld transfers the load through a connection can be complex and varies with respect to the type of weld, the geometry of the connected elements, and the angle of the applied load. The behavior is further convoluted by semi-rigid connections, such as most connections which occur between rectangular HSS, in which the relative flexibility of the connected elements has a significant effect on the weld strength.

Welded connections between rectangular HSS should be established around the entire perimeter of a branch member by means of a PJP flare-bevel-groove weld, a fillet weld, or a combination of the two (Packer et al., 2009). While fillet welds are preferred for cost, PJP flare-bevel-groove welds arise and are necessary in matched connections ($\beta = 1$) along the longitudinal walls of the branch, and when $\theta < 60°$ at the toe or heel. Various situations in HSS welding are illustrated in Figure 2-4.

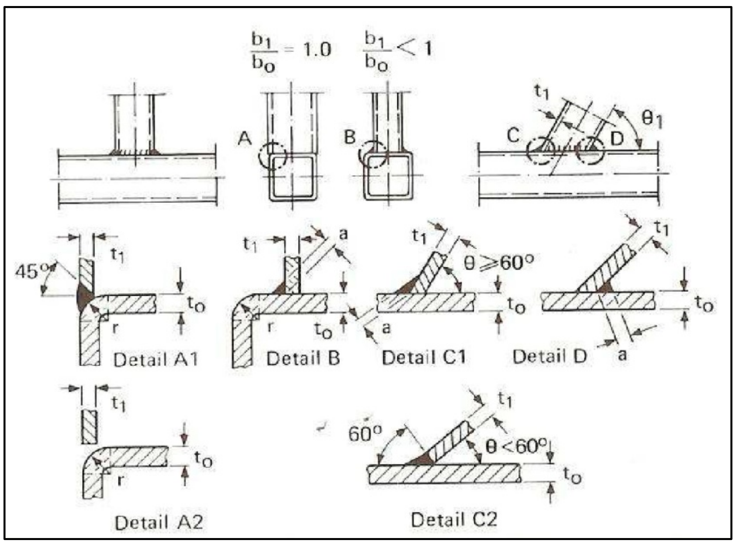

Figure 2-4 Typical situations in HSS welding and suggested welding details (Packer et al., 2009)

With welded connections between rectangular HSS, there are currently two design methods used to proportion welds. Welds which are automatically prequalified for any branch member load are covered under Method (i): Develop the Branch Yield Strength. Using this method, significant overwelding may occur and there must be attention to ensure that fabricators achieve the required weld sizes. A “fit-for-purpose” approach that is intended as an alternative to designing welds for the capacity of the branch member is covered under Method (ii): Effective Weld Properties. This approach typically results in smaller weld sizes which provide a more economical design.

2.2.1. Method (i): Develop Branch Yield Strength

By Method (i), welds are proportioned to develop the capacity of the connected branch wall at all locations around the branch perimeter (Packer et al., 2009; Packer et al., 2010). This approach may be appropriate if there is low confidence in the design forces, uncertainty regarding Method (ii) or if plastic stress-redistribution is required in the connection. This method will produce an upper limit on the required weld size and may be excessively conservative in some situations. In any respect, it has been shown that there is no definitive international agreement for how to proportion a fillet weld in order to develop the capacity of a member (McFadden et al., 2013), and thus many connections designed using this approach, despite merit, have larger-than-necessary welds. A comparison of the effective throats required by various national and international standards to develop the capacity of the connected branch member wall for an axially-loaded 90° T-connections is shown in Table 2-2.

Table 2-2 Comparison of fillet weld effective throats required to develop the yield strength of the connected branch member wall for an axially-loaded 90° T-connection between rectangular HSS made to ASTM A500 Grade C with matching electrodes (McFadden et al., 2013)

Specification or Code	t_w
ANSI/AISC 360-10 Table J2.5	1.43 t_b
AWS D1.1/D1.1M: 2010 Clause 2.25.1.3 and Fig. 3.2	1.07 t_b
CAN/CSA S16-01 Clause 13.13.2.2	1.14 t_b
CSA S16-09 Clause 13.13.2.2	0.95 t_b
CEN (2005): Directional method	1.28 t_b

2.2.2. Method (ii): Effective Weld Properties

By Method (ii), the welds may be designed as “fit-for-purpose” and proportioned to resist the applied forces in the branch (Packer et al., 2009; Packer et al., 2010). This requires the use of effective weld properties to account for the highly non-uniform distribution of stress around the weld perimeter due to the relative flexibility of the connecting chord face. This approach may be appropriate when there is high confidence in the design forces or if the branch forces are particularly low relative to the branch member capacity.

2.2.2.1. Historical Development

Subcommission XV-E of the International Institute of Welding (IIW) produced the first design recommendations for predominantly statically-loaded HSS connections in 1981. A second edition of the design recommendations based solely on Method (i) was released 8 years following. This document (IIW, 1989), is accepted as the basis for nearly all current design rules dealing with statically-loaded connections in onshore HSS structures including those in Europe (CEN, 2005), Canada (Packer & Henderson, 1997) and the United States (AISC, 2010). Over the past three decades, research at the University of Toronto (Frater & Packer, 1992a, 1992b;

Packer & Cassidy, 1995; McFadden et al., 2013; McFadden & Packer, 2014) on statically-loaded rectangular HSS connections has contributed to the development of effective weld properties, or Method (ii), which is now mentioned in the latest edition of the recommendations from the IIW (2012).

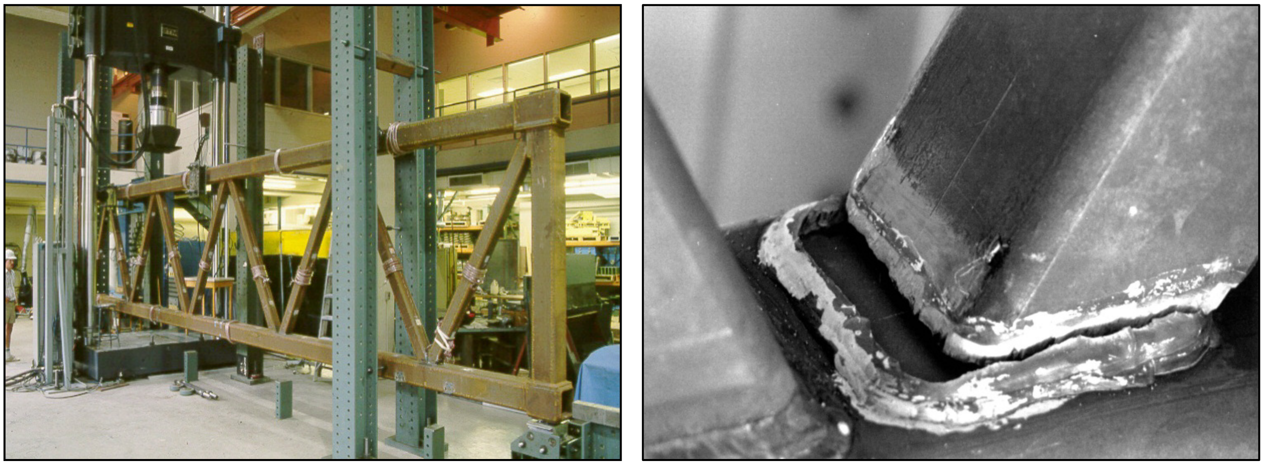

(a) Warren truss with gapped and overlapped K-connections

(b) Weld rupture in gapped K-connection

Figure 2-5 Full-scale tests on RHS Warren trusses with weld-critical gapped K-connections at the University of Toronto (Frater & Packer, 1992b)

Prevenient research by Frater & Packer (1992a, 1992b) on fillet-welded rectangular HSS gapped K-connections in two full-scale Warren trusses (shown in Figure 2-5) revealed that fillet welds in that context can be proportioned on the basis of the branch member loads, a more modern design approach that generally results in smaller weld sizes compared to IIW (1989). It was concluded simplistically that the welds along all four sides of the rectangular HSS branch contribute to the resistance of the joint when the angle of inclination of the branch relative to the chord (θ) is 50° or less (Equation 2-7), but that the weld along the heel should be considered as ineffective when the angle is 60° or more (Equation 2-8). For θ between 50° and 60°, a linear interpolation was recommended. Based on this research, the formulas for the effective length of branch member welds in planar, gapped, rectangular HSS K- and N-connections, subject to predominantly static axial load, were taken as (Packer & Henderson, 1992):

When $\theta \leq 50°$:

$$l_e = \frac{2H_b}{\sin\theta} + 2B_b \qquad \textbf{2-7}$$

When $\theta \geq 60°$:

$$l_e = \frac{2H_b}{\sin\theta} + B_b \qquad \textbf{2-8}$$

A subsequent study by Packer & Cassidy (1995) developed, by means of 16 full-scale connection tests (see Figure 2-6) designed to be weld-critical, new effective length formulas for rectangular HSS T-, Y- and X- (Cross-) connections. It was found that for such joints, more of the weld perimeter is effective for lower branch member inclination angles. Thus, in a later edition of the text by Packer & Henderson (1997), the formulas for the effective length of branch member welds in planar T-, Y- and Cross- (or X-) rectangular HSS connections, subjected to predominantly static axial load, were taken as:

When $\theta \leq 50°$:

$$l_e = \frac{2H_b}{\sin\theta} + B_b \qquad \textbf{2-9}$$

When $\theta \geq 60°$:

$$l_e = \frac{2H_b}{\sin\theta} \qquad \textbf{2-10}$$

A linear interpolation was again recommended for θ between 50° and 60°.

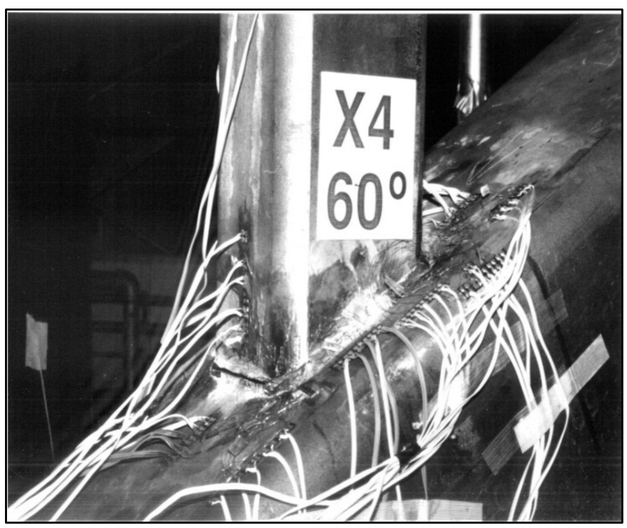

Figure 2-6 Full-scale test on RHS X- (Cross-) connection at the University of Toronto (Packer & Cassidy, 1995)

Another study in the series of programs to investigate effective weld properties in rectangular HSS connections, commissioned by the AISC, was conducted to verify and modify, if necessary, an approach that was speculated in AISC 360 (2010) for the design of branch member welds in planar T-, Y- and Cross- (or X-) rectangular HSS connections, subjected to predominantly static in-plane and out-of-plane bending (McFadden & Packer, 2013, 2014). By means of 12 full-scale experiments on isolated T-connections (see Figure 2-7), it was found that the existing AISC 360 (2010) provisions for weld effective section moduli in such connections were conservative, thus more liberal (but still safe) recommendations were proposed.

The 3rd edition of the recommendations by the IIW (2012) explicitly acknowledges the effective length concept for the design of branch member welds in HSS connections. It recommends that the design resistance of hollow section connections be based on failure modes that do not include weld failure, with the latter being avoided by satisfying either of the two aforementioned Methods ((i) or (ii)).

AISC 360-10 Section K4 is devoted to Method (ii) and – besides containing experimentally-verified weld effective length rules for axially-loaded T-, Y-, Cross- and gapped K-connections – has expanded the scope to also cover weld effective length rules for branch bending in T-, Y- and Cross-connections, plus weld effective length rules for overlapped K-connections under branch axial load.

(a) Weld-critical isolated moment T-connections

(b) Weld rupture in moment T-connection

Figure 2-7 Full-scale rectangular HSS moment T-connection test specimen at the University of Toronto (McFadden & Packer, 2012)

2.2.2.2. Current AISC 360 (2010) Provisions

The available strength formulas in AISC 360-10 Section K4 take into account all of the non-uniform load transfer around the perimeter of the weld due to differences in the relative flexibilities of the chord loaded normal to its surface and membrane stresses carried by the branch members parallel to their surface.

The nominal strengths of welds to rectangular HSS branches subject to axial load or bending are based on the limit state of shear rupture along the plane of the effective weld throat and according to AISC 360 (2010) can be determined according to the following equations:

$$R_n \text{ } or \text{ } P_n = F_{nw} t_w l_e \quad \textbf{2-11}$$

$$M_{n-ip} = F_{nw} S_{ip} \quad \textbf{2-12}$$

$$M_{n-op} = F_{nw} S_{op} \quad \textbf{2-13}$$

where the LRFD resistance factor, ∅, is equal to 0.75 and 0.80 for fillet welds and partial-joint-penetration (PJP) groove welds, respectively, and t_w is the effective weld throat around the perimeter of the branch. The limits of applicability in Section K2.3, which also apply to formulas for connection strength, apply here (see Table 2-1).

The nominal stress of the weld metal, F_{nw}, for fillet welds subject to shear along an effective throat and PJP groove welds subject to tension normal to the weld axis, is specified in Table J2.5 (AISC, 2010) and taken as 0.60 times the minimum tensile strength of the weld metal, F_{EXX}. The use of a directional strength enhancement factor for fillet welds in HSS-to-HSS connections is currently not allowed where Method (ii), using the effective weld length, is used (AISC, 2010; Packer et al., 2010).

The effective weld lengths, l_e , used in conjunction with Equations 2-11,2-12, and 2-13 to calculate R_n , P_n, M_{n-ip}, or M_{n-op} are given in design-guide format in Table K4.1 of AISC 360 (2010). For gapped K- and N-connections under branch axial load, the effective weld length, l_e, associated with Equation 2-11, is calculated as follows:

For θ ≤ 50° :

$$l_e = \frac{2(H_b - 1.2t_b)}{\sin\theta} + 2(B_b - 1.2t_b) \qquad \textbf{2-14}$$

For θ ≥ 60°:

$$l_e = \frac{2(H_b - 1.2t_b)}{\sin\theta} + (B_b - 1.2t_b) \qquad \textbf{2-15}$$

When 50° < θ < 60°, a linear interpolation is used. In contrast to Equations 2-7 and 2-8, however, a reduction to the individual weld element lengths (equal to 1.2 t_b) has been implemented to account for the typical rectangular HSS corner radius. The equations have been simplified compared to the more complex ones that would result if the branch effective widths specified in Section K2.3 (AISC, 2010) were used.

The effective weld properties associated with Equations 2-11, 2-12, and 2-13 for T-, Y- and cross-connections under branch axial load or bending are specified in Table K4.1 of AISC 360 (2010), and are summarized below.

For axial load:

$$l_e = \frac{2H_b}{\sin\theta} + 2b_{eoi} \qquad \textbf{2-16}$$

For in-plane bending:

$$S_{ip} = \frac{t_w}{3}\left(\frac{H_b}{\sin\theta}\right)^2 + t_w b_{eoi}\left(\frac{H_b}{\sin\theta}\right) \tag{2-17}$$

For out-of-plane bending:

$$S_{op} = t_w\left(\frac{H_b}{\sin\theta}\right)B_b + \frac{t_w}{3}\left(B_b^2\right) - \frac{(t_w/3)(B_b - b_{eoi})^3}{B_b} \tag{2-18}$$

where b_{eoi} is calculated using Equation 2-4. An additional requirement imposed by AISC 360 (2010) limits the value of b_{eoi} / 2 to a maximum of $2t$ for connections with β > 0.85 or θ > 50°. In contrast to Equations 2-9 and 2-10, the weld effective length in Equation 2-16 was – for consistency – made equivalent to the branch wall effective lengths used in Section K2.3 (AISC, 2010) for the limit state of local yielding of the branch members due to uneven load distribution. The limit of b_{eoi} / 2 has since been justified as B_b/4 (for β > 0.85 or θ > 50°) in research by McFadden & Packer (2012, 2014) and this will be incorporated into AISC 360-16.

The effective properties associated with Equation 2-11 for welds to member i in overlapped K-connections are dependent on the amount of overlap, O_v, and presented in the following form in AISC 360 (2010) Table K4.1:

When 25% $\leq O_v <$ 50%:

$$l_{e,overlapping\ branch} = \frac{2O_v}{50}\left[\left(1-\frac{O_v}{100}\right)\left(\frac{H_{bi}}{\sin\theta_i}\right) + \frac{O_v}{100}\left(\frac{H_{bi}}{\sin(\theta_i+\theta_j)}\right)\right] + b_{eoi} + b_{eov} \tag{2-19}$$

When 50% $\leq O_v <$ 80%:

$$l_{e,overlapping\ branch} = 2\left[\left(1-\frac{O_v}{100}\right)\left(\frac{H_{bi}}{\sin\theta_i}\right) + \frac{O_v}{100}\left(\frac{H_{bi}}{\sin(\theta_i+\theta_j)}\right)\right] + b_{eoi} + b_{eov} \tag{2-20}$$

When 80% $\leq O_v \leq$ 100%:

$$l_{e,overlapping\ branch} = 2\left[\left(1-\frac{O_v}{100}\right)\left(\frac{H_{bi}}{\sin\theta_i}\right) + \frac{O_v}{100}\left(\frac{H_{bi}}{\sin(\theta_i+\theta_j)}\right)\right] + B_{bi} + b_{eov} \tag{2-21}$$

where b_{eoi} and b_{eov} are calculated using Equation 2-4 and Equation 2-5, respectively. These too have been made equivalent to the branch wall effective lengths used in Section K2.3 (AISC, 2010) for the limit state of local yielding of the branch members and are governed by a requirement that limits the value of b_{eoi} / 2 to a maximum of $2t$ when $B_{bi}/B >$ 0.85 or $\theta_i >$ 50°, and b_{eov} / 2 to a maximum of $2t_{bj}$ when $B_{bi}/B_{bj} >$ 0.85 or (180 – θ_i – θ_j) > 50°.

The terms b_{eoi} and b_{eov} were empirically derived from laboratory tests in the 1970s and 1980s (Davies & Packer, 1982) and already include a partial resistance factor, $\emptyset = 0.90$. They are used to determine the effective width of the welds transverse to the chord and are thus a main topic of the investigation into the performance of welds in rectangular HSS overlapped K-connections. These terms are illustrated in Figure 2-8, alongside the terms contained in square parentheses in Equations 2-19 through 2-21, which sum to the total effective length of weld along the height of the overlapping HSS branch member. Thus, according to the equations, the longitudinal weld elements are partially effective when $O_v < 50\%$, and fully effective when $O_v \geq 50\%$.

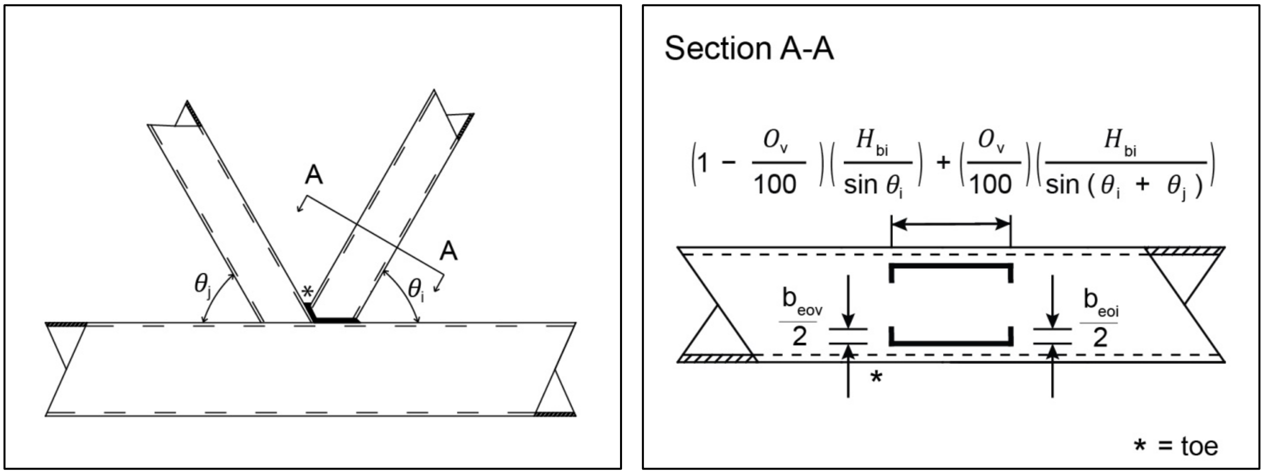

(a) Connection Profile (b) Weld effective length dimensions

Figure 2-8 Weld effective length terminology for rectangular HSS overlapped K-connections subject to branch axial load

While being based on informed knowledge of the behavior of rectangular HSS connections and agreed upon by the AISC 360 TC6 HSS Subcommittee, Equations 2-19, 2-20, and 2-21 have not been validated by experimental tests and therefore, while thought to be conservative, are speculative.

2.3. Methods of Analysis for Rectangular HSS Trusses

Previous large-scale testing of planar rectangular HSS trusses has been performed by Dasgupta (1970), de Koning & Wardenier (1979), Czechowski et al. (1984), Coutie et al. (1987), Philiastides (1988), and Frater & Packer (1992c). The results of these truss tests have validated the many more isolated connection tests, which in total form the basis for international design recommendations by CIDECT and the IIW.

2.3.1. Force Distribution

A key outcome of the investigations into the behavior of planar rectangular HSS trusses has been the validation of analytical methods to predict the axial forces, bending moments, and deflections for static design. For rectangular HSS Warren and Pratt trusses, having either gapped or overlapped connections, Packer et al. (2009) recommend that a force distribution be obtained from an elastic analysis of the truss with either:

a) all of the members pin-connected, or
b) the web members pin-connected to continuous chord members (see Figure 2-9).

In method (b), the truss can be modeled by considering a continuous chord with web members pin-connected to it at distances of $+e$ or $-e$ from it. The links to the pins are treated as being extremely stiff, and thus the forces in the web members acting at a distance of $+e$ or $-e$ automatically produce a sensible distribution of bending moments in the chord. In method (a), the same process needs to be carried out manually if there is a noding eccentricity, e (by distributing the chord moments induced by web member horizontal force components in proportion to the stiffness of the chord on either side of the connection).

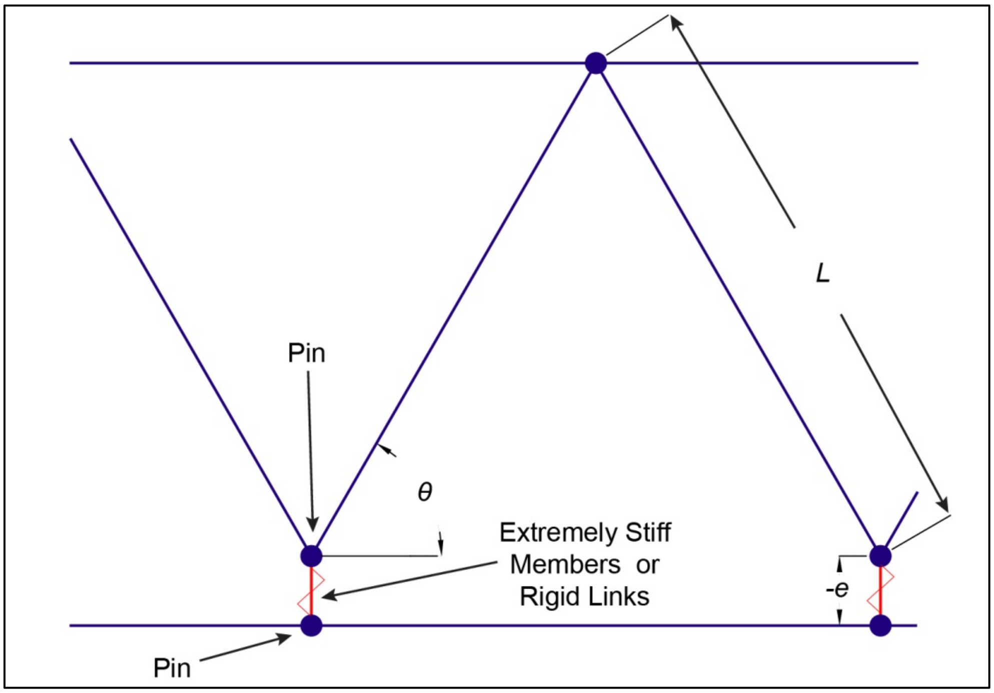

Figure 2-9 Plane frame joint modeling assumptions to obtain realistic forces for member design

An analysis with all members rigidly connected is not recommended for most planar, triangulated, single-chord, directly-welded trusses as it generally exaggerates web member moments, and gives an axial force distribution not significantly different from pin-jointed analysis (Packer et al., 2009).

2.3.2. Overall Deflection

For rectangular HSS trusses with gapped connections, a pin-jointed analysis, which represents the most flexible theoretical structure, generally underestimates overall elastic truss deflections by 12-15% (Czechowski et al., 1984; Coutie et al., 1987; Philiastides, 1988; Frater, 1991). This occurs since frame modeling does not implicitly account for the contribution of joint flexibility to the overall truss behavior. Thus, in such cases, Packer et al. (2009) suggest multiplying the deflections obtained from a pin-jointed analysis by a correction factor of 1.15.

For rectangular HSS trusses with overlapped connections, a pin-jointed analysis should provide a conservative (over-) estimate of the overall elastic truss deflections. If necessary, a more accurate estimate of the overall elastic deflections can be obtained by using a model that comprises continuous chord members and pin-jointed web members – or method (b), above. This analysis method has been shown to agree well with experimental data in previous large-scale, overlap-jointed truss experiments (Coutie et al., 1987; Philiastides, 1988).

The deflections calculated in accordance with these methods are used in conjunction with the requirements of Chapter L of AISC 360 (2010). These requirements, which limit allowable static deflections for certain load combinations, are in existence to prevent the manifestation of short- and long-term serviceability limit states such as visually objectionable deformations, repairable cracking and damage to interior finishes, as well as creep, settlement, and similar long term effects.

2.3.3. Member Continuity and Design

In design, it is generally accepted to treat the web members of a truss as pin-connected and the chords as beam-columns. The latter elements resist the majority of the primary bending moments produced by joint noding eccentricities and transverse loads between panel points. Secondary moments resulting from end fixity of the web members to a flexible chord wall can generally be ignored for both members and joints provided that there is deformation and rotation capacity adequate to redistribute stresses after some local yielding at the connections. This is the case when the prescribed geometric limits of validity for design formulas, such as those given in Section K2.3 of AISC 360-10, are followed, and adequate welds are provided.

According to simplified rules (Packer et al., 2009), KL for web members and chords can be taken as $0.75L$ and $0.9L$, respectively, both in- and out-of-plane of the truss. K is an effective length factor and L is the member buckling length being considered. For web member buckling and chord in-plane buckling, L is always the panel point to panel point (or “work point”) length of the member. For chord out-of-plane buckling, L is the distance between points of lateral support to the compression chord. The design requirements for overlap-jointed Warren truss members in accordance with AISC 360 (2010) are summarized in Table 2-3.

Table 2-3 Forces to be considered for rectangular HSS truss design, with web members pinned at ends, and overlapped K-connections

Type of Loading	Axial Loads	Moments		
		Primary*		Secondary**
		Noding eccentricity ($-0.55H \leq \mathrm{e} \leq 0.25\mathrm{H}$)	Transverse member loading	Local deformations
Chord design	Yes	Yes	Yes	No
Design of web members	Yes	No	Yes	No
Design of connections and welds	Implicit in Section K4	No†	No†	No, subject to Section K2.3 and $L/H_b \geq 6$

† $Q_f = 1$ for all overlap connection criteria.
* Primary bending moments are those required for equilibrium of the structure.
** Secondary bending moments are those produced by connection deformations.

Chapter 3: Experimental Program

3.1. Scope

An experimental program was developed at the University of Toronto to test large-scale rectangular HSS overlapped K-connections. The objective of this study was to verify or adjust the current effective weld length rules defined by Equations K4-10 to K4-12 in Table K4.1 of ANSI/AISC 360 (2010). Nine overlapped K-connections within one large-scale, 33-foot span, simply-supported Warren truss, were designed to be weld-critical under the application of tension to the overlapping branch. Key parameters, such as the branch member overlap (O_v), the branch-to-chord width ratio (β-ratio) and the chord wall slenderness (B/t), were investigated, and varied within the Limits of Applicability of Section K2.3 of the Specification (AISC, 2010). The non-uniform distribution of normal strain in the branch near the connection was measured with strain gages oriented along the longitudinal axis of the branch at uniform increments around the branch perimeter. The truss, and ergo the connections, were fabricated with a continuous effective weld throat using a flux-cored arc welding (FCAW) process by an AWS D1.1 certified fabricator. To induce weld rupture, a single point load was applied to various truss panel points in a quasi-static manner by a 600-kip capacity MTS Universal Testing Frame. The loading strategy was carefully planned to accentuate the force in the critical web member(s) and resulted in all 9 joints failing by shear rupture along a plane through the weld. The experimental program also included tensile coupon tests of the HSS and as-laid weld metal, as well as two truss tests at the service-load level.

3.2. Truss Design

Full-scale truss tests on weld-critical connections have been performed at the University of Toronto for rectangular HSS gapped K-connections (Frater, 1991; Frater & Packer, 1992a, 1992b, 1992c) and are an infallible way to ensure that the appropriate boundary conditions such as member continuity and truss deflection effects are taken into account. The following section summarizes the design of one weld-critical 33-foot span overlap-jointed Warren truss.

3.2.1. Objectives and Constraints

The key objectives and constraints of the experimental program had to be initially outlined in order that they were incorporated into the design process from the outset. They are emphasized here with deductive rationale. According to AISC 360 (2010) Section K2.3, the permissible variation in the key parameters that influences the joint strength of rectangular HSS overlapped K-connections is:

- 25% ≤ O_v ≤ 100%
- 0.25 ≤ β-ratio ≤ 1.00
- B/t ≤ 30

Conceptually, it was desired to produce a good experimental distribution of these parameters, while maintaining effective lengths for the welds on the overlapping web members that are well less than 100%, as predicted by the current AISC 360-10 Section K4 rules.

Objective 1: $\mathrm{O_v}$, β*-ratio and* $\mathrm{B/t}$ *had to be varied within the limits of applicability of Section K2.3 in order to investigate their influence on the effectiveness of the weld at resisting the forces at the rupture limit state.*

A single, quasi-static, compressive point load was to be applied by a 600-kip capacity moveable MTS dynamic loading frame, powered by a computer-controlled electro-hydraulic, closed-loop testing system. Thus, it was imperative that the weld strength at any connection be within the force that could be generated by this equipment. The size of the critical weld elements then dictated the remainder of the strength requirements for the truss members.

Objective 2: Welds had to be critical and a hierarchy of strength needed to be maintained such that weld rupture preceded connection failure, which in turn preceded member cross section and stability failure.

Unlike in practice, where a lower bound approximation is adequate to ensure a safe/conservative design, scientific analysis of experimental data requires accurate input for these parameters in order to eliminate the influence of confounding variables. The two experimental outputs required for a reliability analysis of any current or proposed design rules are the actual weld strength (which relies on the ability to obtain the applied branch load at weld rupture), and the predicted nominal weld strength using experimentally determined weld throats (t_w), weld lengths (l), and the filler metal ultimate strength (F_{EXX}).

Objective 3: All of the material and geometric weld parameters (t_w*,*l*,* F_{EXX}*) and the branch load at weld rupture had to be obtainable with a high degree of accuracy.*

Constraints were imposed by the physical environment within which the tests were conducted. The Sanford Fleming Laboratory, located in the University of Toronto Structural Testing Facilities, is equipped with approximately 7500 ft.^{2} of laboratory space, occupied in part by testing apparatus, and shared between ongoing projects. The laboratory is serviced by one 10-ton capacity overhead crane. Thus, the length of the truss had to fit within the laboratory space allotted to turning, sliding and maneuvering the truss between tests, and the weight of the truss had to be less than 10 tons. It was decided also that the shipping dimension should be such that the truss could fit fully constructed on a 32 ft. flat-bed truck.

3.2.2. Design Methodology

3.2.2.1. Computer Modeling

Simple 2D static frame analysis was performed with SAP2000 using two separate models with increasing complexity for various stages of the design:

(a) In the preliminary design stage, a simple 2D pin-ended analysis model (with web members concentrically connected to chord members) was used. This model was used to approximate the web and chord member axial forces and verify that the strength of the selected members was adequate in each stage of the intended loading. Engineering judgement was relied upon to approximately consider the influence of chord bending moments since the distribution of primary bending moments was at this time unknown.

(b) For verification of the final design, a continuous chord model was used, with branch members pin-connected to it at distances of $+e$ or $-e$, where e is the noding eccentricity or the distance from the chord centerline to the intersection of the branch member centerlines (Packer et al., 2009). The advantages of this model were discussed in Section 2.3. The links to the pins were modeled as very stiff elements (or "rigid links").

3.2.2.2. Procedure and Analysis

Design was carried out using the LRFD method of AISC 360-10 and in accordance with the AWS D1.1 *Structural Welding Code* (2010). Additional design guidance was taken from CIDECT *Design Guide 3* (Packer et al., 2009), and the CSA design guide *Hollow Structural Section Connections and Trusses* (Packer & Henderson, 1997). All members were specified to conform to CAN/CSA G40.20/G40.21 Class C (CSA, 2013a) or ASTM A1085 Class A (2013) per the Bill of Material provided in Appendix C.1 and weld consumable with a nominal ultimate strength of 70 ksi was assumed.

3.2.2.2.1. Span and Depth

The span-to-depth ratio and web member inclination angles were adopted from previous truss tests which were successfully performed at the University of Toronto (Frater & Packer, 1992b). The overall span, depth and weight were governed by laboratory space and equipment restrictions and addressed in the following order:

1. The depth of the truss was made equal to 6 ½ ft. such that it could be rotated about the longitudinal axis within the MTS frame in order to allow compressive point-loading on either of the truss chords. The span was scaled accordingly to maintain the span-to-depth ratio adopted from Frater & Packer (1992b).
2. The span was checked against the laboratory space allotted to turning, sliding and maneuvering the truss between tests and the target shipping dimensions, and verified.

3. The weight was then estimated based on trusses of similar size and found to be safely below the 10-ton capacity of the overhead crane.

Further refinements were made according to the layout of the truss, but at the outset of design it was estimated that a total of nine weld-critical connections could be designed and tested.

3.2.2.2.2. Member Sizes

Two different chord members were chosen to produce two different B/t values: an HSS 10 x 10 x $^{3}/_{8}$, having a nominal B/t value of 26.7, and an HSS 7 x 7 x $^{1}/_{2}$ having a nominal B/t value of 14.0.

Web members were specified to be HSS 5 x 5 x $^{5}/_{16}$ to address the considerations for connection design in CIDECT *Design Guide 3* (Packer et al., 2009) and for the following other reasons:

- Since the strength of a weld increases proportionally to the size of the branch member (by virtue of a longer length around the perimeter), reasonably small members were used to limit the demand on protected (or "non-critical") elements.
- It is more difficult, when build-up off of the overlapped web is required, to measure the theoretical throat in fillet welds. Matched web members permit a PJP weld along this element which can be more accurately measured to determine the throat.
- The ability to designate either web member at connections as the overlapping member greatly simplifies the design of the loading strategy.

The web member inclination angle ($\theta_i = \theta_j = 60°$) was found to represent a critical case in the current AISC 360-10 Section K4 rules and is unique for truss-type connections in that it permits fillet welds at both the toe and heel of the overlapping web member (according to AWS D1.1-10, the minimum included angle for fillet welds is 60°).

This member selection thus produced β-ratios of 0.50 and 0.71 for webs landing on the HSS 10 x 10 x $^{3}/_{8}$ and the HSS 7 x 7 x $^{1}/_{2}$, respectively.

3.2.2.2.3. Layout (Preliminary Modeling)

A simple 2D pin-ended (or "P model") analysis (with web members concentrically connected to chord members) was performed using SAP2000 to identify the axial force distribution that resulted from applying a compressive load of sufficient magnitude to cause weld rupture in any one joint. The analysis revealed that the factor of safety (FOS), taken as the ratio of capacity to demand, for weld (and connection) failure near the supports, while loading the welds near mid-span of the truss, was low. Thus, the loading strategy was designed to work "from-outside-in" in order to facilitate large weld sizes resulting from repair of the already-broken welds near the supports at the time of testing the welds near mid-span of the truss. Connections were laid out with (nominally) greater connection strength (higher O_v) at the ends of the truss, and web members were designated as overlapping or overlapped at each end in accordance with the tensions loads that could be reasonably produced in the branch members. O_v-values of significant variability were provided such that Equations 2-19, 2-20, and 2-21, could each be validated. Sample calculations for the LRFD connection, axial and flexural strengths using the specified mechanical properties are located in Appendix B.1. The nominal and LRFD resistances for all members and connections are tabulated in Appendix B.2.

3.2.2.2.4. Verification (Final Modeling)

To verify the design, a simulation of the nine tests was performed in SAP2000 using a continuous chord analysis (or "PR model"). The loads at panel points required to induce weld rupture were based on upper-bound weld strengths that were inferred from previous experiments and taken as 1.33 times the nominal weld strength when the entire length of the weld is fully effective ($P_n = 0.80 F_{EXX} t_w l_e$) and t_w= 0.188 in. The interaction of axial forces and bending moments in the chord was checked according to a straight-line interaction diagram. For each of the nine tests, the critical member, MTS location, estimated MTS load and stroke, alternate failure mode and FOS, estimated truss deflection, and support reactions are summarized in Appendix B.3. Web member/ weld loads due to the self-weight of the truss are isolated in Appendix B.4.

Fabrication drawings were subsequently produced with specifications for members, connections and welding. These drawings are located in Appendix C.2. The pertinent information is summarized in an overall elevation of the truss, which shows the location and numbering of the nine welded test joints as well as the labelling scheme for branch members and chords, in Figure 3-1.

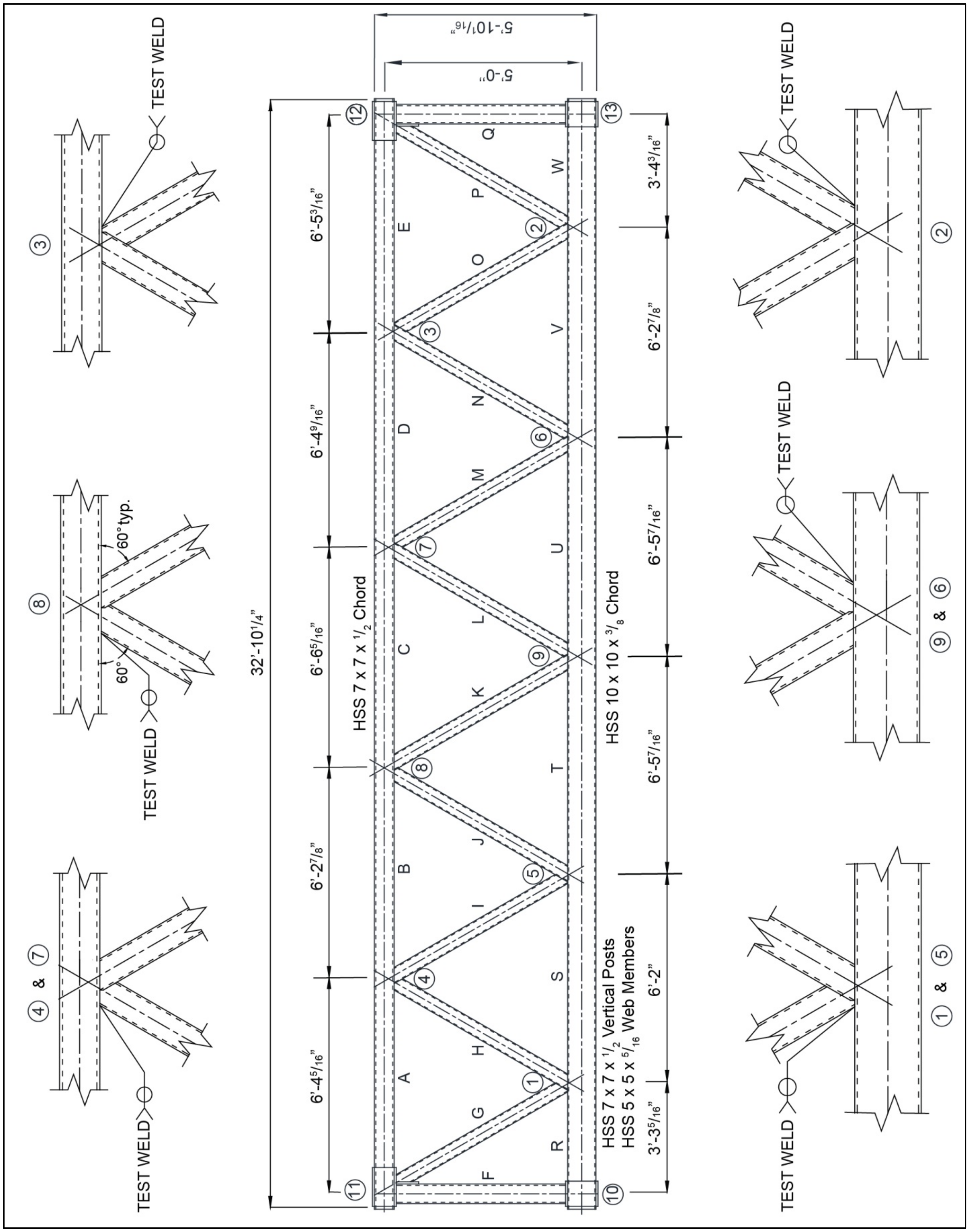

Figure 3-1 Overall elevation of the truss showing labelling scheme for test joints, web members and chord spans

3.3. Welded Test Joints

Matched HSS 5 x 5 x $^{5}/_{16}$ web members inclined at 60° were welded to two different chord sections: HSS 7 x 7 x $^{1}/_{2}$ and HSS 10 x 10 x $^{3}/_{8}$ with nominal B/t values of 26.7 and 14.0, respectively, thus producing β-ratios equal to 0.71 and 0.50. In order to validate the current speculative equations postulated in Table K4.1 (AISC, 2010), O_v values of 30%, 60%, and 90% were included in the connections. Panel point (or "connection") number, experimental designation, and a summary of the key test parameters for each joint are presented in Table 3-1.

Table 3-1 Experimental designation and summary of the key test parameters for each joint

Connection No.	Experimental Designation	O_v	Eccentricity (e)	β-ratio	Chord Wall Slenderness (B/t)
		%	in.		
1	K-90-0.50 (a)	90	4.5	0.50	26.7
2	K-60-0.50	60	3.0	0.50	26.7
3	K-90-0.71	90	3.0	0.71	14.0
4	K-60-0.71 (a)	60	1.5	0.71	14.0
5	K-90-0.50 (b)	90	4.5	0.50	26.7
6	K-30-0.50 (a)	30	1.5	0.50	26.7
7	K-60-0.71 (b)	60	1.5	0.71	14.0
8	K-30-0.71	30	0	0.71	14.0
9	K-30-0.50 (b)	30	1.5	0.50	26.7

Note: B_{bj}/t_{bj} constant for all connections by virtue of constant web members and equal to 16.0.

The weld element labelling convention used throughout the experimental program is shown in Figure 3-2. Labels a and a' refer to the fillet weld and PJP flare-bevel-groove weld elements, respectively, on the side of the truss pictured in Figure 3-1. This side is herein referred to as the "near side" of the truss. Elements b and b' refer to those weld elements opposite to a and a', herein referred to as the "far side" of the truss.

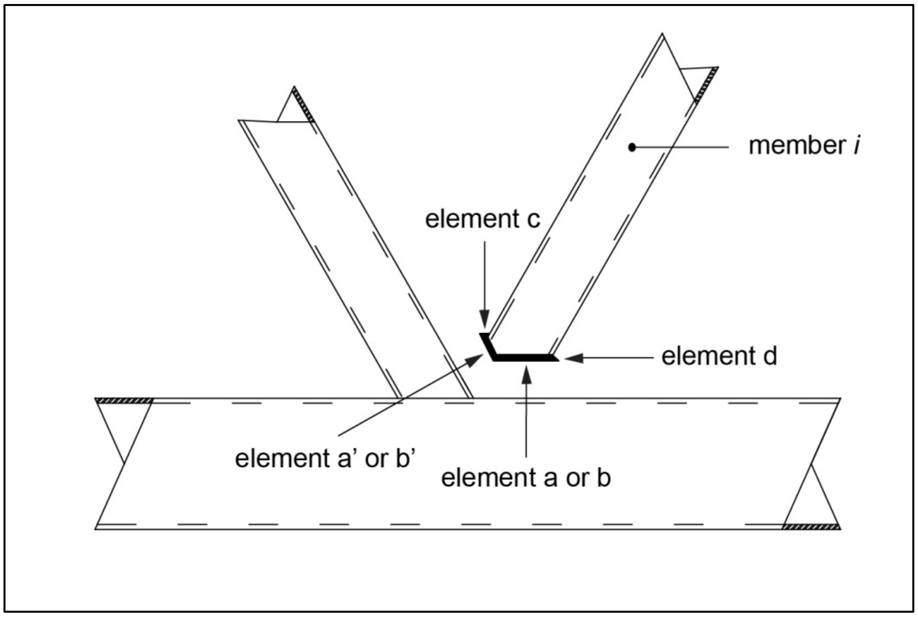

Figure 3-2 Weld element labelling conventions

3.3.1. Weld Element Details

Welded test joints were comprised of three distinct regions: the toe and/or heel region (elements c and d), where 60° fillet welds were permitted with full root penetration (AWS, 2010), the longitudinal 90° fillet-weld region (elements a and b), and the longitudinal PJP-weld region (elements a' and b'), where the butt joint between matched web members forms a flare-bevel groove, as shown in Figure 3-3.

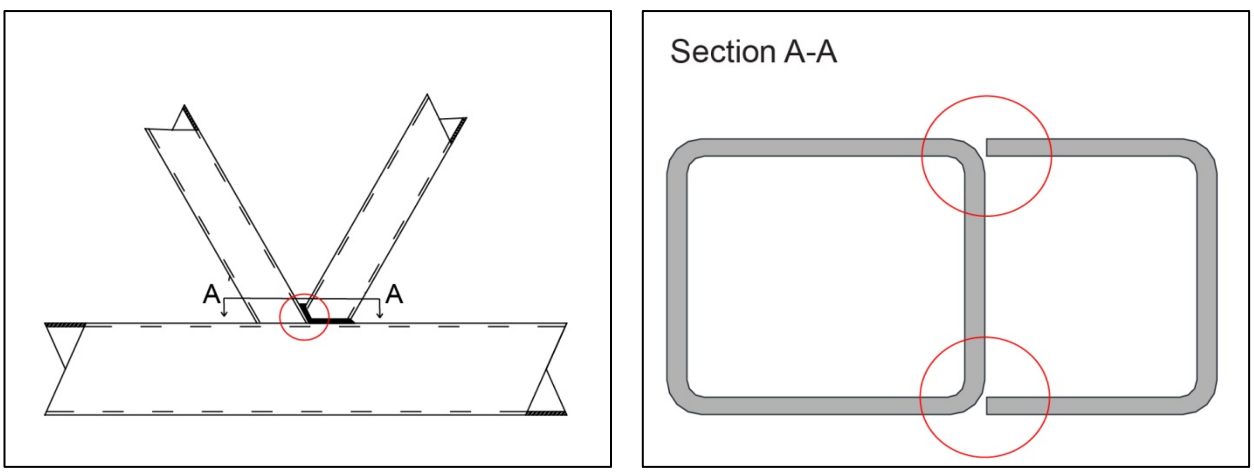

(a) Elevation view of butt joint

(b) Section view of butt joint

Figure 3-3 Flare-bevel groove in the butt joint between matched web members

The deposition of sound weld metal to the bottom of the flare in PJP flare-bevel-groove welds is non-trivial, because the welding puddle bridges between the two surfaces of the butting branch members (Packer & Frater, 2005). Thus, depending on the welding process and the outside corner radius of the HSS, root penetration may not always be achievable. It was shown by McFadden & Packer (2014) that post-rupture macroetch examinations (MEs) of PJP flare-bevel-groove welds produced reliable and accurate measurements of PJP weld throat sizes.

Since post-rupture MEs were not possible due to the sequential nature of the experimental program, a connection detail which utilized a backing bar was imagined in order to circumvent incomplete fusion through the branch thickness, by meeting the qualification requirements of Clause 4.13 (AWS, 2010) for complete joint penetration butt joints in tubular connections. In doing so, the effective throat could be determined in accordance with Table J2.1 (AISC, 2010). Profiles of the final weld details, in which a PJP flare-bevel-groove weld with a complete penetration (CP) detail is employed along elements a’ and b’, are shown in Figure 3-4.

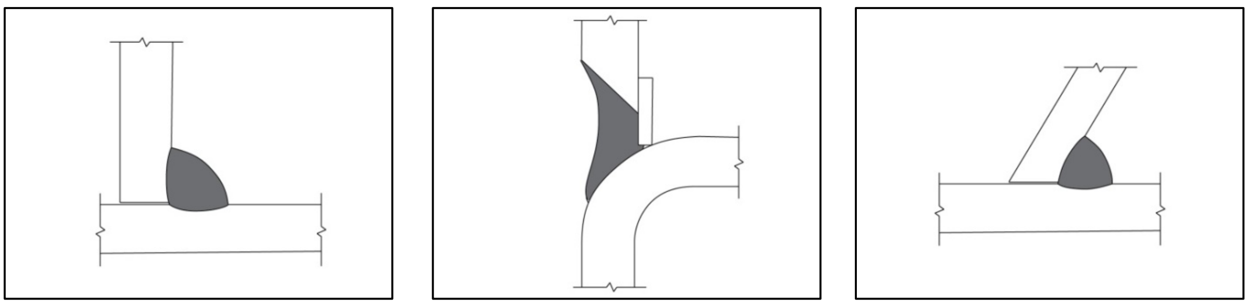

(a) Element a and b (b) Element a’ and b’ (c) Element c and d

Figure 3-4 Weld element details

Minimum weld sizes are specified in Table 5.8 and Table 3.4 of AWS D1.1 (2010) and Table J2.4 and Table J2.3 of AISC 360 (2010) for fillet welds and PJP flare-bevel-groove welds, respectively. These sizes are intended to ensure that there is enough heat input during welding to maintain the soundness of the weld. Since fabricators often grind their welds to produce a desirable profile after welding, these requirements would not be applicable to the result.

Test welds were specified in accordance with these requirements to a uniform effective throat of $^{3}/_{16}$ in. (the minimum size was governed by the required throat for PJP flare bevel groove welds given in Table J2.3 which is less than the minimum equivalent throat size for fillet welds given in Table J2.4 for the joint parameters).

Welds to non-test (or “protected”) members were designed in accordance with AWS D1.1 (2010) to develop the lesser of the branch member yield strength or local strength of the chord member. For fillet welded connections between cold-formed rectangular HSS made to CAN/CSA G40.20/G40.21 Class C or ASTM A1085 Class A with matching electrodes, a prequalified effective throat size (E) is given by AWS in terms of the connected branch wall thickness to develop any branch member load (Equation 3-1):

$$E = t_w = 1.07 \cdot t_b \quad \textbf{3-1}$$

Thus,

$$t_w = 1.07 \cdot t_b$$
$$t_w = 1.07 \cdot (0.313\ in.)$$
$$t_w = 0.334\ in.$$

For practical purposes, t_w was taken as $^3/_8$ in., except along the hidden toe of the overlapped branch (which was always welded to the chord) where the leg sizes (L_V and L_H) were made equal to $^3/_8$ in. A bevel at the toe of the member also helped to accommodate the weld there. Figure 3-5 shows the specified weld sizes and the associated welding symbols in a typical connection detail for a joint with $O_v = 30\%$.

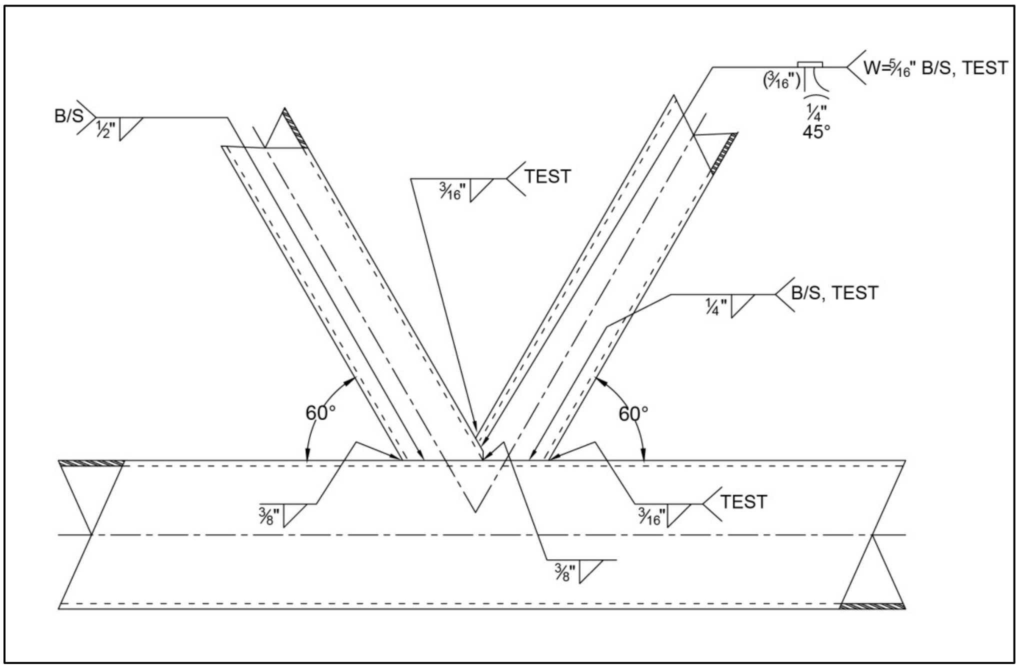

Figure 3-5 Typical connection detail drawing (from K-30-0.50 (a) or (b))

A scale model of the typical connection detail (with $O_v = 60\%$ in contrast to $O_v = 30\%$ as shown in Figure 3-5) is shown in Figure 3-6. The model was designed using SolidWorks and 3D-printed by Cimitrix Solutions Inc. in Oshawa, Ontario in order to emphasize the difference in size between critical and non-critical welds. The model was used to communicate to the welder/ fabricator and proved to be an invaluable asset in demonstrating the objectives of the design.

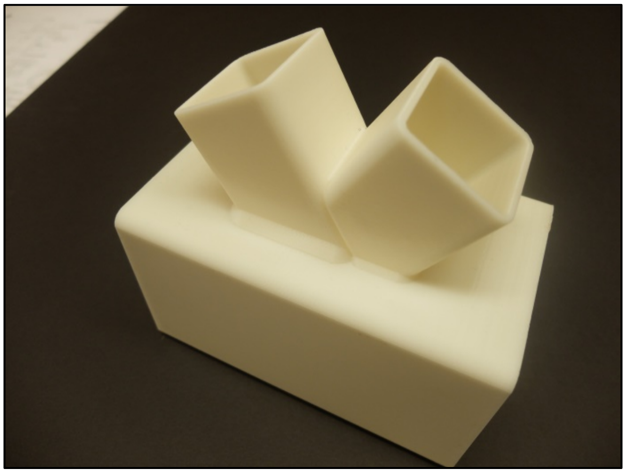

(a) 3D-printed connection

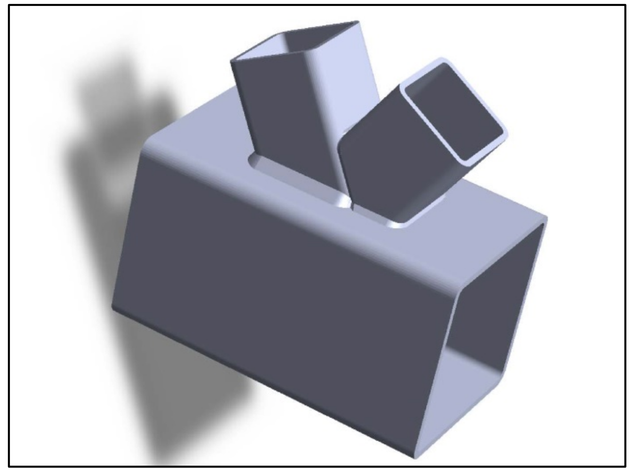

(b) SolidWorks connection model

Figure 3-6 3D-printed connection detail showing critical and non-critical weld elements

3.3.2. Fabrication and Welding Process

All of the fabrication for the truss was performed at Walters Inc. (a professional member of the AISC and fully certified to AWS D1.1) in Hamilton, Ontario and by a CWB-certified welder (see Appendix D.2 for a record of qualification). Trial connections for the critical weld details in Section 3.3.1 were made to calibrate the welding process parameters to achieve the desired weld size, profile, fusion with the base metal and root penetration and to qualify the PJP weld detail in accordance with Clause 4.13 of AWS D1.1 (2010).

For the trial connections, two HSS stub columns were profiled and overlapped at 60°, and tack-welded to a 50 ksi steel plate. A 1/16 in. diameter AWS E71T-1C (Select 720) flux-cored electrode with a nominal tensile strength of 70 ksi and a shielding gas of 100% carbon dioxide supplied at a flow rate of 40 cubic feet per hour (CFH) was used. Welds were made in the flat position with a continuous $^{3}/_{16}$ in. throat around the branch footprint. The weld was cleaned between passes with a pneumatic chipping hammer and wire brush.

Sections were cut normal to the longitudinal axis of each weld element to view the macrostructure of the weld cross-sections. The sections were prepared in accordance with ASTM E340 (2006) using a 10% nital etchant solution, which was applied to the surfaces to examine weld profile, weld/base metal fusion and root penetration. Volumetric discontinuities such as porosity and undercutting, as well as planar discontinuities such as cracks and incomplete fusion were investigated.

It was decided that the PJP flare-bevel-groove weld joint preparation should include a ¼ in. root gap with a backing plate and the overlapping branch member beveled at 45°. This was shown by the MEs to allow consistent penetration into the root and was found to be measurable to a high degree of accuracy in accordance with Table J2.1 (AISC, 2010). The appraisal of the MEs for both the fillet and PJP weld elements is described next.

In Figure 3-7 (a) and (c), the fillet welds have a desirable profile according to ANSI/AWS D1.1 (2010) with a slightly convex face and vertical/horizontal legs of approximately the same size. Fusion with the base metal is thorough and there is good penetration at the root. The weld sizes were measured externally in the shop using fillet weld gages and found to be larger than the minimum sizes specified for fillet welds in Table 5.8 of AWS D1.1 (2010). In Figure 3-7 (b), the PJP flare-bevel-groove weld shows thorough fusion with the base metal and good penetration in both passes along the root. The weld sizes, externally measured using a bridge cam weld gage, were larger than the minimum sizes specified for PJP groove welds in Table 3.4 of AWS D1.1 (2010).

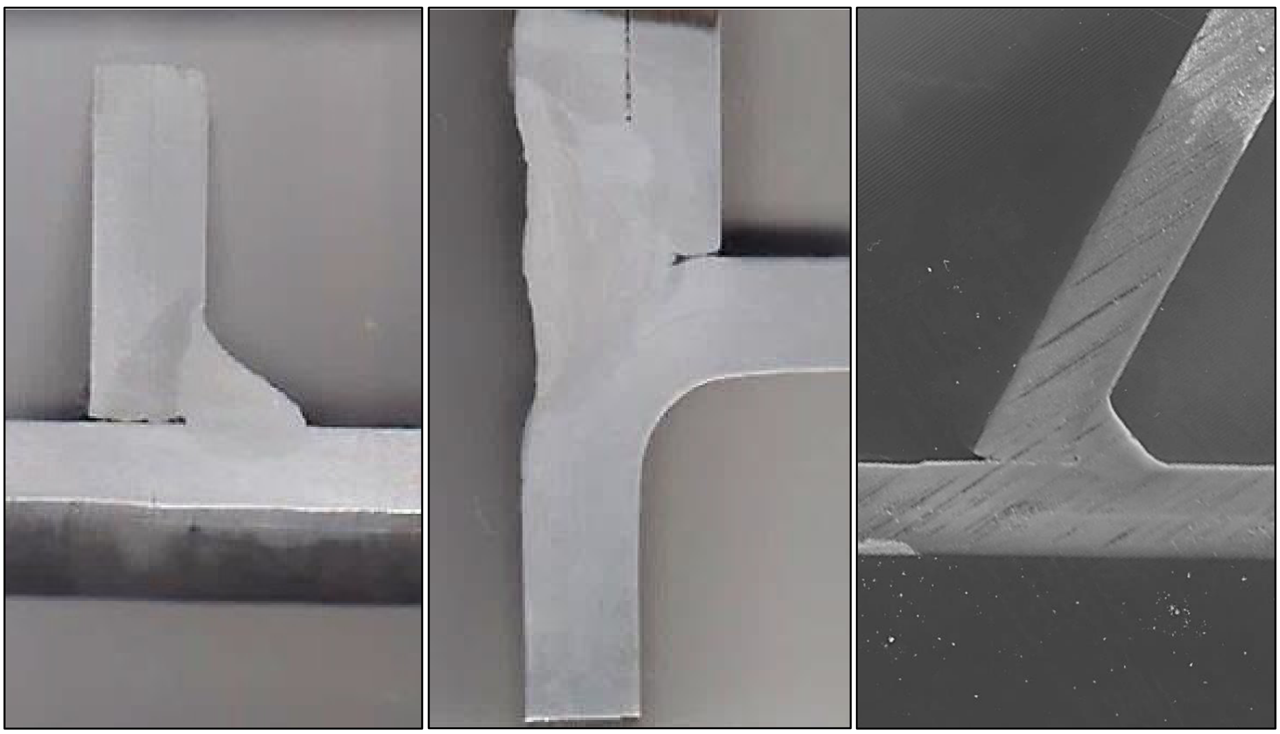

(a) elements a and b (b) elements a' and b' (c) elements c and d

Figure 3-7 Macroetch examinations of welded trial specimens

No visible discontinuities were observed in the any of the macroetch examinations used to qualify the welds and so the welding process parameters used for the trial welds were applied to the full-scale test joints. A welding procedure specification (WPS) is provided in Appendix D.1 and a summary of the final welding process parameters is shown in Table 3-2.

Table 3-2 Average welding process parameters

Weld Element	Specified Weld Leg Size (L_V, L_H)	Voltage	Wire Feed Speed	Average Travel Speed	Number of passes
	in.	V	ipm	ipm	
a	$^1/_4$	28	280	12-14	1
a’	$(^3/_{16})$			10-14	6
b	$^1/_4$			12-14	1
b’	$(^3/_{16})$			10-14	6
c	$^3/_{16}$			12-14	1
d	$^3/_{16}$			12-14	1

Note: The values in parentheses represent the effective throat, t_w.

Photographs from the 4-day long fabrication and welding process are shown in Figure 3-8. A significant amount of effort was put into the preparation and fitting of the web members in order to ensure that the joints were conducive to reproducing the welds exactly as practiced in the trial connections. Welds to test connections were made exclusively in the flat position by rotating the truss throughout the welding process, using the above average welding process parameters and the same electrode coil for all nine joints. The order of welding was as follows:

1. Joint 8 (K-30-0.71)
2. Joint 9 (K-60-0.71 (b))
3. Joint 5 (K-90-0.50 (b))
4. Joint 7 (K-60-0.71 (b))
5. Joint 4 (K-60-0.71 (a))
6. Joint 6 (K-30-0.50 (a))
7. Joint 1 (K-90-0.50 (a))
8. Joint 3 (K-90-0.71)
9. Joint 2 (K-60-0.50)

Non-critical welds were not consistently performed in the flat position, nor were they made using the same electrode coil as for the test joints. This was done so as to not prematurely deplete the electrode coil used for the test welds – of which the mechanical properties were later determined (see Section 3.4.3).

As fabrication was nearly completed, the backing bar on the near side of test joint 2 (K-60-0.50), Member P, backing element a’, was found angled into the HSS with bent tack welds, and thus not flush with the inside face of the HSS as specified by the design. It is believed that this occurred during fitting of Member P (the last web member to be installed) which required some force to position. This complication was not identified until after welding of the far side weld elements had occurred, and thus significant effort causing damage to the test welds was required in order to remove and replace the member. An attempt was made to pry the backing bar upwards with the member still in place, but this attempt was unsuccessful. Ultimately, the resulting gap was filled with weld metal and the welding of the test joint proceeded.

Visual and non-destructive (ultrasonic) testing of all of the PJP flare-bevel-groove welds was performed at the end of the fabrication process, in accordance with CSA W59 (CSA, 2013b) and CAN/CSA S16 (2014). Despite the fault in element a’ of test joint 2 (K-60-0.50), Member P, all of the welds were deemed structurally sound. The non-destructive test report, including measurements of the as-laid weld throats for the PJP flare-bevel-groove weld elements, is provided in Appendix D.3.

(a) Preparation of web members with backing

(b) Fitting of web members

(c) Welding at the “overlapped toe”, in the vertical position (non-critical weld)

(d) Welding in the flat position

(e) close-up view of the fallen-in backing bar at connection K-60-0.50

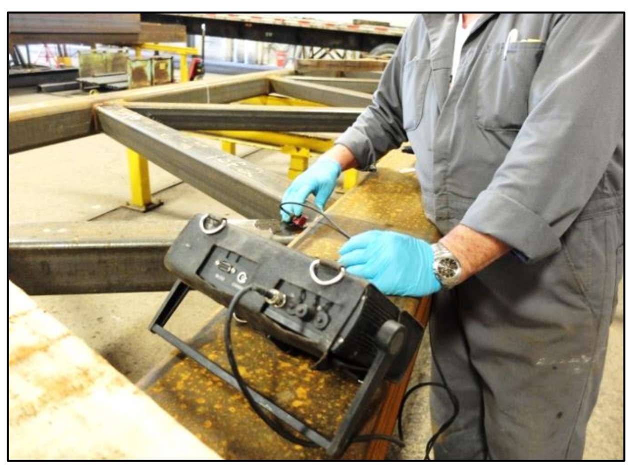

(f) Ultrasonic weld testing of the flare-bevel-groove welds

Figure 3-8 Photographs from the fabrication and welding process

3.4. Material Property Tests

To determine the mechanical properties of the HSS and as-laid weld metal, three tensile coupons (TCs) were created from the HSS stock (specified from the same mill heat) and from the E71T-1C flux-core electrode. The TCs were tested using standard methods to determine the yield stress (F_y, F_{yb}), yield strain (ε_y), ultimate tensile strength (F_u, F_{ub}, F_{EXX}), strain at rupture (ε_{rup}) and Young's Modulus (E). Three Charpy V-notch (CVN) test specimens were also created from the HSS material for the chord members and tested to determine the impact toughness.

3.4.1. HSS Tension Tests

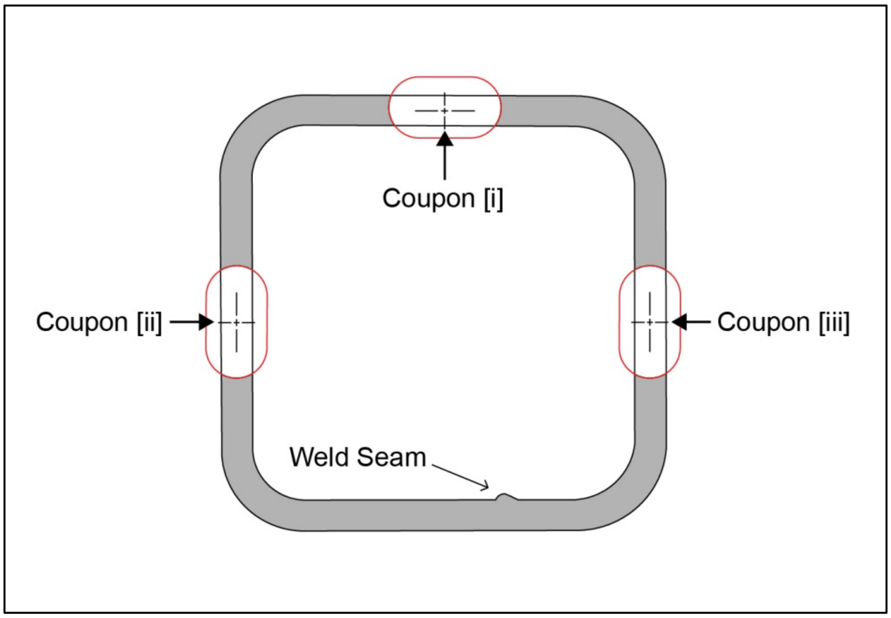

Figure 3-9 HSS Tensile coupon locations

Three rectangular TCs for each size of HSS used in the experimental program were created (9 in total). The coupons were saw-cut from the flat surfaces of the HSS at least 90° from the weld seam and at least twelve inches from the flame-cut ends of the parent tube along the longitudinal axis of the member, as shown in Figure 3-9. One coupon was cut from the face opposite the weld seam, and the other two from the faces adjacent to it.

The TCs were fabricated to the dimensions specified in ASTM A370 (2009) for standard size sheet-type rectangular tension test specimens. The dimensions were measured using a 1-in. Mitutoyo digimatic micrometer and calipers (to the nearest $\pm$000005 in.) prior to testing and recorded in the HSS tension test data forms, located in Appendix E.2. The results are presented in Chapter 4, and were used to modify the mechanical properties of the truss sections in the SAP2000 structural model.

3.4.2. HSS CVN Tests

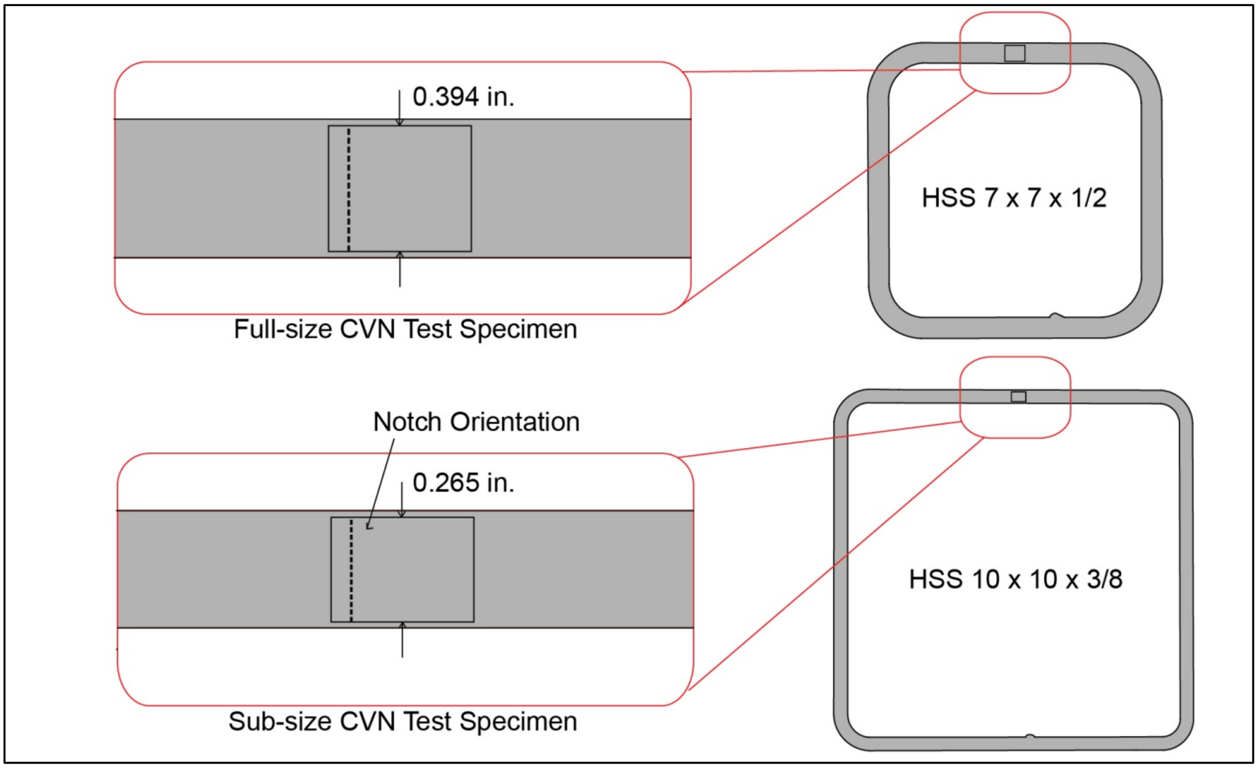

Figure 3-10 Charpy V-notch test specimen orientation and location

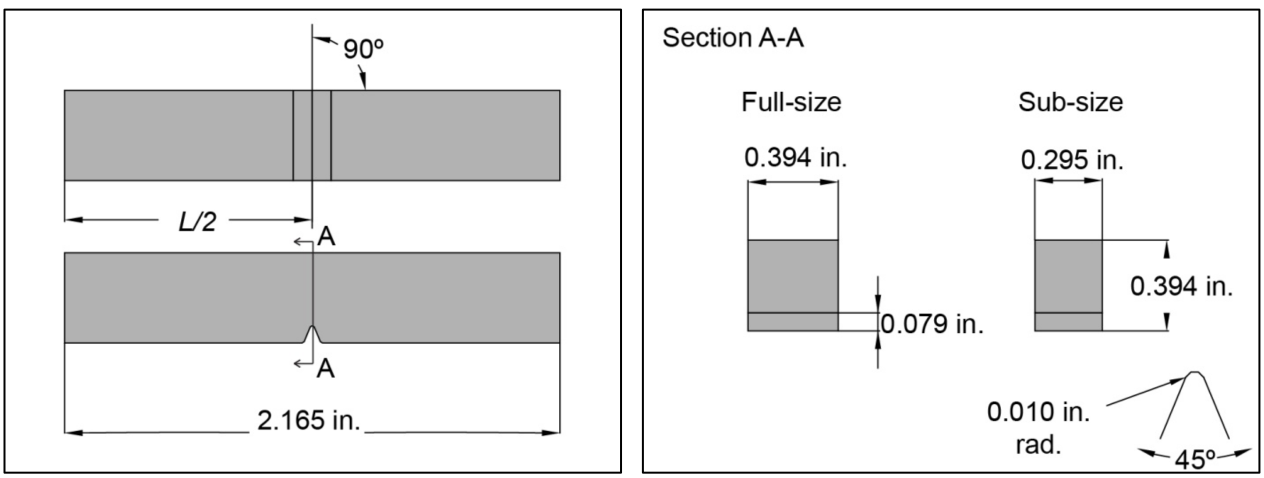

(a) Overall view (b) Detailed section view

Figure 3-11 Machined dimensions of Charpy V-notch test specimens

Three full-size CVN test specimens were carefully saw-cut longitudinally from the flat surface of the HSS 7 x 7 x $^1/_2$ and three sub-size CVN specimens were carefully saw-cut longitudinally from the flat surface of the HSS 10 x 10 x $^3/_8$ 180° away from the weld seam, as shown in Figure 3-10. They were fabricated strictly in accordance with ASTM A370 (2009), to the dimensions specified in Figure 3-11, with the notch oriented vertically through the HSS thickness. Tests were performed at 40°F ± 2°F, in a Tinius Olsen CVN testing machine with very recent calibration, and in immediate succession of one another.

3.4.3. Weld Metal Tension Tests

Three all-weld-metal TCs were created in accordance with Clause 4 of ANSI/AWS D1.1 (2010). Two 1”-thick 50-ksi steel plates were machined at 22.5° to their normal axes and tack-welded, with a ¼” root opening, to a ½” steel plate in order to create a V-groove welding joint. The assembly is shown in Figure 3-12.

(a) Un-welded test plate set-up (b) Welded test plate set-up (C) Weld metal shrinkage

Figure 3-12 All-weld-metal tensile coupon welded test plate set-up

The weld was deposited in the cavity by the same welder and using the same electrode spool, equipment and fabrication processes as the welded joints tested in the experimental program. The following welding process parameters, which are the average values from Table 3-2, were used: arc voltage = 28 V; wire feed speed = 280 ipm; travel speed = 12 ipm; electrode shielding = 100% carbon dioxide; and gas flow rate = 40 CFH.

The TCs were cut from the welded test plate assembly at the University of Toronto and fabricated to the dimensions specified in ASTM A370 (2009) and AWS D1.1 (2010) for standard 0.500-in. round tension test specimens with a 2-in. gage length. The dimensions were measured using the same 1.0-in. Mitutoyo digimatic micrometer and calipers prior to testing and recorded in the weld metal tension test data forms, located in Appendix F.2.

3.5. Geometric Measurement Procedures

The actual geometric properties of the HSS material and as-laid welds were measured such that an accurate analysis of the results from the full-scale tests could be performed. A number of techniques and tools are described herein and shown in Figure 3-13.

(a) 1-in. Mitutoyo digimatic micrometer

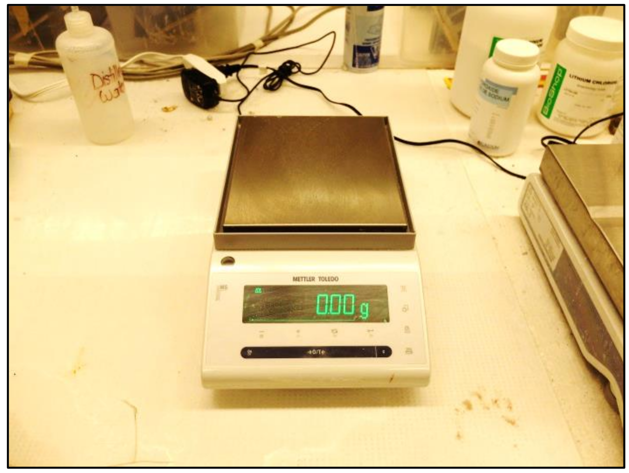

(b) Mettler Toledo digital scale

(c) Skew-T fillet weld gage

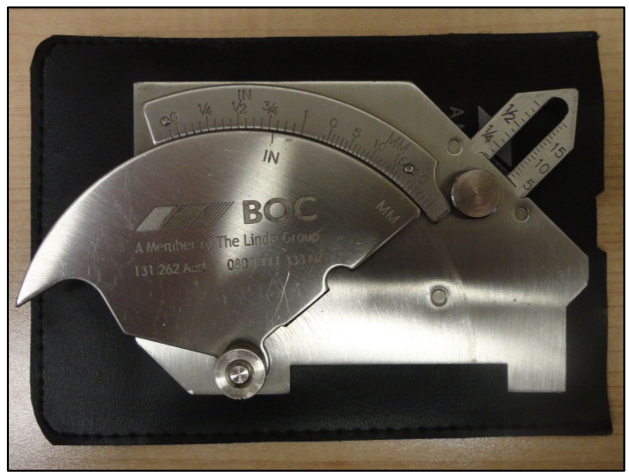

(d) Bridge cam weld gage

Figure 3-13 HSS and as-laid weld geometric measurement tools

3.5.1. HSS Cross-Sectional Dimensions

The cross-sectional dimensions of the HSS were measured in accordance with the recommended methods to check dimensional tolerances on Hollow Structural Sections (HSS) made to ASTM A500 (STI, 1993), a similar manufacturing specification to CAN/CSA G40.20/G40.21(CSA, 2013a) and ASTM A1085 (2013). 1.0-in. thick cross-sections of each rectangular HSS used in the experimental program were saw-cut at least 12-in. away from the flame-cut ends of the parent tube and then machined normal to their longitudinal axis. The wall thickness and section length (or "slice thickness") were measured using the 1.0-in. Mitutoyo digimatic micrometer. The cross sections were scanned and then traced in AutoCAD whereby the corner radii and overall dimensions were determined using built-in measuring tools. The cross-sectional area was determined by weighing the sections on a Mettler Toledo Digital Scale and dividing the measured weight by the product of the density of steel, equal to 0.2836 lb/in3 per the respective material standards, and the slice thickness. The individual HSS geometric measurements were recorded, and are located in Appendix E.5. The average measured dimensions of each section are given in Chapter 4.

Section properties were then computed from the average measured dimensions in a manner consistent with the STI brochure on Dimensions and Section Properties of Hollow Structural Sections (STI, 2010) and the AISC Steel Construction Manual (AISC, 2010) using the formulas located in Appendix E.7. The actual values are presented in Chapter 4, and were used to modify the geometric properties of the truss sections in the SAP2000 structural model.

3.5.2. Weld Element Throats, Legs and Profiles

Fillet weld dimensions were measured using a molding technique, at all locations marked by an 'X' in Figure 3-14, whereby a commercial binary epoxy compound used for "cold welding" was used to cast negative impressions of the weld profile. First, the fillet-weld surface was coated in a release agent. Then the molding material was applied to the measurement locations, as shown in Figure 3-15. After 20 minutes, the material cured in the shape of the weld profile with no perceivable shrinkage. The pieces were knocked free with a rubber hammer and left to harden for 24 hours. Finally, the segments were machined normal to the longitudinal axis of each weld element and scanned in AutoCAD, whereby the legs and throat of the weld were determined using built-in measuring tools.

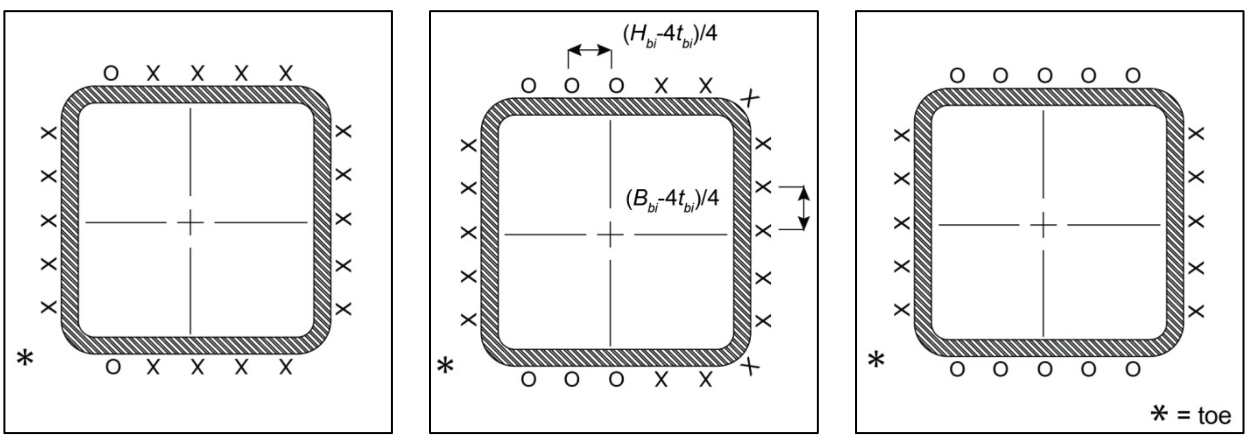

(a) $O_v = 30\%$ (b) $O_v = 60\%$ (c) $O_v = 90\%$

Figure 3-14 Locations and labelling convention for weld size measurements

PJP flare-bevel-groove welds were measured using an external technique at all locations marked by an 'O' in Figure 3-14. A bridge cam weld gage was used to ascertain the greatest perpendicular dimension from the base metal surface to the surface of the PJP flare-bevel-groove weld (or the "crown depth"), d, with which the dimensions of the weld throats could be calculated according to Equation 3-2:

$$t_w = t_{bi} - d \quad \textbf{3-2}$$

where t_{bi} is the thickness of the overlapping branch member. The branch thickness used was the average measured branch thickness recorded with the HSS dimensions, located in Appendix E.5.

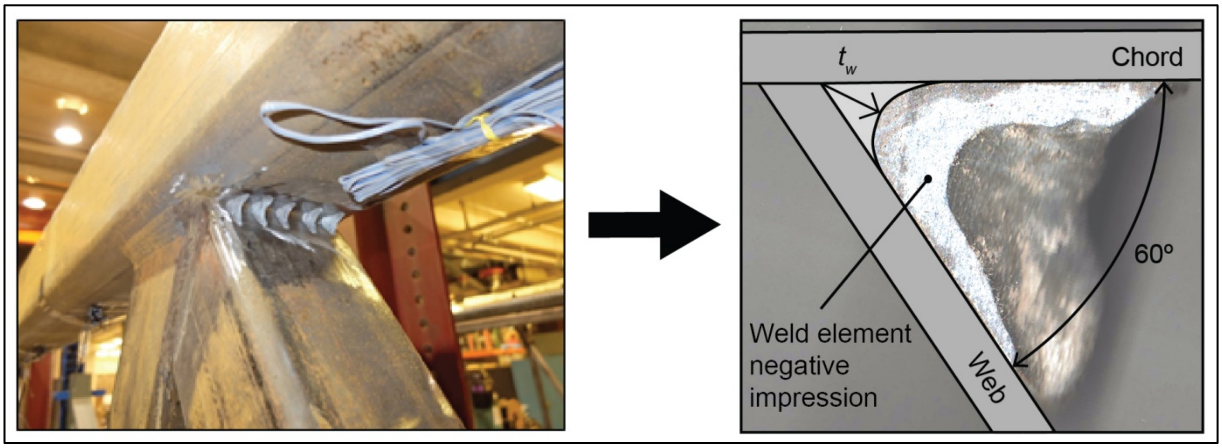

Figure 3-15 Molding technique used to measure fillet-weld dimensions

3.6. Test Setup and Instrumentation

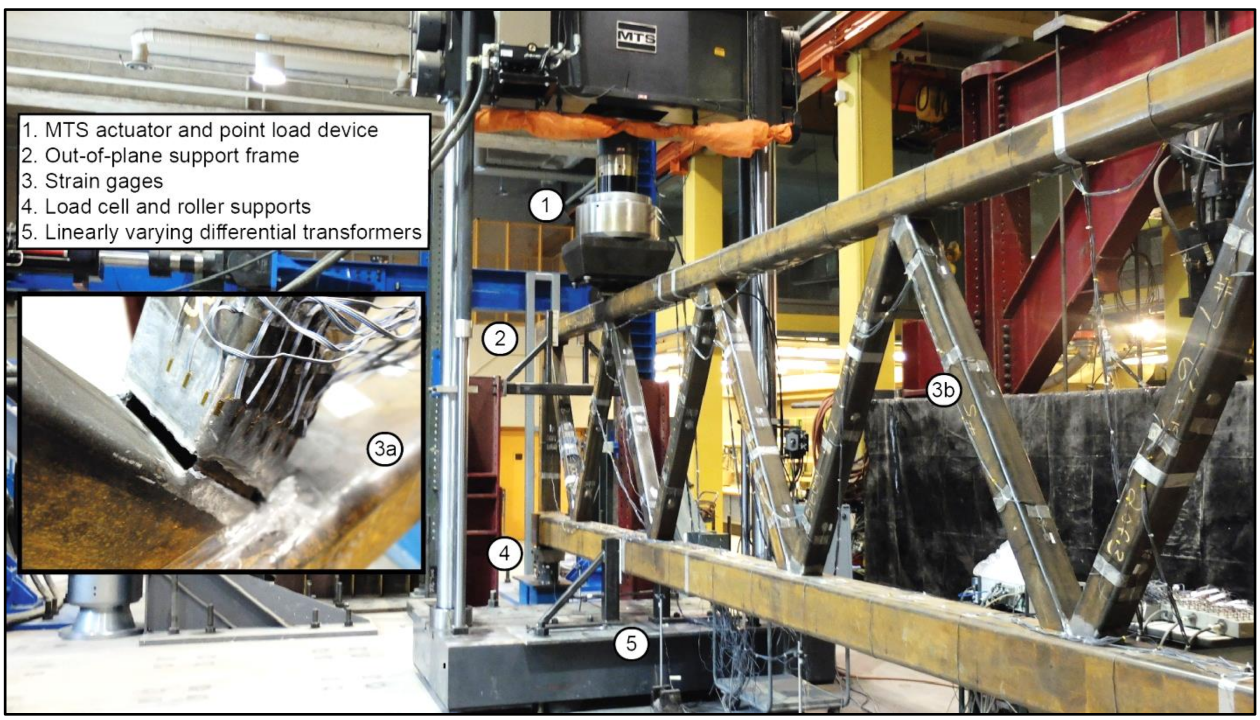

Figure 3-16 Labelled view of the test setup for the full-scale overlap-jointed truss experiments

The test setup employed several of the same components as previous full-scale truss tests that were performed at the University of Toronto for rectangular HSS gapped K-connections (Frater & Packer, 1992a, 1992b) including a 600-kip capacity moveable MTS dynamic loading frame and two 0-675 kip load cells. The remainder of the test setup was designed and then assembled in the University of Toronto Structural Testing Facility using the available materials and resources. An overall view of the test setup for the full-scale experiments is shown in Figure 3-16, with the structural components, equipment and instrumentation labelled. (A full-page photograph of the laboratory at the time of testing appears later in the report on page 88).

3.6.1. Supports and Point Load Device

The single compressive load to panel points was applied using a servo-hydraulically-controlled, 600-kip capacity MTS Universal Testing Frame, operated under stroke- (or displacement) control. A bar-and-socket assembly, which was designed for previous experiments, was used to transfer the load from the actuator to a single point load along the height of the chord, distributed across its width, as shown in Figure 3-17 (a). The line of action of the point load was directed through the intersection of the branch member centerlines transverse to the longitudinal axis of the chord. When load was applied, friction between the top chord and the bar-and-socket assembly provided resistance to horizontal rigid body motion (or “rolling”) in the plane of the truss. The truss reacted at both ends on 225-kip capacity rollers that were oriented transverse to the longitudinal axis of either chord, as shown in Figure 3-17 (b). The entire assembly was lifted 24 in. off the laboratory floor by end-plated HSS pedestals in order to clear the base of the MTS test frame.

Two sets of Meccano-like columns were post-tensioned to the laboratory floor and straddled the compression chord of the truss at various distances from the MTS test frame on either side of the ram head. A bracing system with Teflon pads was fabricated and bolted to the inside of the columns to restrict the movement of the truss to in-plane rotation and translation, as shown in Figure 3-17 (c). A keyed safety system was designed and installed onto the base of the MTS so that in the rare event that the MTS ram head lost contact, clamps fixed to the tension chord and straddled on either side by rigid bumpers would restrain the in-plane longitudinal translation and prevent the truss from rolling off the supports.

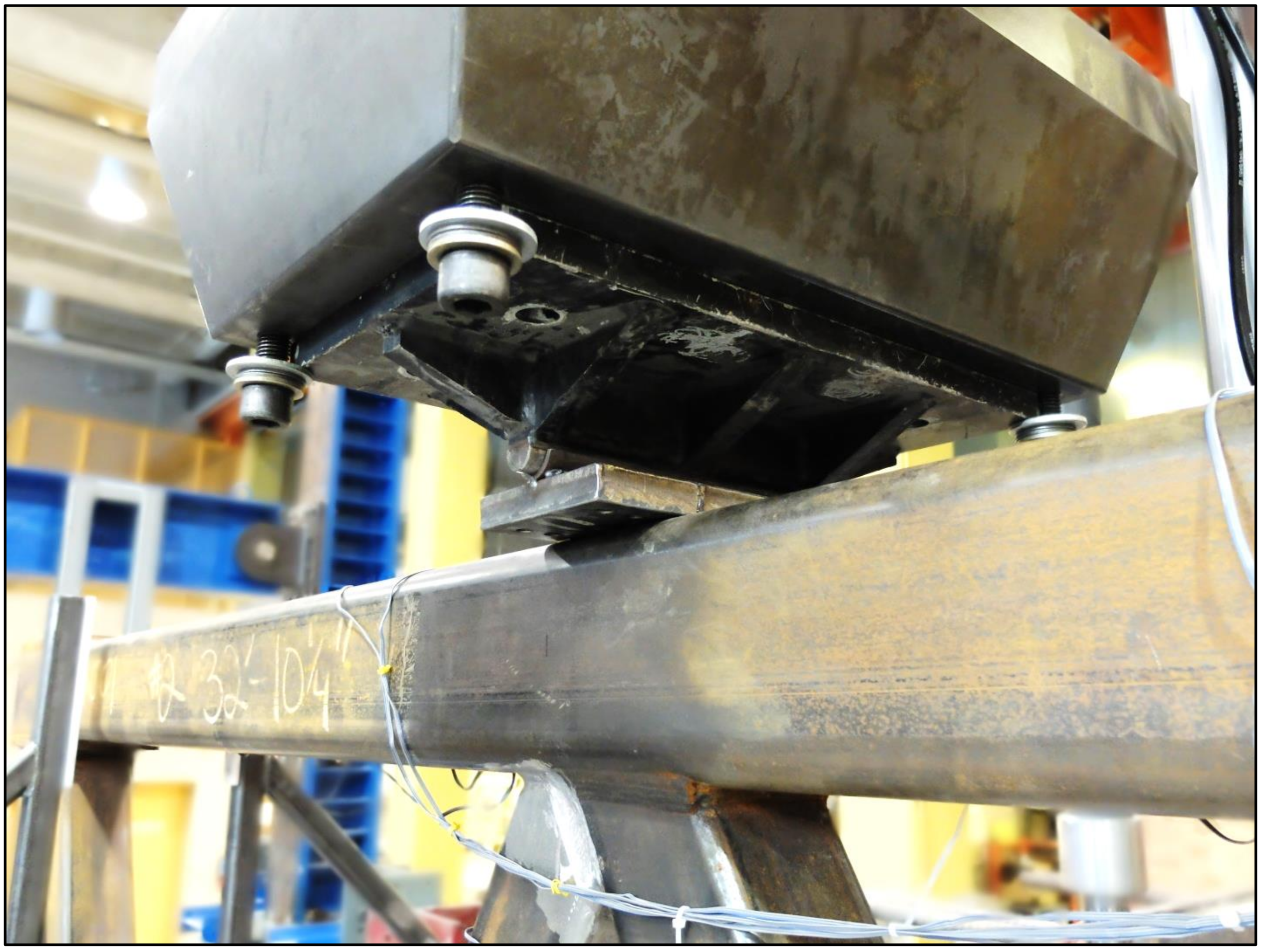

(a) Point load device

(b) Roller end support

(c) Out-of plane compression chord support

Figure 3-17 Load point, reaction and out-of-plane supports

3.6.2. Load Cells

Load cells with a 0 - 675 kip range were calibrated prior to the experimental program by a laboratory technician and placed at the reaction points, underneath the rollers, at either end of the truss to measure the reaction loads. The position of the load cells relative to the reaction points and rollers is shown in Figure 3-17 (b).

Following the experimental program, the load cells were placed one on top of another and loaded in the MTS test frame to check if calibration was maintained after the 11 total loading cycles (nine from weld tests, and two elastic global truss tests). The results indicated that the maximum relative error in any test due to the discrepancy between the load cell measurements and the MTS could be expected to be 1.75%. A comparison of the measurements given by the load cells and the MTS at the end of the experimental program is shown in Figure 3-18 where the load cell denoted “West load cell” was used exclusively under panel points (PPs) 12 and 13, and the load cell denoted “East load cell” was used exclusively under PPs 10 and 11.

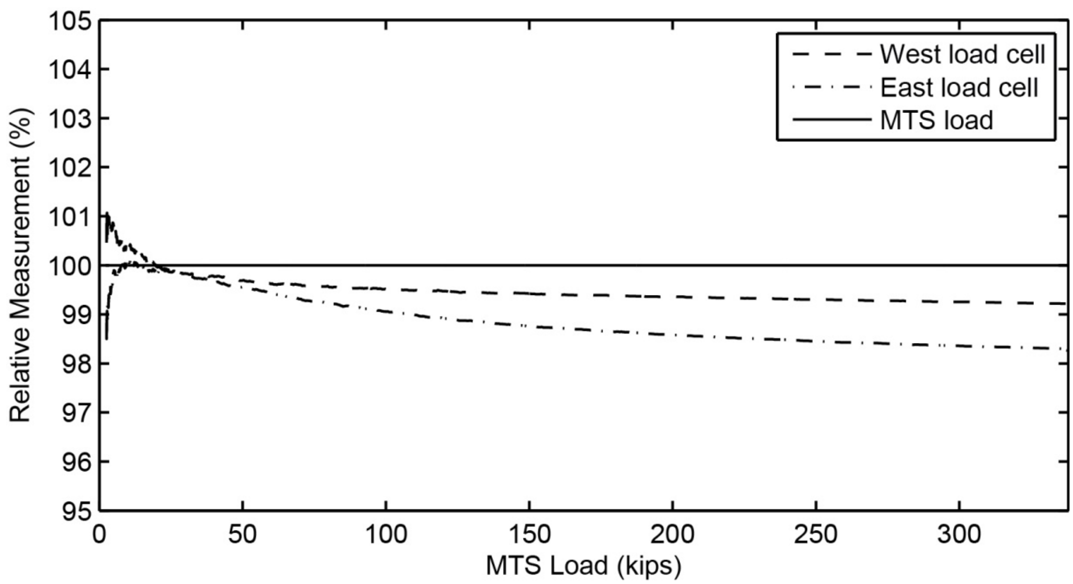

Figure 3-18 Comparison of the measurements given by load cells and the MTS frame at the end of the experimental program

3.6.3. LVDTs

Numerous LVDTs oriented transverse to the longitudinal axis of the chord and in the direction of gravity were installed on the truss to measure panel point deflections and settlements. A total of 7 LVDTs were used in the upright orientation and a total of 6 LVDTs were used in the upside-down orientation. LVDTs were positioned on underside of the bottom (tension) chord at panel points, as shown in Figure 3-19 (a), and on the inside of the chord directly above the rollers, as shown in Figure 3-19 (b), and were calibrated for this purpose by a laboratory technician prior to the tests.

3.6.4. Dial Gages

In order to measure the horizontal component of rigid body motion (or "rolling") and chord elongation, as well as to verify the function of the rollers, dial gages, spanning between the outside edge of the roller support and the outside face of tension chord thickness were installed (see Figure 3-19 (b)). The dial gages were removed at a predetermined load during most of the tests (typically 70-90% of the predicted weld rupture load) to prevent damage to them caused by the violent shaking of the truss that occurred when welds ruptured.

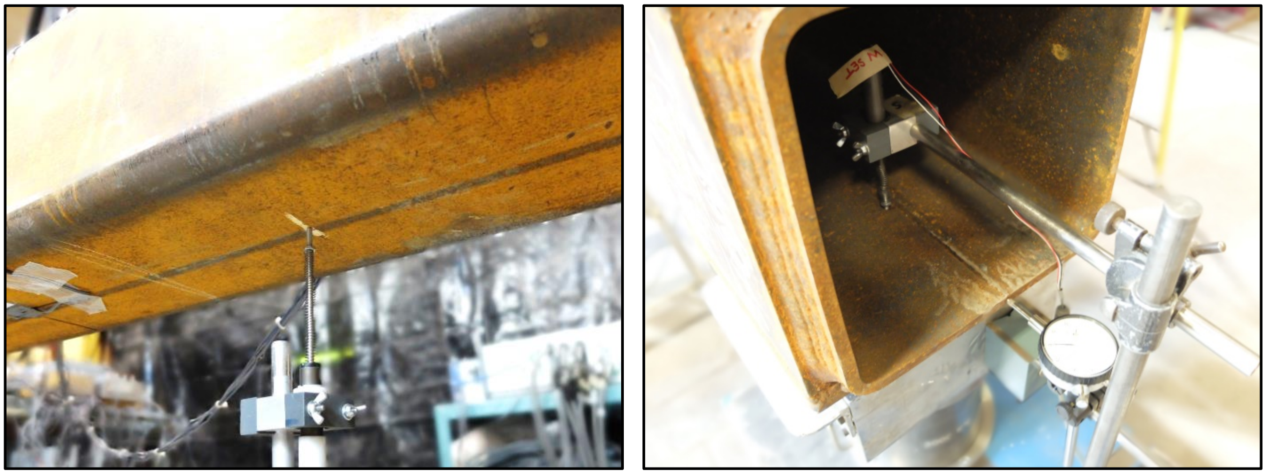

(a) LVDT oriented transverse to the longitudinal axis of the chord and in the direction of gravity

(b) LVDT and dial gage pair at the supports used to measure rigid body motion

Figure 3-19 LVDTs and Dial Gages

3.6.5. Strain Gages

Linear strain gages oriented along the longitudinal axis of the truss members were used to measure axial forces and in-plane bending moments in members as well as to infer the distribution of stress in welds at rupture. The properties of the strain gages that were used (which varied based on availability) are summarized in Table 3-3. It is interesting to note that although not classified as post-yield strain gages, the FLA gages are capable of measuring up to 6000 με and can thus capture the early range of post-yield behavior in steel.

Table 3-3 Strain gage properties and information

	Regular	Post-Yield
Type	FLA-5-11-5LT	YEFLA-5-11-5LT
Adhesive†	CN	CN-Y
Gage Length (in.) Gage Factor (%) Gage Resistance (Ω)	0.20 2.13 ± 0.01 120 ± 0.5	0.20 2.14 ± 0.02 119.5 ± 0.5

†Strain gage performance is sensitive to the type of adhesive used.

A total of 114 global strain gages were installed on opposite faces at various locations along each member in the plane of the truss, as shown in Figure 3-20 (a). Gages on the web members were positioned at mid-length of each member and at a distance of 12.5 in. from the chord face at either end. Gages on the chord members were positioned at mid-length of each chord span (between panel points) and at a distance of 10.5 in. from the heel of the connecting branch. Previous truss testing found that out-of-plane moments were negligible and thus no gages were placed out-of-plane on the near or far side of the truss (Frater, 1991).

To measure the non-uniform distribution of normal strain around the branch footprint, strain gages centered 1 in. from the weld toes and oriented along the longitudinal axis of the branch members were installed. The distance of 1 in. provided from the weld toe is intended to avoid high strain regions caused by the notch effect (Cassidy, 1993).

Theoretically, the distribution of normal strain around the branch footprint is symmetric about the longitudinal centerline of the truss. Hence, strain gages were installed only around half of the branch perimeter (along H_{bi} and half of B_{bi} on two sides). An additional gage was placed at mid-height on the opposite face of the branch member to monitor any significant out-of-plane effects. The spacing of strain gages adjacent to the welded joint around the branch footprint is shown in Figure 3-20 (b), and the (local) strain gage labelling scheme is shown in Figure 3-20 (c).

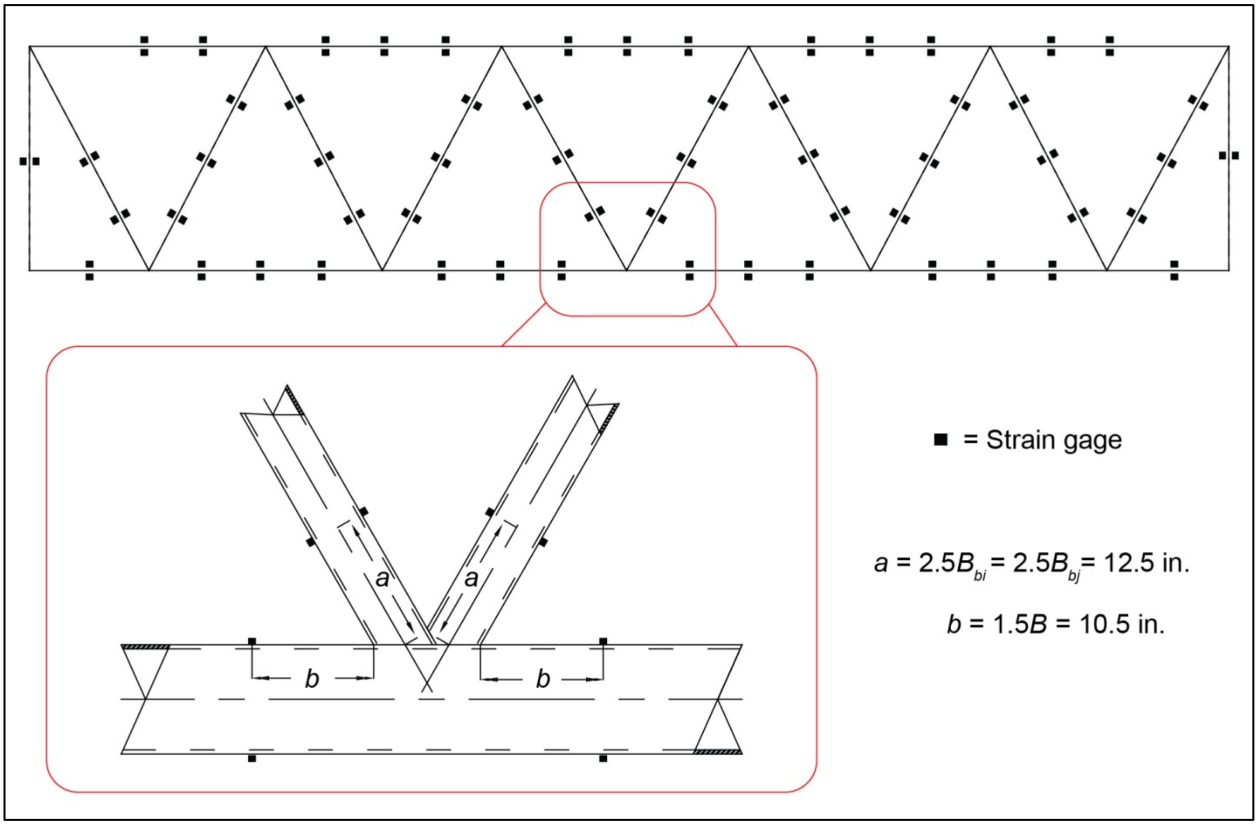

(a) Position of global strain gages (114 total)

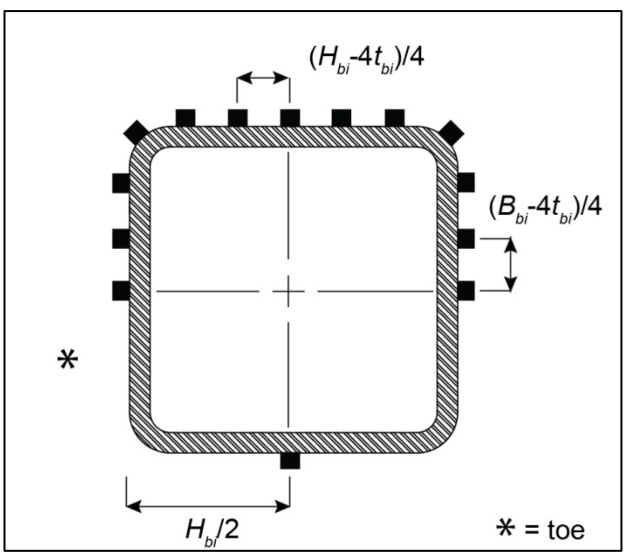

(b) Spacing of strain gages adjacent to the welded joint around the branch footprint

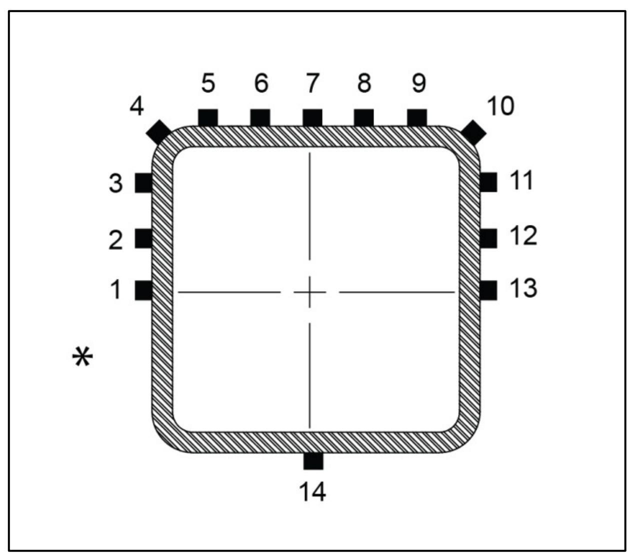

(c) Strain gage labelling scheme adjacent to the welded joint around the branch footprint

Figure 3-20 Strain gage details – global arrangement and around a typical welded joint

3.7. Test Procedure / Loading Strategy

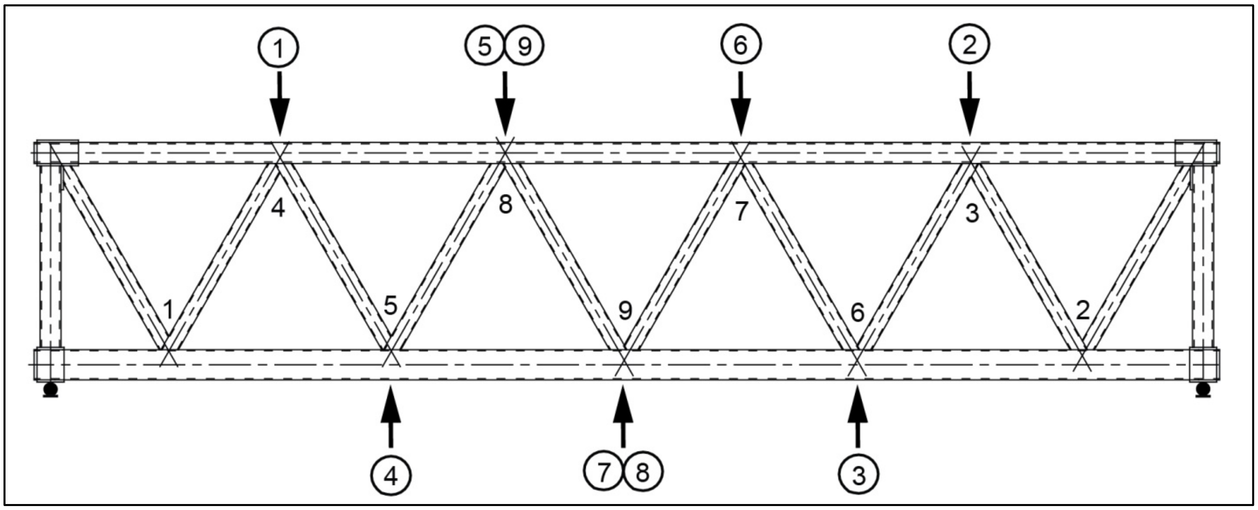

Figure 3-21 Planned sequence of panel point loadings

A single quasi-static point load was applied to a truss panel point using the 600-kip capacity MTS universal testing frame in order to accentuate the force in a predetermined critical branch member, and thereby load the test weld attaching it. Failure of the correct weld was thus achieved by a special distribution of axial forces in the truss that resulted from this loading. After rupture of any weld, the failed joint was repaired by grinding off excess weld meal and re-welding to develop the branch yield strength. In order to perform the subsequent test, the truss was rotated through 180° or inverted (or both) using the 10-ton capacity overhead crane, and repositioned with the MTS cross head centered on a different truss panel point. The supports were moved (by up to 3 panel points), and the procedure was repeated. Before each test, the truss was aligned and levelled by adjusting the lateral supports and shimming the HSS support pedestals. The LVDTs and dial gages were installed and the LVDTs and strain gages were connected to the data acquisition system. All of the data acquisition channels were verified functioning, and once test(s) began data was recorded at a rate of 2 Hz. Test progress was monitored by various real-time plots of the applied MTS load and displacement (or “stroke”), the branch member loads, and longitudinal strain adjacent to weld. All other data was available numerically, in real-time, and was used when necessary to troubleshoot issues with the performance of the test set-up assembly.

A total of nine tests on weld-critical rectangular HSS overlapped K-connections were performed in this manner. The panel point loading sequence, and the order of joint testing, is shown in Figure 3-21. A further two tests, designated as “elastic global truss tests”, were performed whereby a nominal 110-kip point load was applied to PP 4 of the truss. These tests were conducted at the beginning and end of the tests on welded connections and utilized complete, 114-channel, strain gage hook-ups and LVDTs at PPs along the tension chord to investigate axial/bending force distributions and deflection patterns at the serviceability load level.

Chapter 4: Experimental Results

This chapter contains the measured mechanical and geometric properties of the HSS and as-laid welds. These properties were used to calculate the predicted LRFD and nominal branch, connection and weld strengths according to ANSI/AISC 360 (2010) in order to confirm the strength hierarchy discussed in Section 3.2.1 and to make modifications to the test procedure where necessary. The results and observations from nine full-scale tests on rectangular HSS overlapped K-connections, that failed by weld rupture along a plane through the weld, are presented. For each test, the actual weld strength, MTS Load vs. branch load relationship and normal strain distribution around the branch perimeter adjacent to the weld are given. Finally, the measured axial forces, in-plane bending moments, and truss deflection profiles from the global elastic tests are presented.

4.1. HSS Mechanical and Geometric Properties

The yield stress (F_y, F_{yb}), yield strain (ε_y), ultimate tensile strength (F_u, F_{ub}), rupture strain (ε_{rup}) and Young's Modulus (E) determined from TC tests and the CVN values determined from impact tests are reported herein. The results are compared with the minimum specified requirements for cold-formed HSS made to the specification and grade indicated on the mill certificates (CAN/CSA G40.20/G40.21 (CSA, 2013a) for the HSS 5 x 5 x $^5/_{16}$ and HSS 10 x 10 x $^3/_8$, and ASTM A1085 (ASTM, 2013) for the HSS 7 x 7 x $^1/_2$) and with the reported values in the mill certificates provided by the HSS manufacturer. Measured cross-sectional dimensions for each HSS are compared with the dimensional tolerances of the relevant specification above.

4.1.1. HSS Mechanical Properties

The results from nine individual TC tests are summarized here. The TCs for each HSS used in the experimental program were tested in accordance with the standard methods for tension testing of metallic materials (ASTM, 2008). A 225-kip capacity MTS test frame was used to load the TCs to failure (see Figure 4-1 (a)). The TCs were loaded at an initial stroke-rate of 0.0002 in/s. Once the rounded yield region was surpassed, the stroke-rate was increased to 0.0003 in/s. The stroke-rate was increased to 0.0006 in/s. after reaching the ultimate tensile strength until failure. The axial strain was measured by an MTS extensometer (Model #: 632.12C-20) which spanned the initial 2-in. gage length and was attached to the coupon at the beginning of the test. To prevent damage to it, the extensometer was removed prior to rupture.

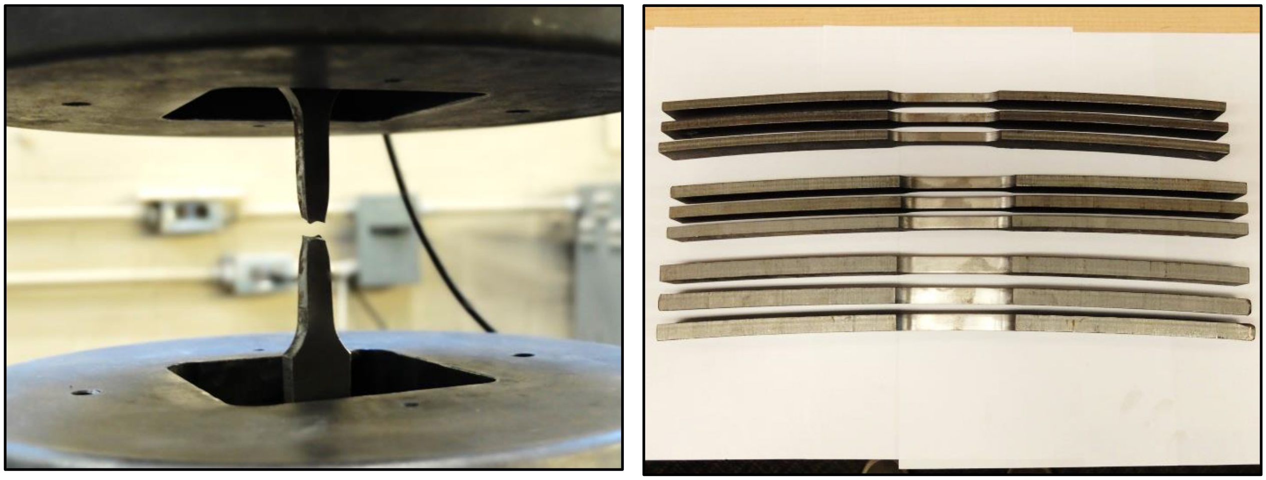

(a) Loading and subsequent failure of TCs in the 225-kip MTS test frame

(b) Curvature of TCs due to residual stresses

Figure 4-1 Rectangular HSS tensile coupon specimens

The yield strength (F_y) and yield strain (ε_y) of the material were located in a rounded yield region and determined using the 0.2% offset method (ASTM, 2008). Stress-strain diagrams for the individual TC specimens are located in Appendix E.3. Typical HSS stress-strain plots are shown in Figure 4-2.

All of the TCs exhibited initial linear elastic behavior up to a proportional limit which occurred well below the yield point. This indicates a large amount of residual stress in the material, which is to be expected for continuously cold-formed HSS along the flat walls. Another indication of high residual stresses is the curvature in the TC specimens immediately after they were extracted from the parent tube which is shown in Figure 4-1 (b). It can also be seen here that sections with smaller wall thicknesses had larger curvatures.

Beyond yield, the TCs underwent minor strain-hardening up to their ultimate strength, at which time necking occurred and the strength gradually decreased until fracture (this stage is cut short in Figure 4-2. since it occurred after the extensometer was removed). The rupture strain (ε_{rup}) was determined after the test was completed by joining the fractured pieces together and recoding the change in gage length divided by the initial gage length. The TCs were ductile and the minimum specified elongation requirement (21% elongation), though not restrictive once the tube has left the manufacturer, was always met. The results are summarized in Table 4-1

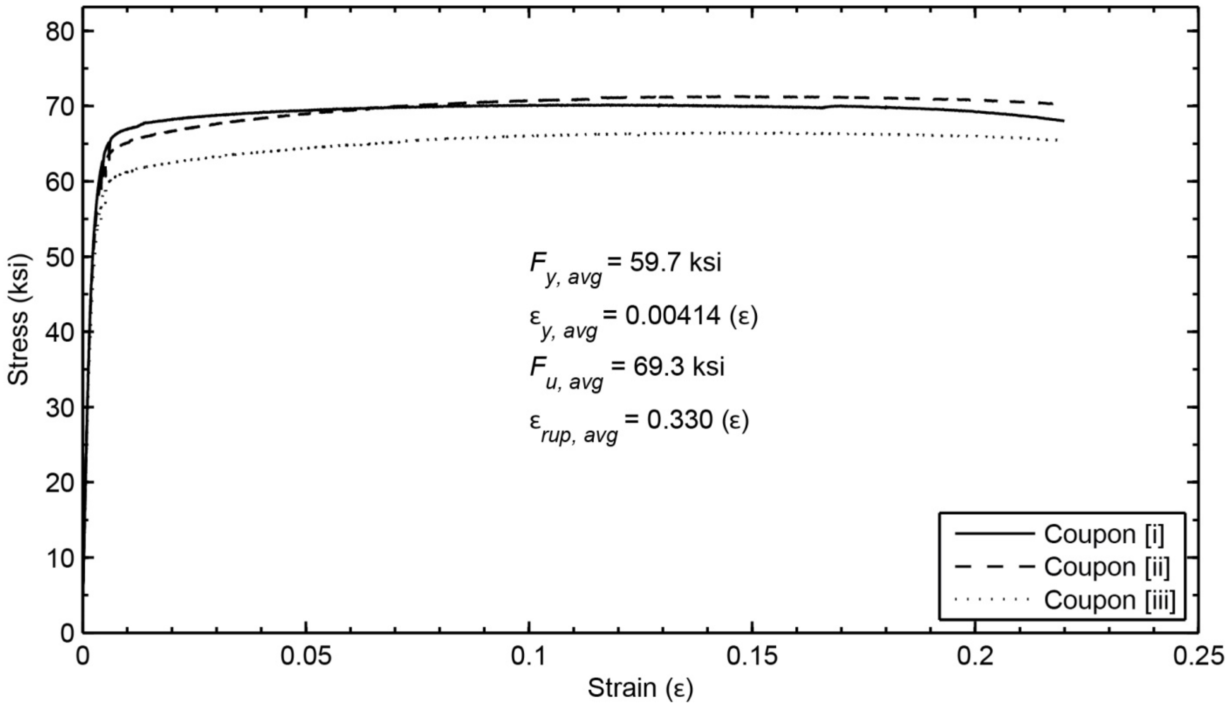

Figure 4-2 Typical stress-strain plot from (HSS 5 x 5 x $^{5}/_{16}$) tensile coupon test

Table 4-1 HSS tensile coupon test results

HSS Specification and Designation	F_y (ksi)	ε_y ($\times 10^3 \mu\varepsilon$)	F_u (ksi)	$Eln.$ (%)	E ($\times 10^3$ ksi)	F_y/F_u
CSA G40 (50W) HSS 5 x 5 x $^{5}/_{16}$	59.7	4.14	69.3	33.0	28.0	0.861
ASTM A1085 HSS 7 x 7 x $^{1}/_{2}$	55.1	3.97	70.9	33.2	28.0	0.777
CSA G40 (50W) HSS 10 x 10 x $^{3}/_{8}$	56.1	4.02	72.2	34.5	27.8	0.777

For the CVN (impact toughness) tests, the full-size specimens for the HSS 7 x 7 x $^{1}/_{2}$ and the sub-size specimens for the HSS 10 x 10 x $^{3}/_{8}$ (shown in Figure 4-3 (a)) were thermally conditioned in a dry ice-methanol liquid coolant mixture for a sufficiently long time in order to reach 40°F before being tested. A thermocouple was used to monitor the temperature of the mixture. The six tests were performed in immediate succession of one another using a Tinius Olsen Charpy pendulum testing machine, shown in Figure 4-3 (b), which was calibrated with National Institute of Standards and Technology (NIST) test blocks prior to the experiment. The results are summarized in Table 4-2 and more detailed results are located in Appendix E.4. It should be noted that the results have no influence on the current research project, as it deals with connection static behavior, and have been included strictly for a comparison to the standard specifications and the mill test certificates.

(a) Sub-size (left) and full-size (right) CVN test specimens

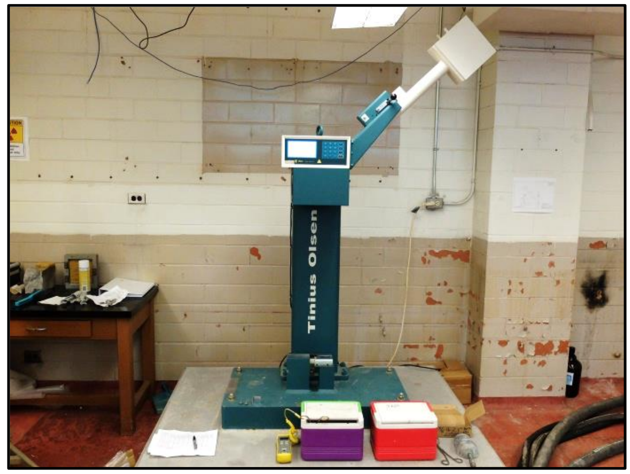

(b) Tinius Olsen CVN Testing Apparatus

Figure 4-3 Charpy V-notch test specimens and testing apparatus

Table 4-2 Charpy V-Notch test results

HSS Specification and Designation	Test 1		Test 2		Test 3		Average Energy (ft-lb)
	T (°F)	Energy (ft-lb)	T (°F)	Energy (ft-lb)	T (°F)	Energy (ft-lb)	
ASTM A1085 HSS 7 x 7 x $^{1}/_{2}$	38.5	10.54	38.7	10.77	38.8	16.96	12.76
CSA G40 (50W) HSS 10 x 10 x $^{3}/_{8}$	38.0	98.97	38.0	46.0	38.3	101.7	82.21

Note: Results from the HSS 10 x 10 x $^{3}/_{8}$ CVN tests have been converted to the equivalent absorbed energy for a full-size test block.

A comparison between the specified minimum required mechanical properties given by the specifications and the actual mechanical properties determined in accordance with ASTM E8/E8-M (2008) and ASTM E340 (2006) is made in Table 4-3. The actual mechanical properties exceeded the specified minimum mechanical properties for all sizes of HSS with the exception of the CVN value for the HSS 7 x 7 x $^{1}/_{2}$ which was 49% below.

Table 4-3 Comparison between the specified minimum requirements and the actual mechanical properties of the rectangular HSS

HSS Specification and Designation	Specified Minimum				Experimental			
	F_y (ksi)	F_u (ksi)	ε_{rup} ($\times 10^5 \mu\varepsilon$)	CVN (ft-lb.)	F_y (%)	F_u (%)	ε_{rup} (%)	CVN (%)
CSA G40 (50W) HSS 5 x 5 x $^5/_{16}$	50	65	2.10	-	+19.4	+6.61	+57.1	-
ASTM A1085 HSS 7 x 7 x $^1/_2$	50	65	2.10	25	+10.2	+9.08	+59.1	**-49.0**
CSA G40 (50W) HSS 10 x 10 x $^3/_8$	50	65	2.10	-	+12.2	+11.1	+64.3	-

Note 1: Values that are in bold typeface are not in compliance with the minimum specified requirements.
Note 2: CVN experimental value is by using a through-thickness notch; the HSS manufacturer is permitted to use a surface notch with full-sized CVN coupons.

Another comparison, between the mechanical properties reported in the mill certificates provided by the product manufacturer and the actual mechanical properties determined from testing, is shown in Table 4-4. The mill certificate for the HSS 5 x 5 x $^5/_{16}$ was not available and hence has no basis for comparison. The actual mechanical properties show reasonable agreement with the mechanical properties reported in the mill certificates for both sizes of HSS, except for the HSS 7 x 7 x $^1/_2$ CVN values which were far below the manufacturer-reported values. The original mill certificates are located in Appendix E.1. The considerable difference in CVN values between the manufacturer and the university testing laboratory may be attributable to Note 2 below Table 4-3.

Table 4-4 Comparison between the mill certificates provided by the manufacturer and the actual mechanical properties of the rectangular HSS

HSS Specification and Designation	Mill Certificates				Experimental			
	F_y (ksi)	F_u (ksi)	ε_{rup} ($\times 10^5 \mu\varepsilon$)	CVN (ft-lbs.)	F_y (%)	F_u (%)	ε_{rup} (%)	CVN (%)
CSA G40 (50W) HSS 5 x 5 x $^5/_{16}$	-	-	-	-	-	-	-	-
ASTM A1085 HSS 7 x 7 x $^1/_2$	59.3	67.8	2.84	69.3	**-7.08**	+4.57	+16.9	**-81.5**
CSA G40 (50W) HSS 10 x 10 x $^3/_8$	60.2	75.0	3.53	-	**-6.81**	**-3.73**	+13.8	-

Note: Values that are in bold typeface are less than the properties declared by the manufacturer on the mill certificate.

4.1.2. HSS Geometric Properties

The cross-sectional dimensions of each HSS used in the experimental program were measured and the average values are reported in Table 4-5. The measured geometric properties were checked against the dimensional tolerances of the manufacturing standard (ASTM, 2013; CAN/CSA, 2010) and a comparative analysis is presented in Table 4-6.

Table 4-5 Average measured cross-sectional dimensions of the rectangular HSS

HSS Specification and Designation	Height and Width (H and B)	Wall thickness (t)	Cross-sectional area (A)	Outer radius	Inner radius
	in.	in.	in.^{2}	in.	in.
CSA G40 (50W) HSS 5 x 5 x $^5/_{16}$	5.00	0.306	5.62	0.625	0.354
ASTM A1085 HSS 7 x 7 x $^1/_2$	7.03	0.494	12.05	1.377	0.922
CSA G40 (50W) HSS 10 x 10 x $^3/_8$	10.02	0.364	13.65	3.87	0.577

The values compared in Table 4-6 are the minimum (or maximum) of the measured values from Appendix E.5. According to ASTM A1085 (2013) and CAN/CSA G40.20/G40.21 (2010), the permissible variation in the outside flat dimensions is $\pm$0.030 in. for the HSS 5 x 5 x $^5/_{16}$ and 1.00% of the larger flat dimension for both the HSS 7 x 7 x $^1/_2$ and the HSS 10 x 10 x $^3/_8$. For all the HSS, the wall thickness is required to be not less than 5.00% and not more than 10.00% of the specified thickness and this is governed by a more restrictive mass tolerance of $\pm$3.00%. The outlines of the scanned cross-sections, which show the locations and values of the individual measurements, are located in Appendix E.5.

Table 4-6 Comparison between the specified minimum requirements and the actual geometric properties of the rectangular HSS

HSS Specification and Designation	Outside dimension tolerance (H and B)	Minimum wall thickness (t)	Mass	Outside corner radius	
				Max.	Min.
	in.	in.	lb/ft.	in.	in.
CSA G40 (50W) HSS 5 x 5 x $^5/_{16}$	+0.023	0.3045 (-2.56%)	+0.525%	0.650 (2.12 t)	0.593 (1.94 t)
ASTM A1085 HSS 7 x 7 x $^1/_2$	+0.050	0.4917 (-1.67%)	-2.12%	**1.440 (3.92 t)**	1.308 (2.65 t)
CSA G40 (50W) HSS 10 x 10 x $^3/_8$	+0.061	0.3608 (-3.79%)	-2.89%	1.037 (2.81 t)	0.885 (2.43 t)

Note: Values that are in bold typeface are not in compliance with the minimum specified requirements.

The violation of the maximum outside corner radius for the HSS 7 x 7 x ½ is non-critical. When comparing the average outside corner radius of this HSS, equal to 1.377 in. or 2.79t, instead of the maximum and minimum measurements, the dimensional tolerances for the outside corner radii in Table 5 of ASTM A1085 (2013) are met. The HSS geometric properties were calculated from the average measured section properties in accordance with the methods of the STI brochure on Dimensions and Section Properties of HSS (2010) and used in the following truss analysis. The calculated values are summarized in Table 4-7.

Table 4-7 HSS Section Properties calculated per the methods of STI brochure on Dimensions and Section Properties of Hollow Structural Sections (STI, 2010)

HSS Specification and Designation	Wt. per Foot	$b/t^{\dagger}$ and $h/t^{\dagger}$	I	S	r	Z	J	C	Surface Area per Foot
	lb/ft.		in.^{4}	in.^{3}	in.				ft.^{2}/ft.
CSA G40 (50W) HSS 5 x 5 x $^5/_{16}$	19.13	12.3	19.8	7.93	1.878	9.58	32.5	13.4	1.578
ASTM A1085 HSS 7 x 7 x $^1/_2$	41.0	8.7	81.5	23.2	2.60	28.6	141.6	41.1	2.15
CSA G40 (50W) HSS 10 x 10 x $^3/_8$	46.4	22.2	206	41.1	3.88	48.3	335	67.4	3.20

Note: All properties based on the average measured HSS dimensions.
† b/t and h/t determined using actual flat lengths, equal to the average overall dimension minus two times the average outside corner radius of the section.

4.2. Weld Mechanical and Geometric Properties

4.2.1. Weld Mechanical Properties

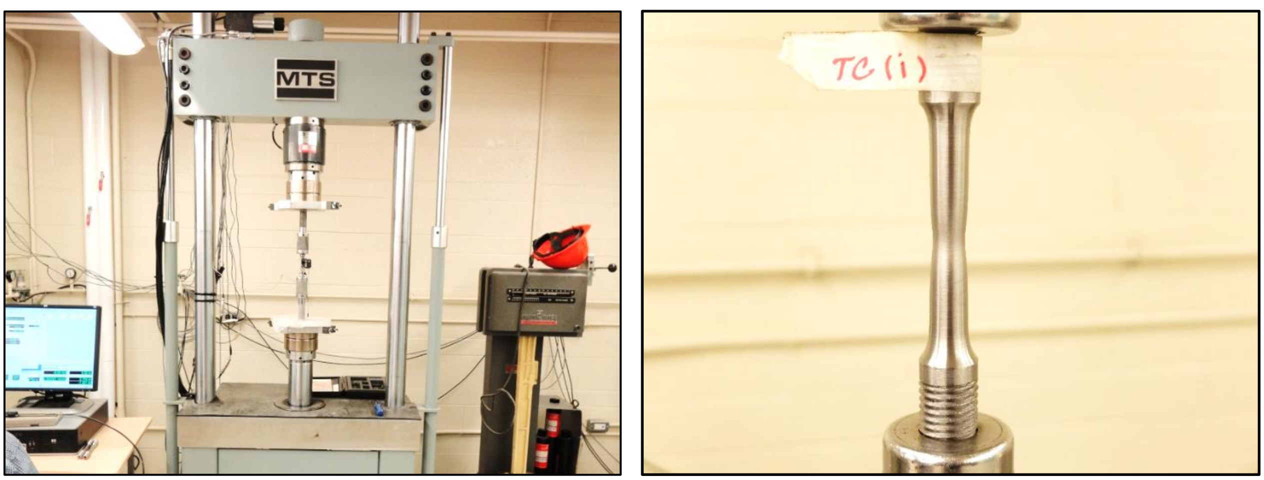

(a) 55-kip MTS test frame

(b) Necking of TC [i]

Figure 4-4 All-weld-metal tensile coupon specimens and apparatus

Three TCs were tested in accordance with the standard methods for tension testing of metallic materials (ASTM, 2008). A 55-kip capacity MTS test frame (shown in Figure 4-4 (a)) was used to load the TCs to failure. The TCs were loaded at an initial stroke-rate of 0.0002 in/s. Once the yield region was surpassed, the stroke-rate was increased to 0.0003 in/s until failure. To prevent damage to it, the extensometer was removed prior to rupture.

The yield strength (F_y) and corresponding yield strain (ε_y) of the material was determined using the 0.2% offset method with an elastic modulus (E) taken as the average slope over the un-yielded linear region of the stress-strain diagram (ASTM, 2008). Stress-strain diagrams for the individual TC specimens are located in Appendix E.3. Figure 4-5 shows the average stress-strain plot.

Every all-weld-metal TC exhibited linear-elastic behavior until the upper yield point which was followed by an immediate drop in stress and a subsequent yield plateau. Beyond the yield plateau, the TCs underwent minor strain-hardening up to their ultimate tensile strength (F_{EXX}), at which time necking occurred, as shown in Figure 4-4 (b), and the strength gradually decreased until rupture. (The latter stage of necking occurred after the extensometer was removed and is therefore cut short in Figure 4-5). The rupture strain (ε_{rup}) was determined after the test was completed by joining the fractured pieces together and recording the change in gage length divided by the initial gage length.

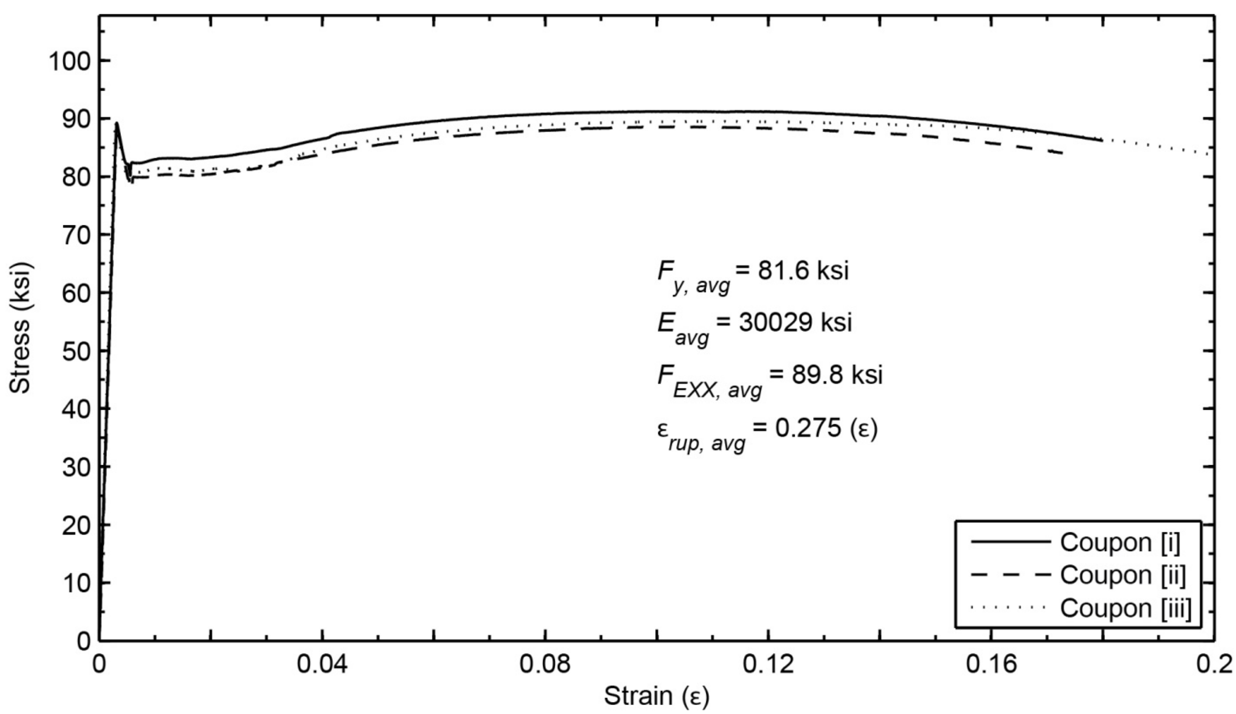

Figure 4-5 Stress-strain plot from the all-weld-metal tensile coupon tests

The measured mechanical properties exceeded the minimum requirements for AWS E71T-1C flux-core electrodes which were used in this project. The tensile strength of the as-laid weld metal was 28% stronger than the specified tensile strength. Similar results were observed by McFadden & Packer (2013) for ER70S-6 solid wire electrodes which, in their case, were 26% stronger than the specified tensile strength. The results are summarized in Table 4-8.

Table 4-8 All-weld-metal tensile coupon test results

Coupon Designation	F_y (ksi)	E ($\times 10^3$ ksi)	F_{EXX} (ksi)	ε_{rup} (%)
[i]	81.0	29.3	91.2	27.0
[ii]	81.4	29.0	88.7	26.4
[iii]	82.3	31.8	89.5	29.2
Average	**81.6**	**30.0**	**89.8**	**27.5**

4.2.1.1. Size Reduction

An upper-bound to the weld effective throat, to ensure weld-critical behavior, was re-determined accounting for the actual measured tensile strength of the as-laid weld metal. Using the same upper-bound prediction method as in Section 3.2.2.2.4, but omitting 1.33 times the nominal weld strength and including the actual measured weld strength, a $^1/_8$ in. effective throat was found to be necessary at all locations around the branch perimeter to develop the capacity of the weld and protect the non-critical elements. The welds thus underwent weld size reductions (by grinding) of slightly more than $^1/_{16}$ in., since their actual cross-sectional dimensions were provided by the fabricator even larger than specified. Measurements, made using the fillet weld gages, bridge cam weld gage, and a skew-T fillet weld gage, were made at interim stages during grinding of the welds to approximate the sizes.

(a) Weld sizes provided by the fabricator

(b) Weld sizes after reduction

Figure 4-6 Comparison of connection K-30-0.71 before and after weld size reduction

Although the final effective weld throats were below the minimum value specified in Table 3.4 of AWS D1.1 (2010) for a PJP groove weld, no adverse effects are expected to have occurred as a result of the weld size reduction (recall that the rationale for the minimum sizes is based on the quench effect). The resulting weld faces were nearly perfect 45° triangles along elements a and b, and concave along elements a’, b’, c and d. A comparison of one welded joint before and after reducing the weld size is shown in Figure 4-6.

4.2.2. Weld Element Geometric Properties

The theoretical weld throats of the critical test connections were measured externally prior to testing to:

a) ensure that the connections would be weld-critical; and
b) collect accurate weld measurements for the evaluation/ analysis of the full-scale tests.

A total of 180 cross-sections of the size-reduced welds were measured, which consisted of 20 measurements for each of the nine weld-critical overlapped K-connections within the truss. The average values for the external measurements of the individual weld elements tested, at the time of testing, are summarized in Table 4-9. Included amongst the results are the average measured values for the weld elements in two previous tests on weld-critical overlapped K-connections (Frater, 1992) which are analysed in conjunction with the nine current tests in Chapter 5.

Table 4-9 Average weld theoretical throat sizes and predicted joint failure loads

Experimental Designation	Theoretical Throat of Weld Element (in.)						Predicted Failure Load (kips)
	a	a’	b	b’	c	d	
K-90-0.50 (a)	0.136	0.125	0.123	0.141	0.148	0.168	217
K-60-0.50	0.105	0.150	0.094	0.140	0.152	0.166	201
K-90-0.71	0.125	0.153	0.125	0.150	0.143	0.151	228
K-60-0.71 (a)	0.157	0.138	0.152	0.123	0.149	0.152	201
K-90-0.50 (b)	0.181	0.136	0.150	0.144	0.151	0.168	227
K-30-0.50 (a)	0.132	0.181	0.116	0.156	0.171	0.143	191
K-60-0.71 (b)	0.135	0.140	0.127	0.148	0.151	0.156	205
K-30-0.71	0.180	0.194	0.134	0.188	0.168	0.149	213
K-30-0.50 (b)	0.129	0.169	0.120	0.169	0.158	0.139	187
T2 Joint 4[†]	0.177	0.177	0.173	0.173	0.283	0.264	-
T2 Joint 6[†]	0.280	0.280	0.256	0.256	0.358	0.417	-

[†] (Frater, 1991)

Since the current design requirements of ANSI/AISC 360 (2010) are based on the limit state of shear rupture along the plane of the weld effective throat, the measured values for the vertical and horizontal leg sizes for fillet welds, L_V and L_H (respectively), are not shown. Instead, they are provided in the comprehensive list of external measurements located in Appendix F.4.

The fillet weld throat dimension, t_w, was taken as the minimum distance between the root of the fillet weld and the face of the triangular weld profile. The fillet weld legs were measured between the root of the fillet and the point of intersection of the weld face with the wall of the overlapping HSS member (L_v) or the wall of the chord/overlapped web member (L_h). These dimensions are shown in Figure 4-7 (a), where the value of θ is equal to 90° for the longitudinal fillet welds (elements a and b) and 60° for the transverse fillet welds (elements c and d).

The crown depth of a PJP groove-weld was measured adjacent to the 45° beveled end of the HSS which corresponded to the greatest perpendicular dimension from the base metal surface to the surface of the weld (d). This was a situation that was created intentionally during the weld-size reductions to take advantage of a designed-in crack that results from the backing bar, which theoretically lies on the rupture plane through the weld throat. The dimension d is shown in Figure 4-7 (b).

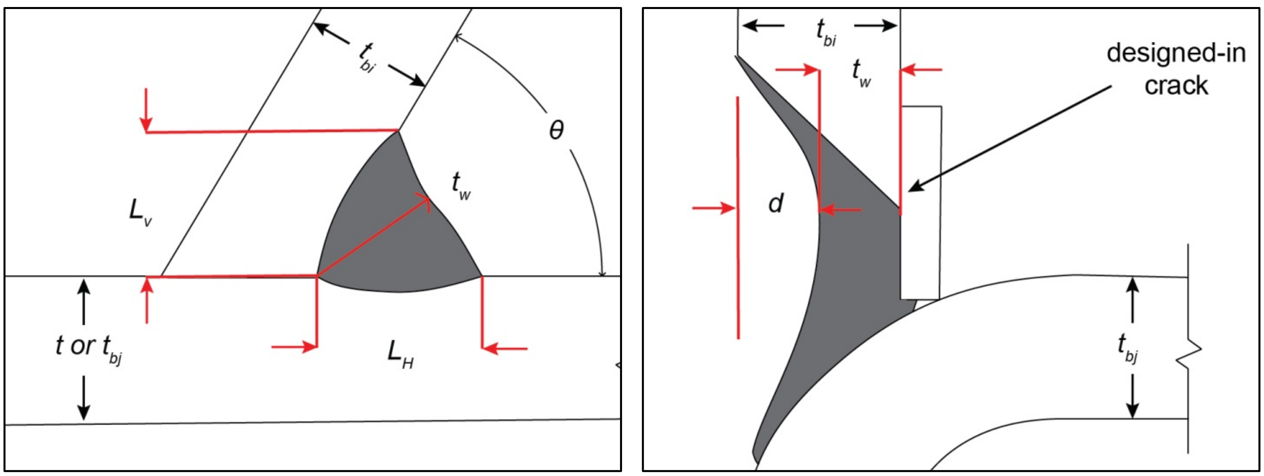

(a) fillet weld cross-section from the molding technique

(b) PJP groove-weld cross section from the macroetch examinations

Figure 4-7 Example of a fillet weld and PJP groove weld throat (and fillet weld leg) measurement

The nominal weld strength (i.e. omitting any resistance factors) was then calculated for each of the nine connections using the *actual* tensile strength and the *average measured* throat dimensions of the size-reduced weld elements. The following section summarizes the general approach that was adopted to calculate the strength of the welds and is applicable to any of the predicted strength models discussed in Chapter 5.

4.3. Weld Strength Prediction Method

The equations for the effective length of welds in HSS overlapped K-connections in Table K4.1 are based on the load carrying capacity of each weld element. As such, they can be discretized to isolate the contribution of each individual weld element to the overall resistance. The resistance of the joint can thus be computed according to Equation 4-1:

$$R_n = \sum_i F_{nw} l_{ei} t_{wi} \tag{4-1}$$

where t_{wi} is the measured effective throat of any i^{th} weld element, and l_{ei} is the effective length of any i^{th} weld element. By assuming that the entire weld length is effective (i.e. no effective length rules are applied), and using the overall dimensions (i.e. using H_{bi} and B_{bi} everywhere and neglecting the HSS corners) the effective length of each weld element can be calculated using the equations for l_{ei} shown in Table 4-10.

Table 4-10 Summary of weld strength prediction method (shown for the "upper-bound" method)

Weld Element Convention†	F_{nw} (ksi)	l_{ei} (in.)	t_{wi}
a b	$0.60F_{EXX}$	$\left(1-\frac{O_v}{100}\right)\left(\frac{H_{bi}}{\sin\theta_i}\right)$	Average measurement from Table 4-9
a' b'	$1.00F_{EXX}$	$\frac{O_v}{100}\left(\frac{H_{bi}}{\sin(\theta_i+\theta_j)}\right)$	
c	$0.60F_{EXX}$	B_{bi}	
d	$0.60F_{EXX}$	B_{bi}	

†For weld element labelling convention, see Figure 3-2.

As shown in Table 4-10, the term for the shear strength, F_{nw}, of the fillet welds was taken as:

$$F_{nw} = 0.60F_{EXX} \tag{4-2}$$

This same equation is given in Table J2.1 (AISC, 2010) for the tensile strength, F_{nw}, of PJP welds; however, according to the AISC 360-10 commentary:

> *"The factor of 0.6 on F_{EXX} for the tensile strength of PJP groove welds is an arbitrary reduction that has been used since the early 1960s to compensate for the notch effect of the unfused area of the joint, uncertain quality on the root of the weld due to the inability to perform non-destructive evaluation, and the lack of a specific notch-toughness requirement for filler metal. It does not imply that the tensile failure mode is by shear stress on the effective throat, as in fillet welds."*

Thus, a more appropriate equation for the nominal tensile strength of PJP flare-bevel-groove welds, shown in Equation 4-3, has been used.

$$F_{nw} = 1.00F_{EXX} \tag{4-3}$$

Table 4-11 summarizes the predicted strengths for each limit state in the welded test joints prior to testing. The predicted weld rupture load was calculated by regarding the entire weld length as effective, and thus a predicted connection resistance marginally less than the predicted weld rupture load was deemed acceptable. Preliminary results from the first several experiments would dictate the need to revisit the weld sizes if they were found to still be stronger than predicted using this method.

Table 4-11 Pre-experiment strength prediction summary

Joint Designation	O_v	β	B/t	Nominal Axial Strength of Branch (kips)	Predicted Nominal Connection Strength (kips)	Predicted Weld Rupture Load (kips)
K-90-0.50a	90	0.5	26.7	335.4	307.9	217.3
K-60-0.50	60	0.5	26.7		253.5	200.6
K-90-0.71a	90	0.714	14		307.9	228.3
K-60-0.71a	60	0.714	14		307.9	200.7
K-90-0.50b	90	0.5	26.7		307.9	226.8
K-30-0.50b	30	0.5	26.7		189.3	191.0
K-60-0.71b	60	0.714	14		307.9	204.8
K-30-0.71	30	0.714	14		243.7	213.1
K-30-0.50b	30	0.5	26.7		189.3	186.8

Plane-frame truss modelling was re-done using the PR model and the appropriate property modifiers for the rectangular HSS sections in the SAP2000 structural model to account for the actual measured material and geometric properties. The test process was simulated using the upper-bound prediction method and a detailed test plan, including the sequence of joint loading and fracture, the required MTS loads, alternate global limit state, the corresponding factor of safety (taken as the ratio of capacity to demand), and the support reactions, was produced. The detailed test plan is located in Appendix G.3. Included with it is a schematic of the truss motions required to load the nine welded test joints in the loading sequence.

4.4. Results from Full-Scale Welded Connection Tests

Each weld-critical test joint failed by rupture along a plane through the weld and at an axial load considerably higher than the nominal strength predicted by the current provisions of Section K4.1 (AISC, 2010) for welds in overlapped K-connections. Figure 4-8 shows the nine connections with the reduced-size welds immediately prior to testing, and Figure 4-9 shows the shear/tensile rupture failure modes observed during the experimental programs for fillet welds and PJP welds, respectively.

Rupture loads were generally taken from a strain gage pair located at mid-height of the critical tension-loaded web member. The load in the web member was kept below the LRFD predicted tensile capacity of the web member computed on the basis of the actual mechanical properties and dimensions ($\emptyset T_r = 302$ kips) for all tests. Hence, members remained elastic throughout the test and loads were calculated as the product of the average strain ($\bar{\varepsilon}$), the Young's modulus (E), and the cross-sectional area (A_b).

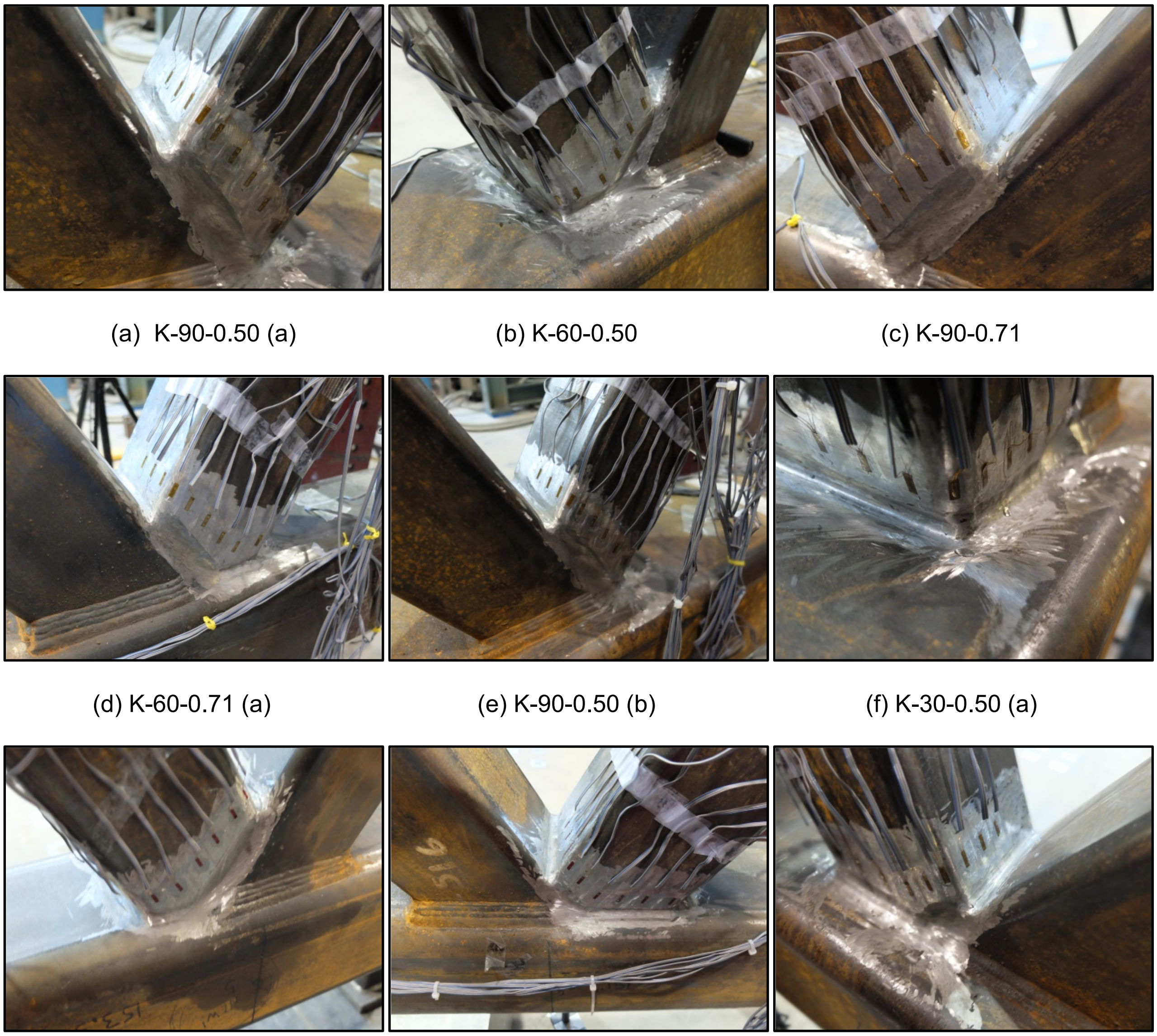

(a) K-90-0.50 (a) (b) K-60-0.50 (c) K-90-0.71

(d) K-60-0.71 (a) (e) K-90-0.50 (b) (f) K-30-0.50 (a)

(g) K-60-0.71 (b) (h) K-30-0.71 (i) K-30-0.50 (b)

Figure 4-8 Test joints with instrumentation immediately prior to testing

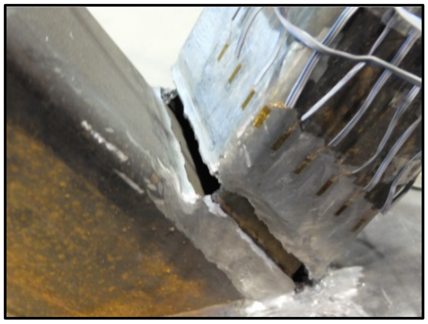

(a) K-90-0.50 (a)

(b) K-60-0.50

(c) K-90-0.71

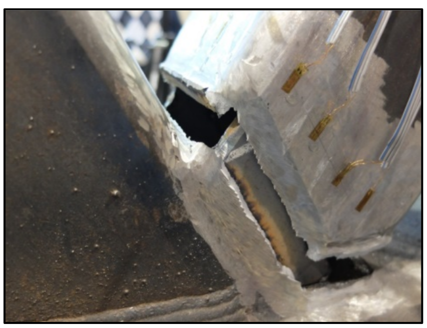

(d) K-60-0.71 (a)

(e) K-90-0.50 (b)

(f) K-30-0.50 (a)

(g) K-60-0.71 (b)

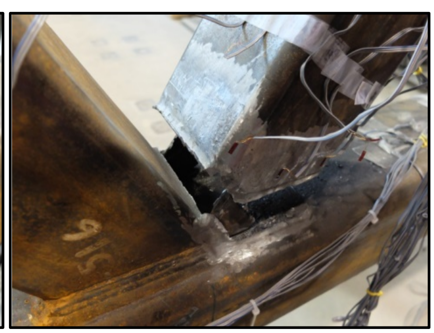

(h) K-30-0.71

(i) K-30-0.50 (b)

Figure 4-9 Test joints with instrumentation immediately after testing

4.4.1. Discussion on the Performance of the Test Setup

As tests progressed, minor changes were made to the original test setup in order to optimize the performance for subsequent tests. A non-critical issue with the truss support at panel point (or "PP") 10 was encountered during the first test, K-90-0.50 (a), whereby softening of the reinforcement plate under the reaction load resulted in a near pin-ended support condition for the majority of the test. Residual deformations in the reinforcement plate and chord face after the point load was removed indicated that the chord face had yielded. For subsequent tests, two 1.5 in. thick hardened steel plates were tack welded to the reinforcement plates at the susceptible PPs (10 and 13); see Figure 3-1. A rigid steel block assembly (or a hydraulic jack) was also employed inside the chord beneath the MTS ram head in order to prevent a similar failure mode (web crippling/yielding). Where the hydraulic jack was used, the pressure was increased at a rate of 25.4 psi per kip of the applied MTS load.

Following the second test, K-60-0.50, and after noting slight variations in the load measured at 12.5 in. from the weld and at mid-length of the web member, a third strain gage pair located at 12.5 in. from the opposite end of the web member was monitored in order to produce a greater redundancy in the number of web member load measurements.

Finally, following a number of tests in which the weld strength prediction models were preliminarily evaluated, the testing sequence was revised to reduce the total number of truss movements and instrumentation resets, and to thereby mitigate additional risk of causing equipment damage. The connections were finally tested in the following order:

1. Joint 1 (K-90-0.50 (a))
2. Joint 2 (K-60-0.50)
3. Joint 3 (K-90-0.71)
4. Joint 4 (K-60-0.71 (a))
5. Joint 6 (K-30-0.50 (a))
6. Joint 5 (K-90-0.50 (b))
7. Joint 9 (K-30-0.50 (b))
8. Joint 8 (K-30-071)
9. Joint 7 (K-60-0.71 (b))

This revision to the testing sequence from Figure 3-21 is shown in Figure 4-10. As a final note, the measured load from all of the strain gages used in the experimental program, and the actual weld rupture loads used for the analysis, neglect the effects of the self-weight of the truss and the forces due to member fitting. The former loads for the web members are located in Appendix B.4 should the reader be interested, but they account for less than 1% of the experimental rupture loads of the joints.

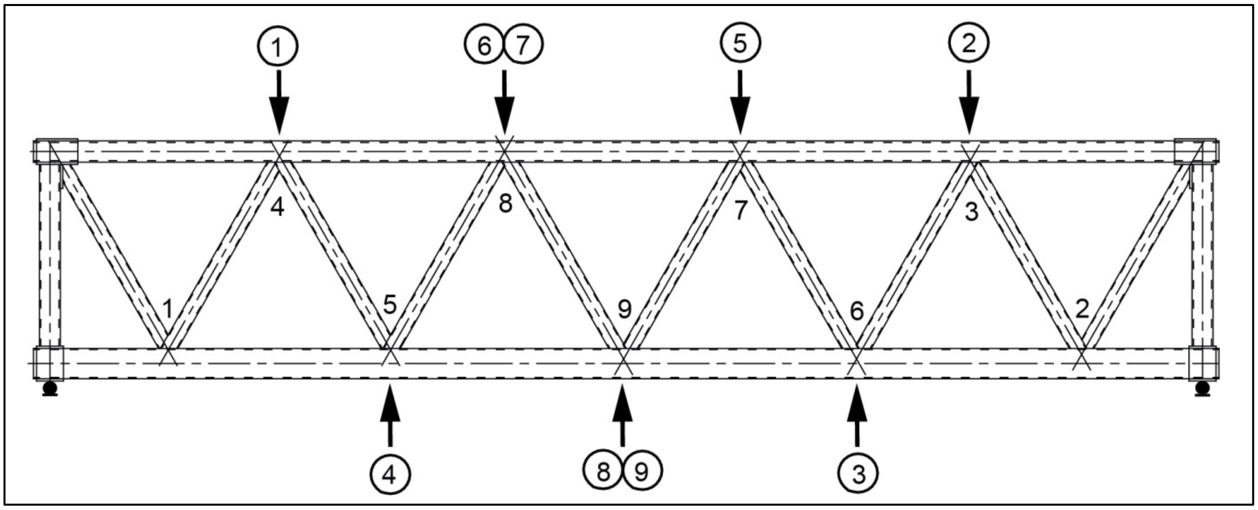

Figure 4-10 Actual sequence of panel point loadings (similar to Figure 3-21)

4.4.2. K-90-0.50 (a)

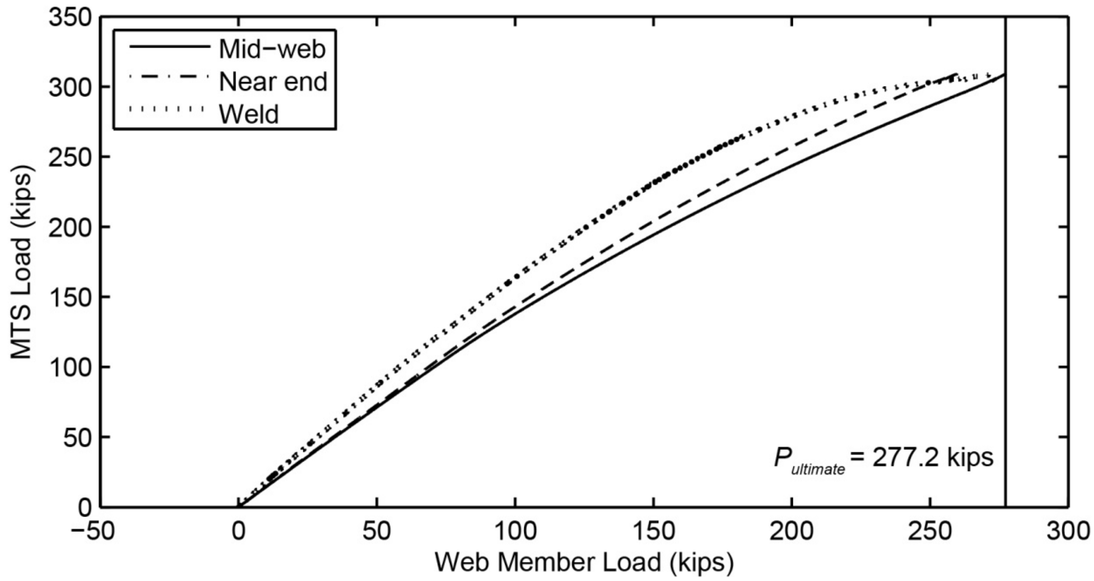

Figure 4-11 MTS load vs. web member load measured at multiple locations along the branch length for K-90-0.50 (a)

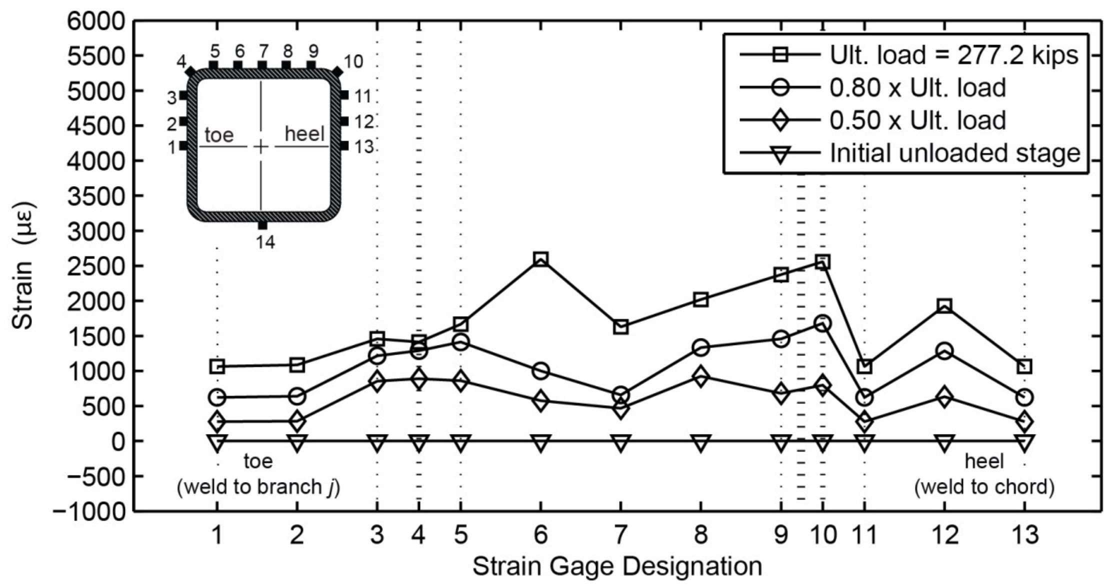

Figure 4-12 Distribution of normal strain around the branch perimeter for K-90-0.50 (a)

K-90-0.50 (a) was loaded at an MTS stroke rate of 0.0002 in/s. Failure occurred in a brittle manner by rupture along a plane through the weld. Early in the test, cracking in a weld at an HSS corner was observed. Before failure, there was visible joint rotation and deformation of the HSS chord face. Several small "pings" signaled that weld rupture was imminent, and upon failure, the load measured by the load cells rapidly dropped. The weld ruptured simultaneously at all locations around the branch perimeter and the release of energy caused the truss to briefly (but violently) jolt, knocking free the two dial gages and one of the load cell cables.

The weld ruptured at a web member load of 277.2 kips, measured by the strain gage pair at mid-height of the web member. This was 48% higher than the predicted nominal strength according to the current effective weld length rules in Section K4.1 of AISC 360 (2010), and 28% higher than the upper-bound prediction method (regarding the entire weld length as fully effective). One must bear in mind, however, that the appropriate safety margins, or a sufficient safety index, still need to be implemented. The relationship between the applied MTS load and the measured branch member load at 12.5 in. from the weld and at mid-length of the web member is shown in Figure 4-11.

Initially, linear-elastic behavior was observed, followed by a gradual decrease in stiffness caused by rotation of the joint and deformation of the HSS chord face. The levelling-off of the load measured adjacent to the weld in Figure 4-11 indicates some ductility in the welded joint. The relationship between the applied MTS load and the *individual strain gage measurements* at various locations on the branch is given in Appendix H.4.

Figure 4-12 shows the distribution of normal strain measured around the branch perimeter at the start of the experiment and at 50%, 80% and 100% of the weld rupture load. Note that in all of these plots, the toe of the test branch sits on the overlapped branch, and the heel sits on the chord. Strain distributions at each stage are erratic but, on average, uniform. The non-uniform increments in strain at many of the locations indicate that the weld had the capacity for stress redistribution without premature failure. However, this phenomenon was more pronounced in joints with $\beta = 0.71$. The magnitude of strain along the branch transverse faces decreases towards the mid-wall location (SG 1 or 13), but the decrease at the heel of the branch is less than what was observed for specimens with lower O_v. In general, the observations were consistent with the expectations for a connection with $O_v = 90\%$, $B/t = 26.7$, and $B_{bj}/t_{bj} = 16.0$.

4.4.3. K-60-0.50

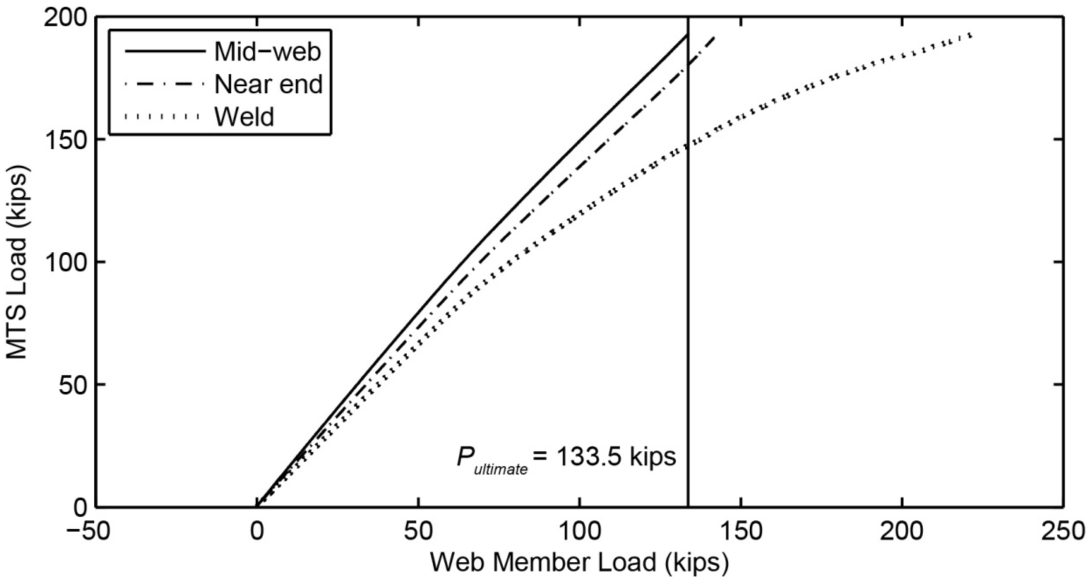

Figure 4-13 MTS load vs. web member load measured at multiple locations along the branch length for K-60-0.50

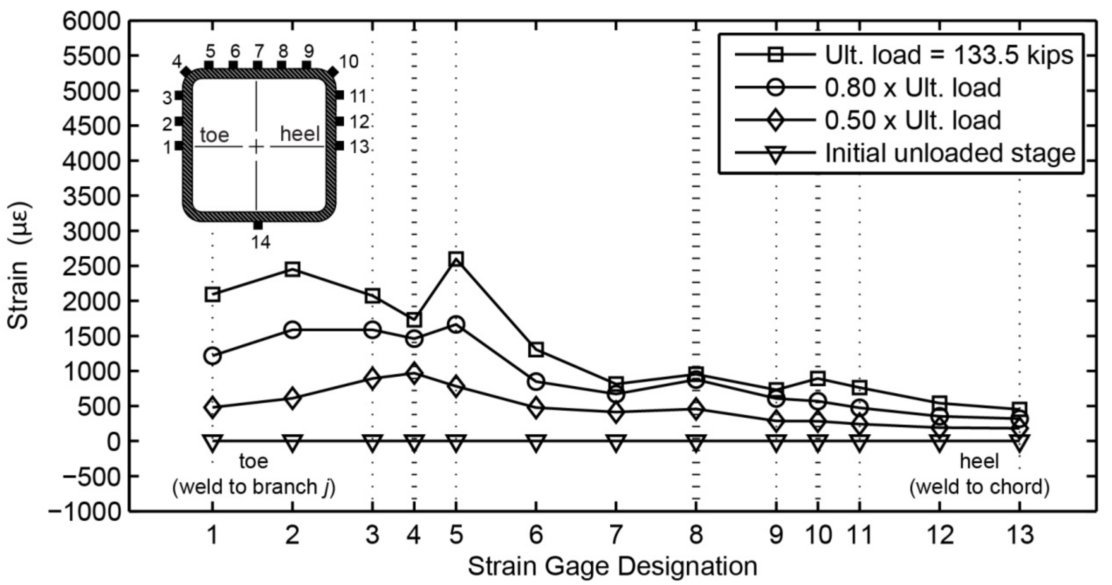

Figure 4-14 Distribution of normal strain around the branch perimeter for K-60-0.50

K-60-0.50 was loaded at an initial test rate of 0.0004 in/s which was increased throughout the experiment to a maximum rate of 0.00045 in/s. Failure occurred in a brittle manner by rupture along a plane through the weld. Early in the test, cracking in weld at the HSS corner was observed. Before failure, there was no visible joint rotation or deformation of the HSS chord face. Several small “pings” signaled that weld rupture was imminent, and upon failure, the load measured by the load cells rapidly dropped. The weld ruptured simultaneously at all locations around the branch perimeter and the release of energy caused the truss to briefly (but violently) jolt, knocking free the two dial gages.

The weld ruptured at a load of 133.5 kips, measured by the strain gage pair at mid-height of the web member. This was 3% lower than the predicted nominal strength according to the current weld effective length rules in Section K4.1 of AISC 360 (2010), and 33% lower than the upper-bound prediction method (regarding the weld as fully effective). The effect of overlap on strength is visible in SG 11 to 13, which appear particularly lightly loaded in Figure 4-14, when compared to the first test. However rupture did occur at lower average strains. The premature failure was thus attributed to the “fallen-in” backing bar that was identified in Section 3.3.2.

The relationship between the applied MTS load and the measured branch member load at 12.5 in. from the weld and at mid-length of the web member is shown in Figure 4-13. Linear-elastic behavior was approximately maintained throughout the test. The relationship between the applied MTS load and the *individual strain gage measurements* at various locations on the branch is given in Appendix H.4. Figure 4-16 shows the distribution of normal strain measured around the branch perimeter at the start of the experiment and at 50%, 80% and 100% of the weld rupture load. Strain distributions at each stage are less erratic than for the first test and decrease as a function of the distance from the toe of the connection. This may be explained by the difference in relative stiffness between the chord member (B/t =26.7) and the overlapping branch (B_{bj}/t_{bj} = 16.0) which attracts more load. The magnitude of strain along the branch transverse faces decreases towards the mid-wall location (SG 1 or 13), and the decrease in the magnitude of strain along the heel of the branch is expectedly more pronounced than in the first test which was expected.

4.4.4. K-90-0.71

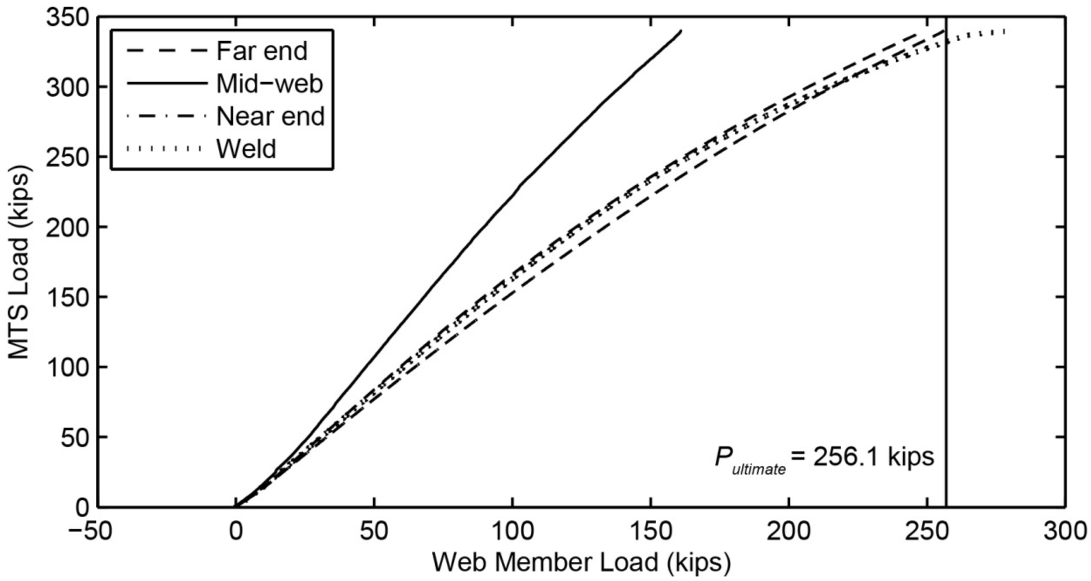

Figure 4-15 MTS load vs. web member load measured at multiple locations along the branch length for K-90-0.71 test

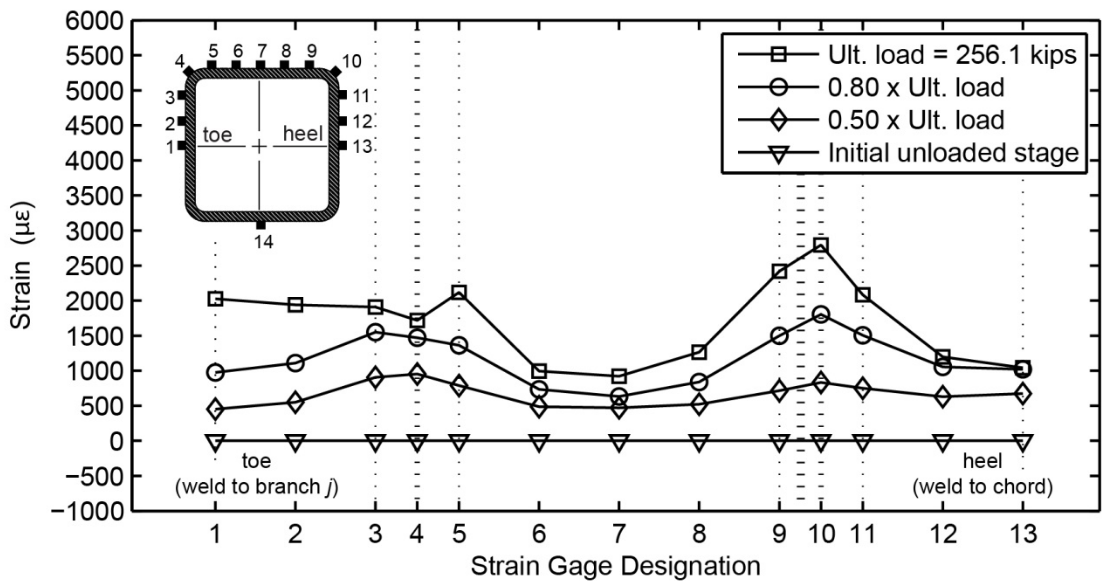

Figure 4-16 Distribution of normal strain around the branch perimeter for K-90-0.71 test

K-90-0.71 was loaded at an MTS stroke rate of 0.0003 in/s, which was less than in previous tests due to a higher ratio of the web member load to the MTS load. Failure occurred in a brittle manner by rupture along a plane through the weld. Early in the test, there was no apparent cracking in the weld anywhere around the perimeter and, due to a much stockier chord member, no apparent joint rotation or deformation of the HSS chord face. Several small "pings" signaled that weld rupture was imminent, and upon failure, the load measured by the load cells rapidly dropped. The weld ruptured simultaneously at all locations around the branch perimeter. Failure in this connection was more sudden than in the previous two tests with $\beta = 0.50$.

The weld ruptured at a load of 256.1 kips. This was 29% higher than the predicted nominal strength according to the current effective weld length rules in Section K4.1 of AISC 360 (2010), and 12% higher than stronger than the upper-bound prediction method (regarding the entire weld length as fully effective). The relationship between the applied MTS load and the measured branch member load at 12.5 in. from the weld, mid-length of the web member, and 12.5 in. from the opposite end of the web member is shown in Figure 4-15. The force that was measured at mid-height of the branch appeared spurious; an observation later confirmed by the individual strain gage measurements from the elastic tests, located in Appendix I.1. Hence the rupture load was taken from the strain gage pair 12.5-in from the weld. The relationship between the applied MTS load and the *individual strain gage measurements* at various locations on the branch is given in Appendix H.4.

Figure 4-16 shows the distribution of normal strain measured around the branch perimeter at the start of the experiment and at 50%, 80% and 100% of the weld rupture load. The highest measured strains were located at the corners of the branch which is typical for connections between rectangular HSS because of the relative flexibility in the connected chord face and the stiffness of the branch corners. The magnitude of strain along the branch transverse faces decreases towards the mid-wall location (SG 1 or 13) by approximately the same amount at the toe and heel of the connection. At the ultimate load, the strain distribution became slightly erratic and the transverse weld element at the toe picked up more of the load. This may indicate a significant capacity for stress redistribution prior to failure.

4.4.5. K-60-0.71 (a)

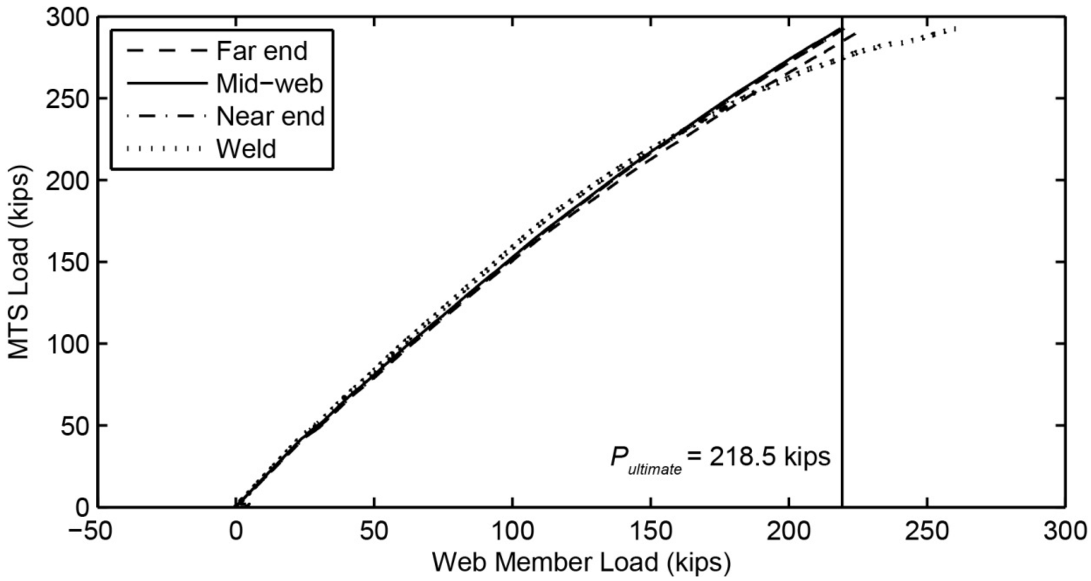

Figure 4-17 MTS load vs. web member load measured at multiple locations along the branch length for K-60-0.71 (a)

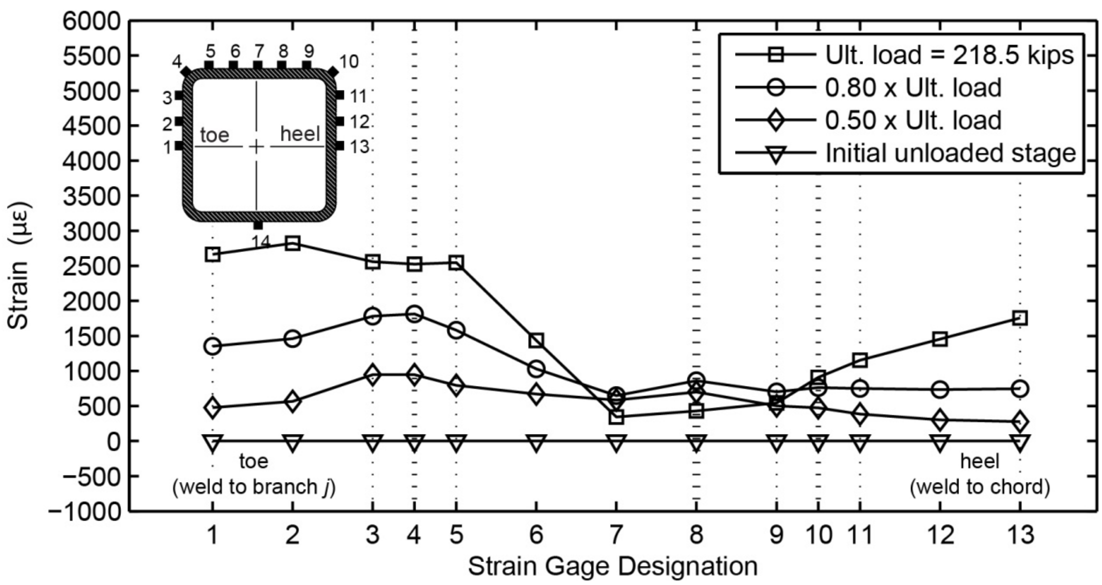

Figure 4-18 Distribution of normal strain around the branch perimeter for K-60-0.71 (a)

K-60-0.71 (a) was loaded at an MTS stroke of 0.0003 in/s. Failure occurred in a brittle manner by rupture along a plane through the weld. Early in the test, cracking in the weld along the transverse weld element at the heel of the HSS was observed. Before failure, there was visible joint rotation and deformation of the HSS chord face. Several small “pings” signaled that weld rupture was imminent, and upon failure, the load measured by the load cells rapidly dropped.

The weld ruptured simultaneously at all locations around the branch perimeter. Like in the previous test, failure in this connection was sudden.

The weld ruptured at a load of 218.5 kips measured by the strain gage pair at mid-height of the web member. This was 50% higher than the predicted nominal strength according to the current effective weld length rules in Section K4.1 of AISC 360 (2010), and 9% higher than the upper-bound prediction method (regarding the entire weld length as fully effective). The relationship between the applied MTS load and the measured branch member load at 12.5 in. from the weld, mid-length of the web member, and 12.5 in. from the opposite end of the web member is shown in Figure 4-17. The relationship between the applied MTS load and the *individual strain gage measurements* at various locations on the branch is given in Appendix H.4.

Figure 4-18 shows the distribution of normal strain measured around the branch perimeter at the start of the experiment and at 50%, 80% and 100% of the weld rupture load. The magnitude of strain along the branch transverse face adjacent to the weld at the toe of the HSS decreases slightly towards the mid-wall location (SG 1); however, the magnitude of strain along the branch transverse face adjacent to the weld at the heel of the HSS is approximately uniform. This is explained by the larger wall slenderness (of the member on which the branch lands) at the heel relative to the toe. At the ultimate load, the strain distribution becomes very erratic and the transverse weld element at the toe picks up more of the load, indicating a significant capacity for stress redistribution prior to failure.

4.4.6. K-30-0.50 (a)

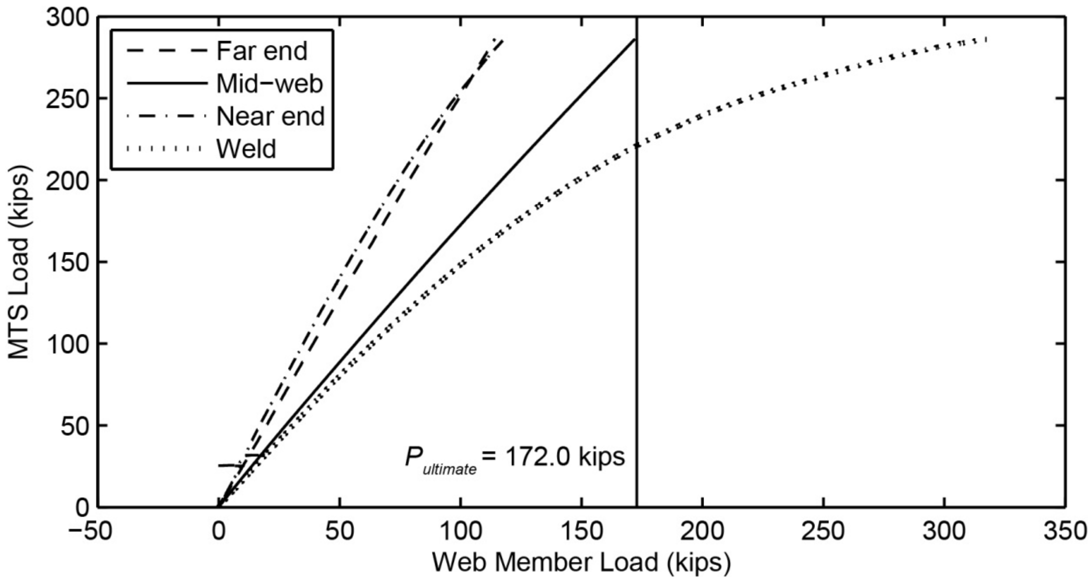

Figure 4-19 MTS load vs. web member load measured at multiple locations along the branch length for K-30-0.50 (a)

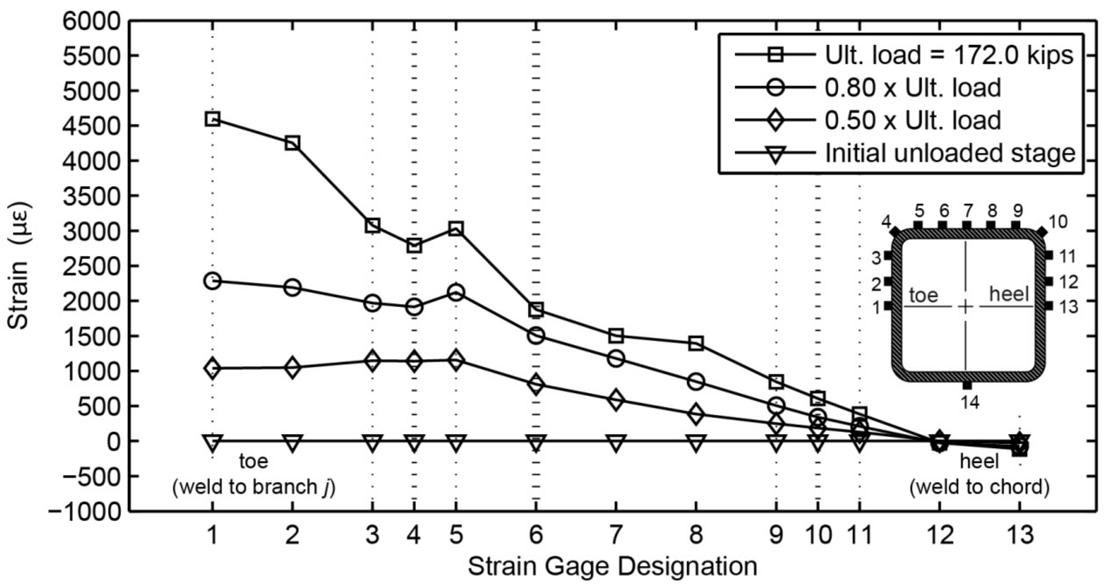

Figure 4-20 Distribution of normal strain around the branch perimeter for K-30-0.50 (a)

K-30-0.50 (a) was loaded at an initial MTS stroke of 0.0003 in/s which was increased at an MTS load of 60 kips to 0.0035 in/s until failure. Failure occurred in a brittle manner by rupture along a plane through the weld. Early in the test, cracking in the weld at the HSS corner at the toe of the connection was observed. Before failure, there was significant joint rotation and deformation of the HSS chord face. Several small "pings" signaled that weld rupture was imminent, and, upon failure, the load measured by the load cells rapidly dropped. The weld ruptured simultaneously at all locations around the branch perimeter.

The weld ruptured at a load of 172.0 kips measured by the strain gage pair at mid-height of the web member. This was 99% higher than the predicted nominal strength according to the current effective weld length rules in Section K4.1 AISC 360 (2010), and 10% lower than the upper-bound prediction method (regarding the entire weld length as fully effective). The relationship between the applied MTS load and the measured branch member load at 12.5 in. from the weld, mid-length of the web member, and 12.5 in. from the opposite end of the web member is shown in Figure 4-19. The measured branch member load at mid-length of the member showed poor agreement with the loads measured at 12.5 in. from the weld and 12.5 in from the opposite end of the web member. This was consistently observed for load measurements on this branch member (member "M"), but was not erroneous based on the individual strain gage measurements. A possible explanation may be more significant local effects on the web member relative to others. The relationship between the applied MTS load and the *individual strain gage measurements* at various locations on the branch is given in Appendix H.4.

Figure 4-20 shows the distribution of normal strain measured around the branch perimeter at the start of the experiment and at 50%, 80% and 100% of the weld rupture load. As was observed in K-60-0.50, strains decrease as a function of the distance from the toe of the connection. The explanation is likely the same. The magnitude of strain measured along the transverse weld at the heel of the connection shows a large region of ineffectiveness, even at the ultimate load. The reduced effective length is consistent with the expectations for a connection with $O_v =$ 30%, B/t =26.7, and $B_{bj}/t_{bj} =$ 16.0. The magnitude of strain measured along the transverse weld at the toe of the connection is approximately uniform from the corner to the mid-wall location (SGs 4-1) throughout the loading, but increases at the mid-wall location just prior to rupture, indicating some capacity for stress redistribution.

4.4.7. K-90-0.50 (b)

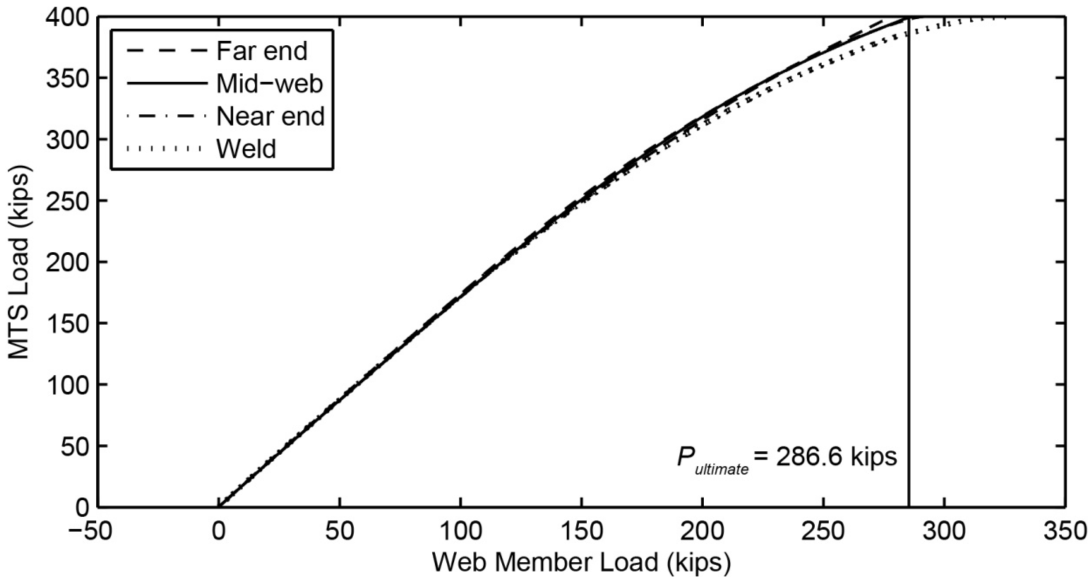

Figure 4-21 MTS load vs. web member load measured at multiple locations along the branch length for K-90-0.50 (b)

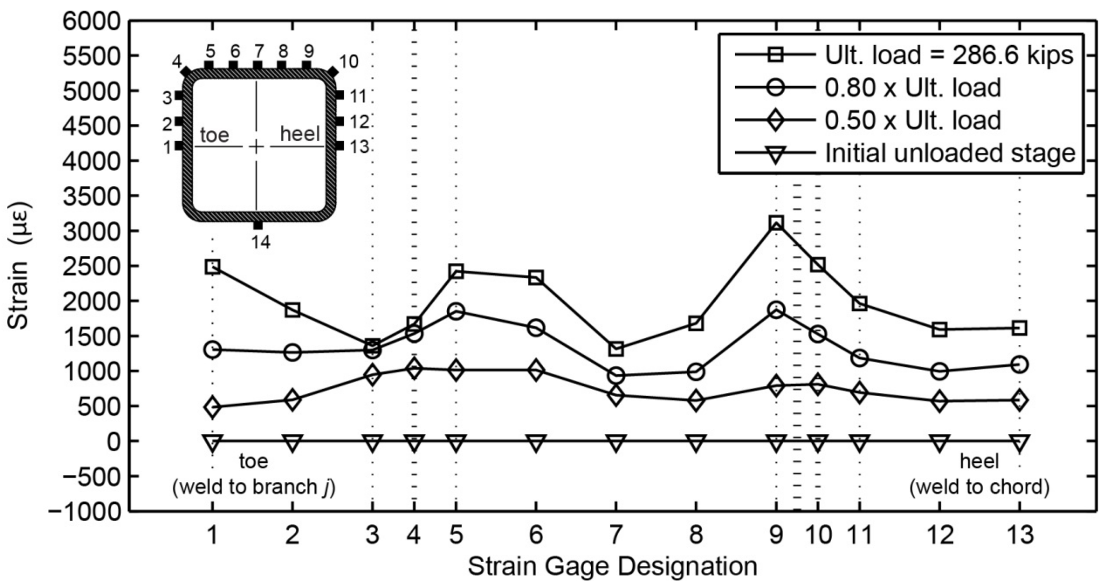

Figure 4-22 Distribution of normal strain around the branch perimeter for K-90-0.50 (b)

As the test program progressed, the margin of safety against adverse failure away from the critical joint became smaller. During this test, there was a non-negligible probability of failing the weld at joint K-30-0.50 (b) so the joint was instrumented and monitored alongside K-90-0.50 (b). K-90-0.50 (b) was a redundant test that was planned in order to verify the results of the previous test on K-90-0.50 (a). K-90-0.50 (b) was loaded at an MTS stroke rate of 0.0003 in/s. Failure of the weld occurred in a brittle manner by rupture along a plane through the weld. Early in the test, cracking in the weld at the HSS corner at the toe of the connection was observed. Later in the test, a second crack along the heel weld element was visibly growing in size. Before failure, there was significant joint rotation and deformation of the HSS chord face. Several small “pings” signaled that weld rupture was imminent, and, upon failure, the load measured by the load cells rapidly dropped. The weld ruptured simultaneously at all locations around the branch perimeter and after unloading the resulting gap between the connection and the separated web member was significant.

Failure occured at a load of 286.6 kips measured by the strain gage pair at mid-height of the web member. This was 46% higher than the predicted nominal strength according to the current effective weld length rules in Section K4.1 of AISC 360 (2010), and 26% higher than the upper-bound prediction method (regarding the entire weld length as fully effective). The relationship between the applied MTS load and the measured branch member load at 12.5 in. from the weld, mid-length of the web member, and 12.5 in. from the opposite end of the web member is shown in Figure 4-21. Initially, linear-elastic behavior was observed, followed by a gradual decrease in stiffness caused by rotation of the joint and deformation of the HSS chord face. The relationship between the applied MTS load and the *individual strain gage measurements* at various locations on the branch is given in Appendix H.4.

Figure 4-22 shows the distribution of normal strain measured around the branch perimeter at the start of the experiment and at 50%, 80% and 100% of the weld rupture load. Strain distributions at each stage are erratic but, on average, uniform. The highest measured strains were located at the corners of the branch. The results were thus similar to K-90-0.50 (a).

Despite the 1 in. thick hardened steel plate, the roller support at PP 10 was immobile. This resulted in a near pin-ended support condition for the majority of the test. It was thought to be attributable to internal damage in the roller assembly.

4.4.8. K-30-0.50 (b)

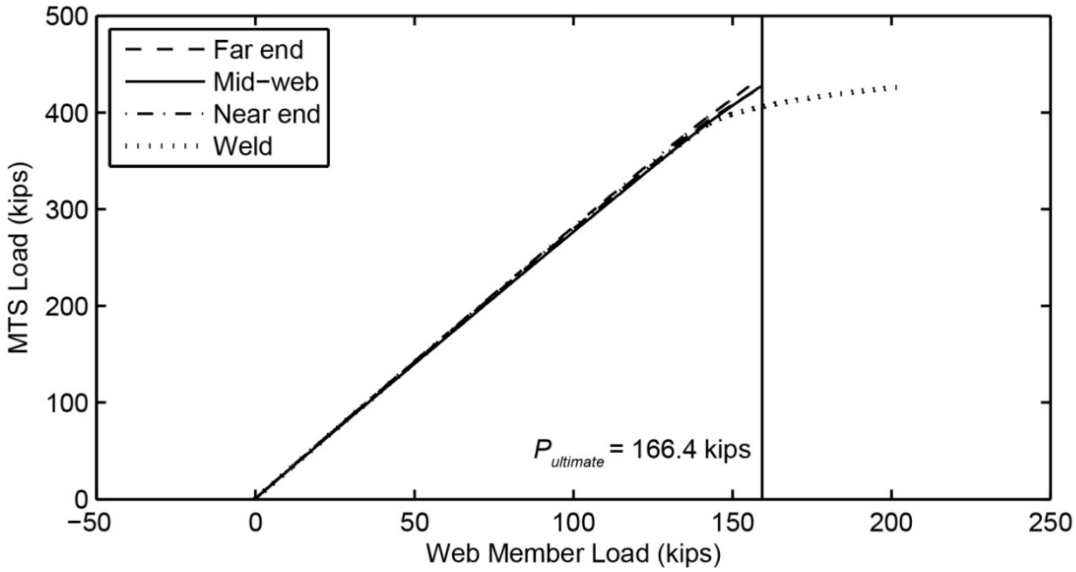

Figure 4-23 MTS load vs. web member load measured at multiple locations along the branch length for K-30-0.50 (b)

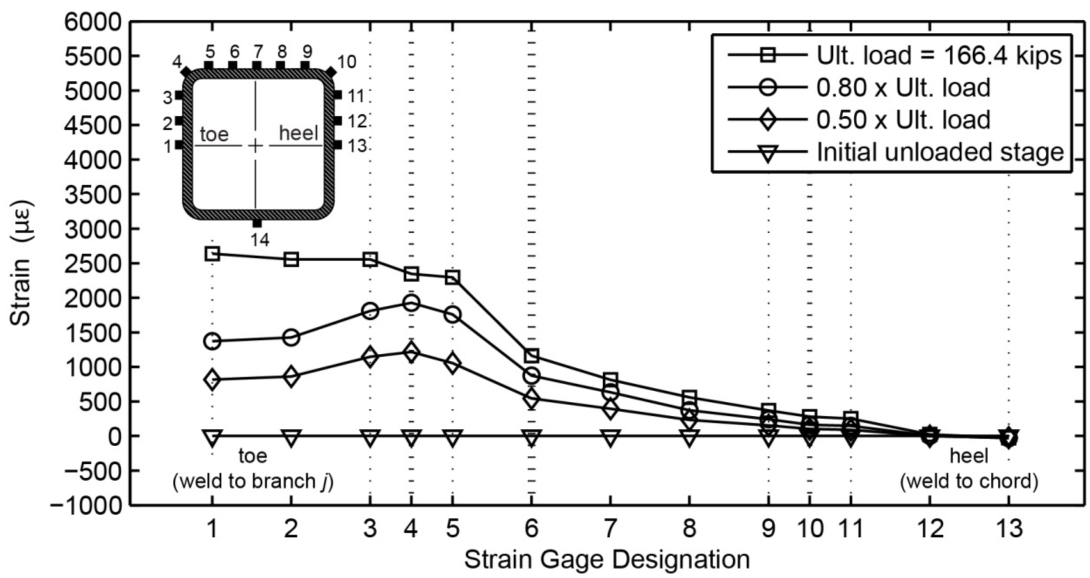

Figure 4-24 Distribution of normal strain around the branch perimeter for K-30-0.50 (b)

K-30-0.50 (b) was a redundant test that was planned in order to verify the results of the previous test on K-30-0.50 (a). K-30-0.50 (b) was loaded at an initial MTS stroke of 0.0004 in/s. At an MTS load of 403 kips, the operator-controlled safety limit of the MTS actuator was reached which caused the ram head to retract and the load to drop. At this point, the connection was unbroken. The truss was then loaded at an MTS stroke of 0.0006 in/s up to 85% of the previous load, and at 0.0004 in/s afterwards. As failure of K-30-0.50 (b) seemed imminent (due to cracking of the weld along the heel of the branch), K-90-0.50 (b) (which was previously tested and over-welded) ruptured. The load was completely removed and K-90-0.50 (b) was repaired with plate stiffeners on the webs of the branch to prevent future inadvertent failures. The truss was loaded again at an MTS stroke of 0.0006 in/s up to 85% of the previous load, and at 0.0004 in/s afterwards, and K-30-0.50 (b) was ruptured. The welded joint failed in a brittle manner by rupture along a plane through the weld and with visible joint rotation and deformation of the HSS chord face – more so than had been observed in any of the previous tests. The weld ruptured simultaneously at all locations around the branch perimeter.

Failure occurred at a load of 166.4 kips measured by the strain gage pair at mid-height of the web member. This was 95% higher than the predicted nominal strength according to the current effective weld length rules in Section K4.1 of AISC 360 (2010), and 11% lower than the upper-bound prediction method (regarding the entire weld length as fully effective). The relationship between the applied MTS load and the measured branch member load at 12.5 in. from the weld, mid-length of the web member, and 12.5 in. from the opposite end of the web member is shown in Figure 4-23. Because the un-loading curve from the second stage of loading was followed back to the point of failure, complete linear-elastic behavior was observed during the test. The relationship between the applied MTS load and the *individual strain gage measurements* at various locations on the branch is given in Appendix H.4.

Figure 4-24 shows the distribution of normal strain measured around the branch perimeter at the start of the experiment and at 50%, 80% and 100% of the weld rupture load. The load-strain relationships for the individual SGs around the perimeter of the branch member are located in Appendix H.5. As was explained for the other joints, strains decrease as a function of the distance from the toe of the connection. The magnitude of strain measured along the transverse weld at the heel of the connection shows a large region of ineffectiveness, even at the ultimate load. The reduced effective length is consistent with the expectations for joints with O_v = 30%, B/t =26.7, and B_{bj}/t_{bj} = 16.0. The magnitude of strain measured along the transverse weld at the toe of the connection is approximately uniform from the corner to the mid-wall location (SGs 4-1) throughout the loading, but increases at the mid-wall location just prior to rupture, indicating some capacity for stress redistribution.

4.4.9. K-30-0.71

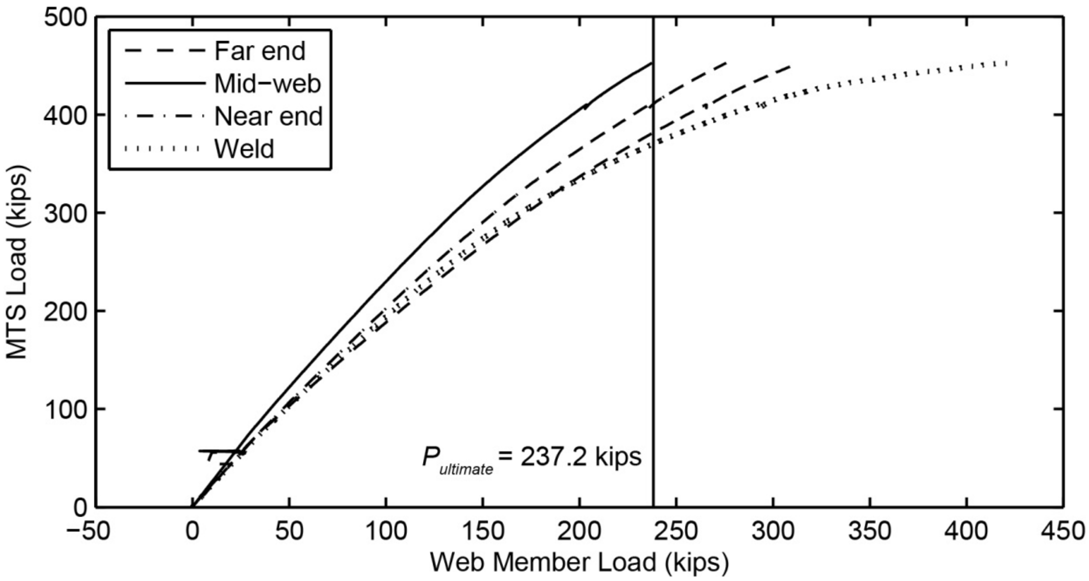

Figure 4-25 MTS load vs. web member load measured at multiple locations along the branch length for K-30-0.71

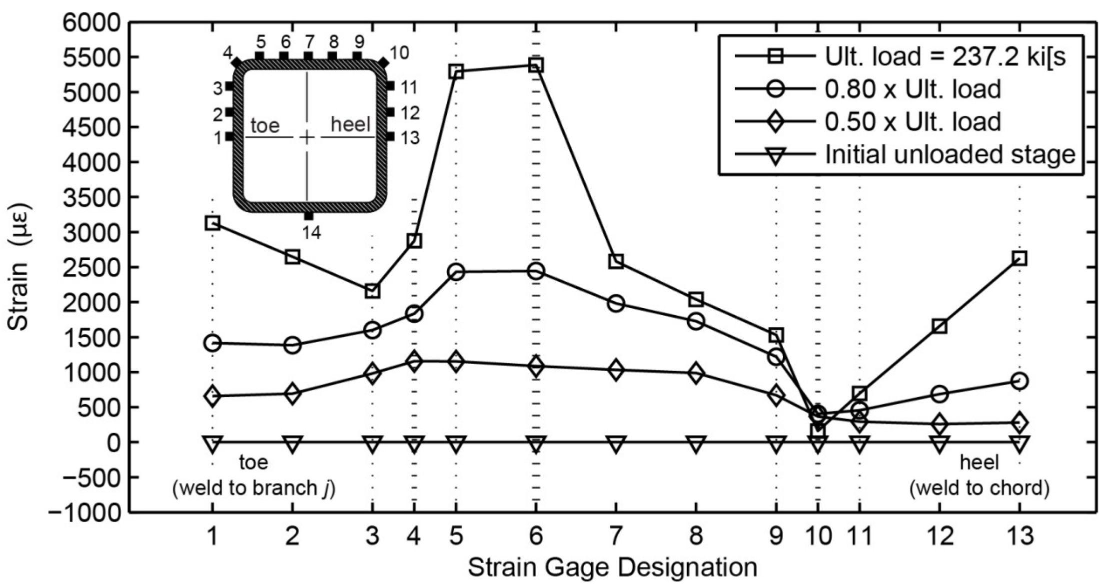

Figure 4-26 Distribution of normal strain around the branch perimeter for K-30-0.71

K-30-0.71 was loaded at an MTS stroke rate of 0.0005 in/s. Failure of the weld occurred in a brittle manner by rupture along a plane through the weld. Early in the test, cracking in the weld was observed beginning at the heel-side corner of the HSS and then propagating towards the mid-wall location. Before failure, there was no apparent joint rotation or deformation of the HSS chord face. Several small “pings” signaled that weld rupture was imminent, and, upon failure, the load measured by the load cells rapidly dropped. Several strain gages were detached by the elastic rebound of the web member at rupture.

Failure occured at a load of 237.2 kips measured by the strain gage pair at mid-height of the web member. This was 129% higher than the predicted nominal strength according to the current effective weld length rules in Section K4.1 of AISC 360 (2010), and 11% higher than the upper-bound prediction method (regarding the entire weld length as fully effective). The relationship between the applied MTS load and the measured branch member load at 12.5 in. from the weld, mid-length of the web member, and 12.5 in. from the opposite end of the web member is shown in Figure 4-25. The small blip in the curve coincides with a transient change in the pressure applied by the in-chord jack assembly which inadvertently occurred during the experiment. The relationship between the applied MTS load and the *individual strain gage measurements* at various locations on the branch is given in Appendix H.4.

Figure 4-26 shows the distribution of normal strain measured around the branch perimeter at the start of the experiment and at 50%, 80% and 100% of the weld rupture load. The load-strain relationships for the individual SGs around the perimeter of the branch member are located in Appendix H.5. The magnitude of strain along the branch transverse faces decreases towards the mid-wall location (SG 1 and 13), but the heel transverse weld element (SGs 10 to 13) contributes very little to the overall resistance until immediately prior to rupture at which point the strain distribution becomes very erratic, which may indicate a capacity for stress redistribution prior to failure.

After unloading, a substantial gap between the overlapping web member and the rest of the connection remained. Plate stiffeners were thus added to the webs of the HSS at the joint to help with welding over the large gap.

4.4.10. K-60-0.71 (b)

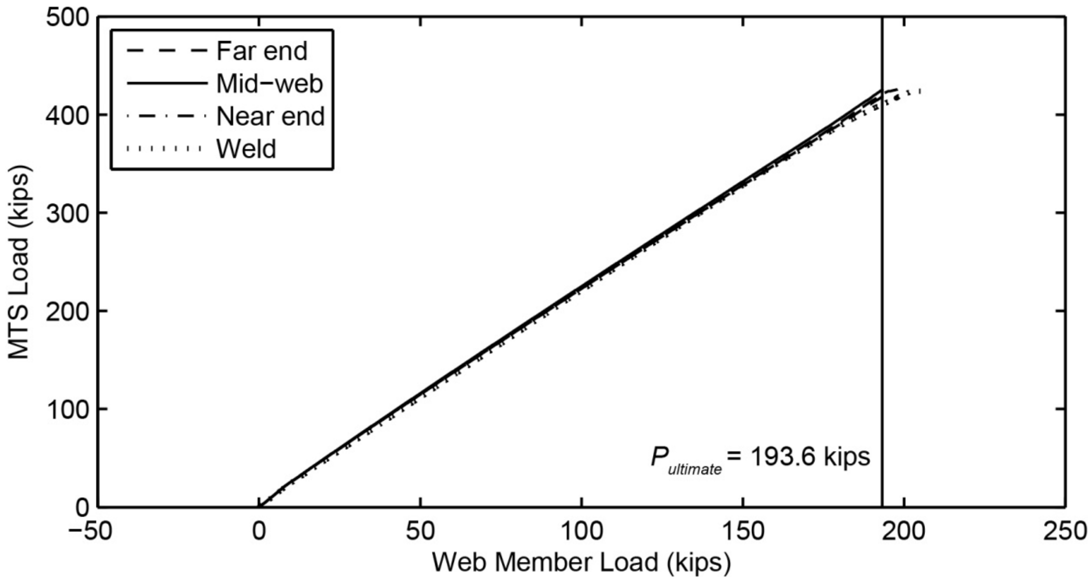

Figure 4-27 MTS load vs. web member load measured at multiple locations along the branch length for K-60-0.71 (b)

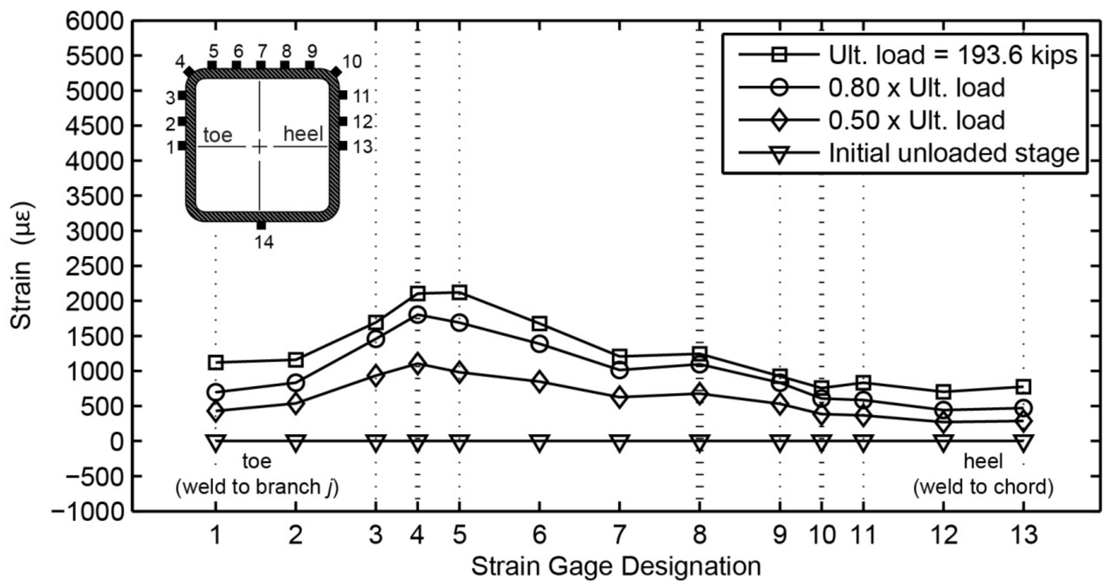

Figure 4-28 Distribution of normal strain around the branch perimeter for K-60-0.71 (b)

K-60-0.71 (b) was a redundant test that was planned in order to verify the results of the previous test on K-60-0.71 (a). It was loaded at an MTS stroke rate of 0.005 in/s. Failure of the connection occurred in a brittle manner by rupture along a plane through the weld. Early in the test, there was no apparent cracking in the weld anywhere around the perimeter and no apparent joint rotation or deformation of the HSS chord face. Several small "pings" signaled that weld rupture was imminent, and, upon failure, the load measured by the load cells rapidly dropped. The weld ruptured simultaneously at all locations around the branch perimeter.

Failure occured at a load of 193.6 kips measured by the strain gage pair at mid-height of the web member. This was 30% higher than the predicted nominal strength according to the current effective weld length rules in Section K4.1 ANSI/AISC 360 (2010), and 6% lower than the upper-bound prediction method (regarding the entire weld length as fully effective). The relationship between the applied MTS load and the measured branch member load at 12.5 in. from the weld, mid-length of the web member, and 12.5 in. from the opposite end of the web member is shown in Figure 4-27. Because the previous loading for K-30-0.71 occurred at the same panel point, K-60-0.71 (b) was previously heavily loaded and the un-loading curve from the previous test was followed back to the point of failure. The relationship between the applied MTS load and the *individual strain gage measurements* at various locations on the branch is given in Appendix H.4.

Figure 4-28 shows the distribution of normal strain measured around the branch perimeter at the start of the experiment and at 50%, 80% and 100% of the weld rupture load. At the ultimate load, there is very little plastic stress redistribution, indicating that the joint may have been very close to failure in the previous experiment. The load-strain relationships for the individual SGs around the perimeter of the branch member are given in Appendix H.5, where this observation is further apparent.

4.4.11. Summary

All nine welded joints failed in a brittle manner by rupture along a plane through the weld at a mean rupture load that was 58% higher than the predicted nominal strength according to current effective weld length rules in Section K4.1 ANSI/AISC 360 (2010). The most conservative predictions were for joints with O_v = 30%. Connections with B/t = 26.7 were accompanied by significant joint rotation and deformation of the HSS chord face at failure. Strain gage readings at loads up to 80% of ultimate were the most useful, in indicating relative amounts of load distribution to the overlapping branch welds, because erratic strain gage readings were generally obtained at failure. For all tests, the toe of the branch landed on a relatively stiff branch (with B_{bj}/t_{bj} = 16.0) so the effectiveness of the transverse weld at that location was always relatively high. Strain gages at the heel of the overlapping branch, however, did show reduced effectiveness of the transverse weld at that location, particularly for the more slender walled chord member with B/t = 26.7.

As the load required by the MTS to produce fracture became greater, so became the separation between the overlapping web member and chord at rupture, and the residual truss deformations. Pinning (as opposed to rolling) occurred at the support at panel point 10 during tests on K-90-0.50 (a) and K-90-0.50 (b). Joints K-90-0.50 (b) and K-30-0.71 were stiffened with reinforcing plates at the end of their tests.

Table 4-12 Summary of experimental performance parameters

Joint Designation	Panel Point Location of MTS Point Load	Tension (Overlapping) Branch Member†	Predicted Branch Load‡ / Measured Branch Load	Sum of Load Cell Readings / MTS Load Reading
K-90-0.50 (a)	4	G	1.01*	0.96
K-60-0.50	3	P	1.07	0.98
K-90-0.71	6	O	1.00	0.98
K-60-0.71 (a)	5	H	1.00	0.98
K-90-0.50 (b)	8	I	1.04*	0.98
K-30-0.50 (a)	7	N	1.03	0.99
K-60-0.71 (b)	9	M	1.10	0.98
K-30-0.71	9	J	0.97	0.98
K-30-0.50 (b)	8	L	1.07	0.98

† According to the branch member labelling scheme in Figure 3-1.
‡ According to the PR (pin-ended web and continuous chord) model.
* Predicted loads by assuming a pin-ended support at PP 13 (caused by reinforcement plate softening).

The mean of the ratio of the branch load, predicted by the continuous chord (PR) model, to the load measured by experiment was 1.03. The maximum of this ratio, equal to 1.10, occurred in test K-60-0.71 (b), at which time residual deformations had caused visible changes in truss geometry. The sum of load cell readings at the reaction points was always less than the MTS readings, with an average ratio (of the former to the latter) equal to 0.98. These points of interest, recorded at rupture for each of the nine tests, are summarized in Table 4-12, and a comparison of the actual to predicted weld rupture loads is given in Table 4-13.

Table 4-13 Actual versus predicted (A/P) strength of the welds in the rectangular HSS overlapped K-connections

Joint Designation	O_v (%)	β	B/t	Predicted Rupture Load† (kips)	Actual Rupture Load (kips)	Location of Rupture Load Measurement	Actual/ Predicted Ratio
K-90-0.50 (a)	90	0.50	26.7	217.3	277.2	Mid-web	1.28
K-60-0.50	60	0.50	26.7	200.6	133.5	Mid-web	0.67
K-90-0.71	90	0.71	14.0	228.3	256.1	$2.5B_i$	1.12
K-60-0.71 (a)	60	0.71	14.0	200.7	218.5	Mid-web	1.09
K-90-0.50 (b)	90	0.50	26.7	226.8	286.6	Mid-web	1.26
K-30-0.50 (a)	30	0.50	26.7	191.0	172.0	Mid-web	0.90
K-60-0.71 (b)	60	0.71	14.0	204.8	193.6	Mid-web	0.94
K-30-0.71	30	0.71	14.0	213.1	237.2	Mid-web	1.11
K-30-0.50 (b)	30	0.50	26.7	186.8	166.4	Mid-web	0.89
T2 Joint 4‡	50	0.63	16.0	256.7	379.3	-	1.48
T2 Joint 6‡	50	0.63	16.0	378.0	375.0	-	0.99

† Loads predicted based on assuming the entire weld length is effective.
‡ (Frater, 1991)

The results from the full-scale welded overlapped connection tests were generally consistent with the observations for other rectangular HSS connections, in that the strength and rigidity of an unreinforced welded connection decrease as the branch-to-chord width ratio (β-ratio) decreases, as the branch member overlap (O_v) decreases, and as the chord wall slenderness value (B/t) increases (Packer & Henderson, 1997). The effect of branch overlap on weld strength was especially apparent for element d at the heel (see Figure 3-2), in joints with $B/t = 26.7$, where the effectiveness of the welds (at this location), as shown by the distributions of normal strain measured around the branch perimeter, and also the strength of the connections, decreased as O_v decreased. Appendix G contains additional data from the full-scale tests.

4.5. Results from Global Elastic Truss Tests

The results and observations from the two global elastic truss tests are presented in this section. The results from each test include 57 instantaneous axial force and in-plane bending moment measurements obtained by 114 SGs on the truss, and truss deflection profiles at various stages of loading.

For both tests, the truss was loaded at PP 4 (see Figure 3-1) to a maximum load of 110 kips at an MTS stroke rate of 0.0002 in/s. Data was continuously sampled at a rate of 2 Hz. There was a discrepancy between the load measured by the load cell in the MTS ram head and the sum of the loads measured by the two load cells at the supports (up to 2%, as shown in Figure 3-18). The sum of the load cells was used as the basis for all comparisons. Upon reaching the maximum load (nominally 110 kips as indicated by the load cells), the test was paused momentarily to ensure that data was collected. Elastic Test 1 (E1) was performed on the virgin truss before fracturing any welds, hence the truss was subsequently unloaded. Elastic Test 2 (E2) was performed on the truss after nine welded joints had been fractured and repaired. For this "elastic" test, the load was increased until buckling of member H (see Figure 3-1) occurred leaving the truss unrepairable.

Aside from the truss failure portion of E2, all of the members remained essentially elastic throughout the two tests validating the use of the following equation to calculate the axial loads:

$$P_n = \bar{\varepsilon} E A \qquad \textbf{4-4}$$

where $\bar{\varepsilon}$ is the average strain; E is the Young's modulus of elasticity of the member (as determined by the TC tests), and A is the measured cross sectional area of the particular member. Plane sections were assumed to have remained plane and thus the in-plane bending moments were calculated from the curvature of the member, φ, according to:

$$\begin{aligned} M_n &= \varphi E I \\ &= [(\varepsilon_1 - \varepsilon_2)/H] E I \end{aligned} \qquad \textbf{4-5}$$

Material linearity was verified by examining the load-strain relationships for all of the gages on the truss, located in Appendix I.1 for test E1 and in Appendix I.2 for test E2. In Equation 4-5, ε_1 and ε_2 are the strain on opposite faces of the HSS member and H is the member depth.

4.5.1. Elastic 1

An overall view of the test set-up assembly, for test E1, is shown in Figure 4-29. The measured axial force and in-plane bending moment distributions from the global elastic truss test E1 are shown in Figure 4-30 and Figure 4-31, respectively. It is interesting to note that even at a distance of 2.5B_b from the chord face along the branch members and 1.5B from the heel of the branch members along the chord (see Figure 3-20 (a)), shear lag effects are present, indicated by the non-uniform axial force measured at different locations along a member.

The measured deflection profile at the start of the experiment and at 50%, 80% and 100% of the maximum load (109.1 kips) is shown in Figure 4-32. Measured values of the support settlement and displacement at 50%, 80% and 100% of the maximum load are shown in Table 4-14 and Table 4-15, respectively.

The load-strain relationships for each of the 114 strain gages are located in Appendix I.1 and from them, spurious readings can be noted in strain gages E-3-O, L-9-O, N-3-I, O-N, O-P, T-9-I, V-6-I, and V-2-I, despite them having been checked following application. The strain gage labelling scheme is located in Appendix G.3.

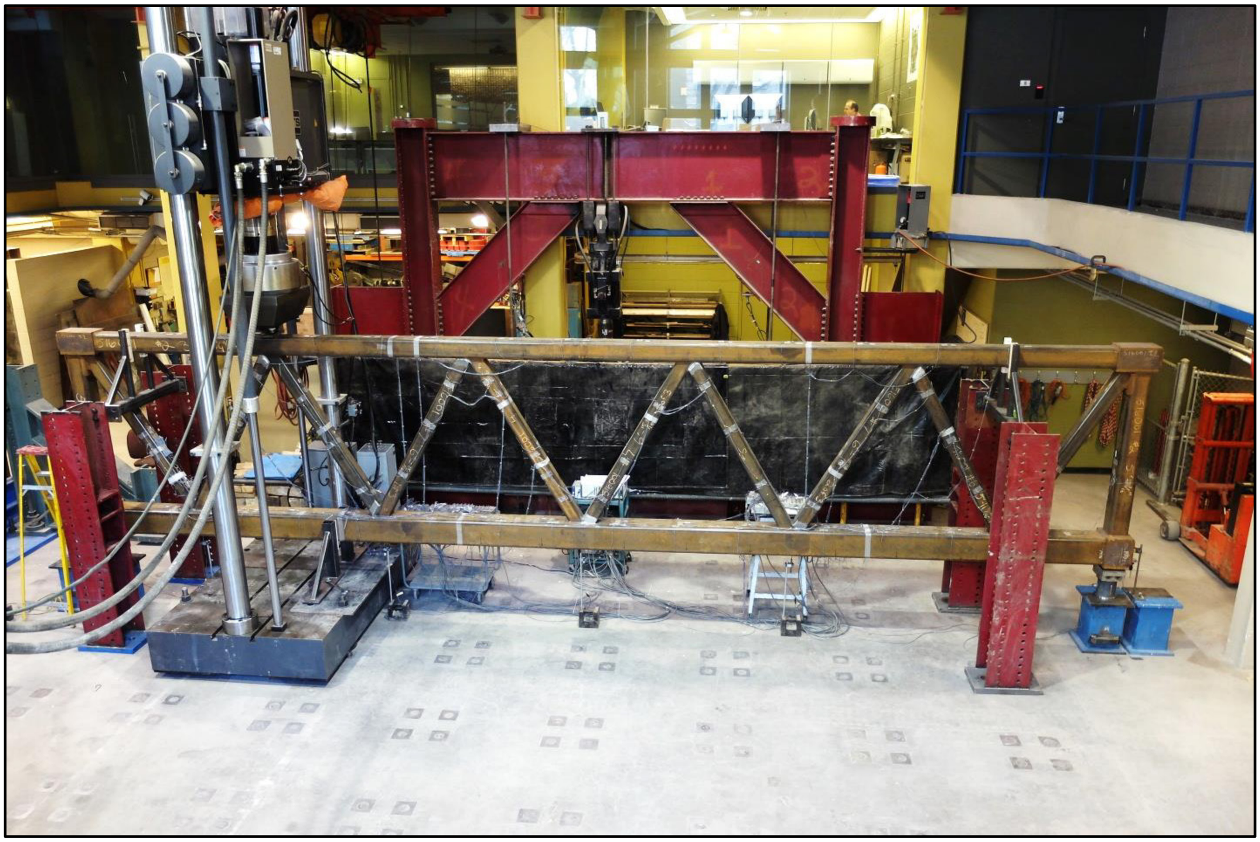

Figure 4-29 Overall view of the test set-up assembly for test 'Elastic 1' and K-90-0.50 (a)

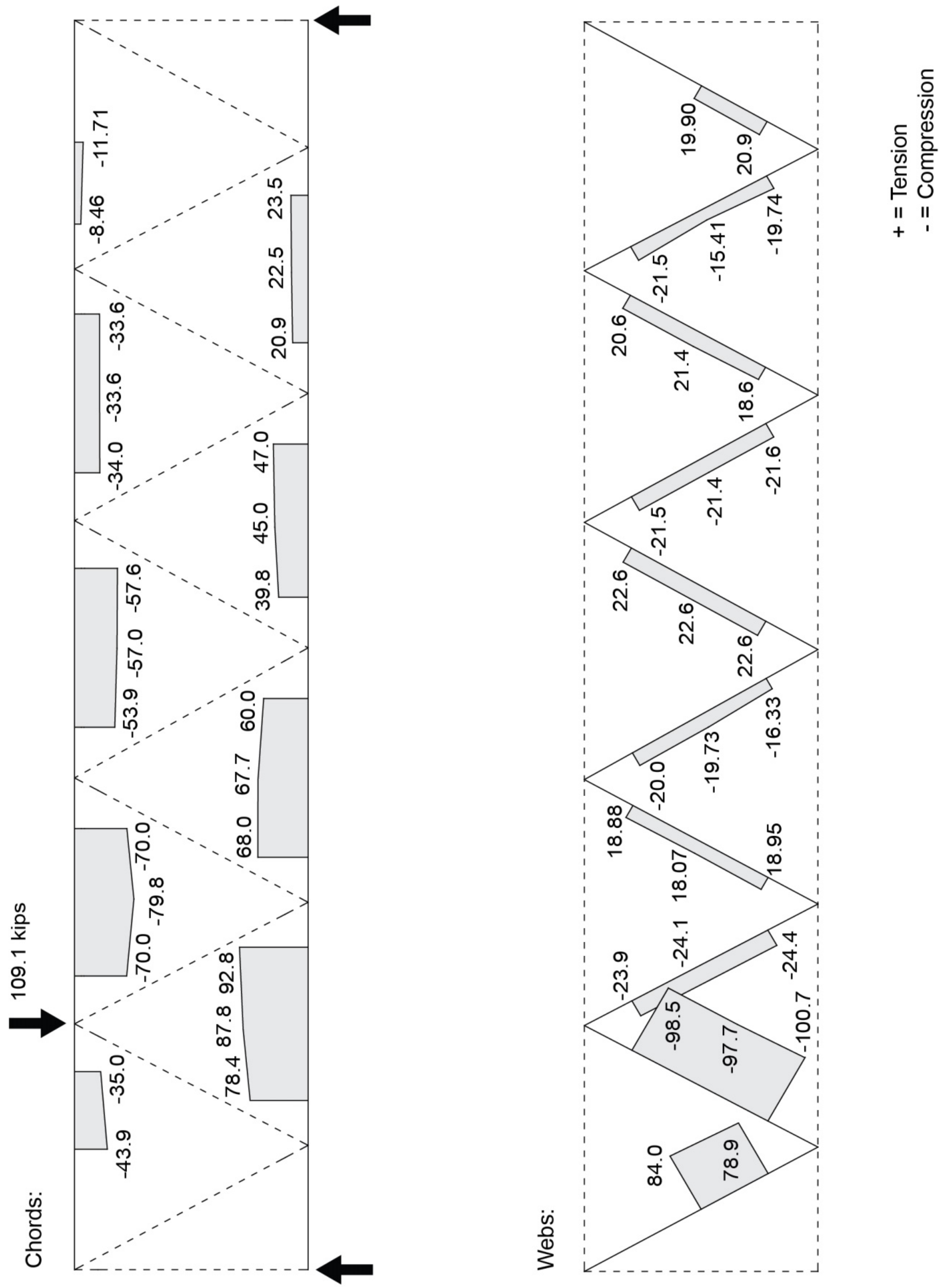

Figure 4-30 Experimental axial force distribution (in kips) for test 'Elastic 1'

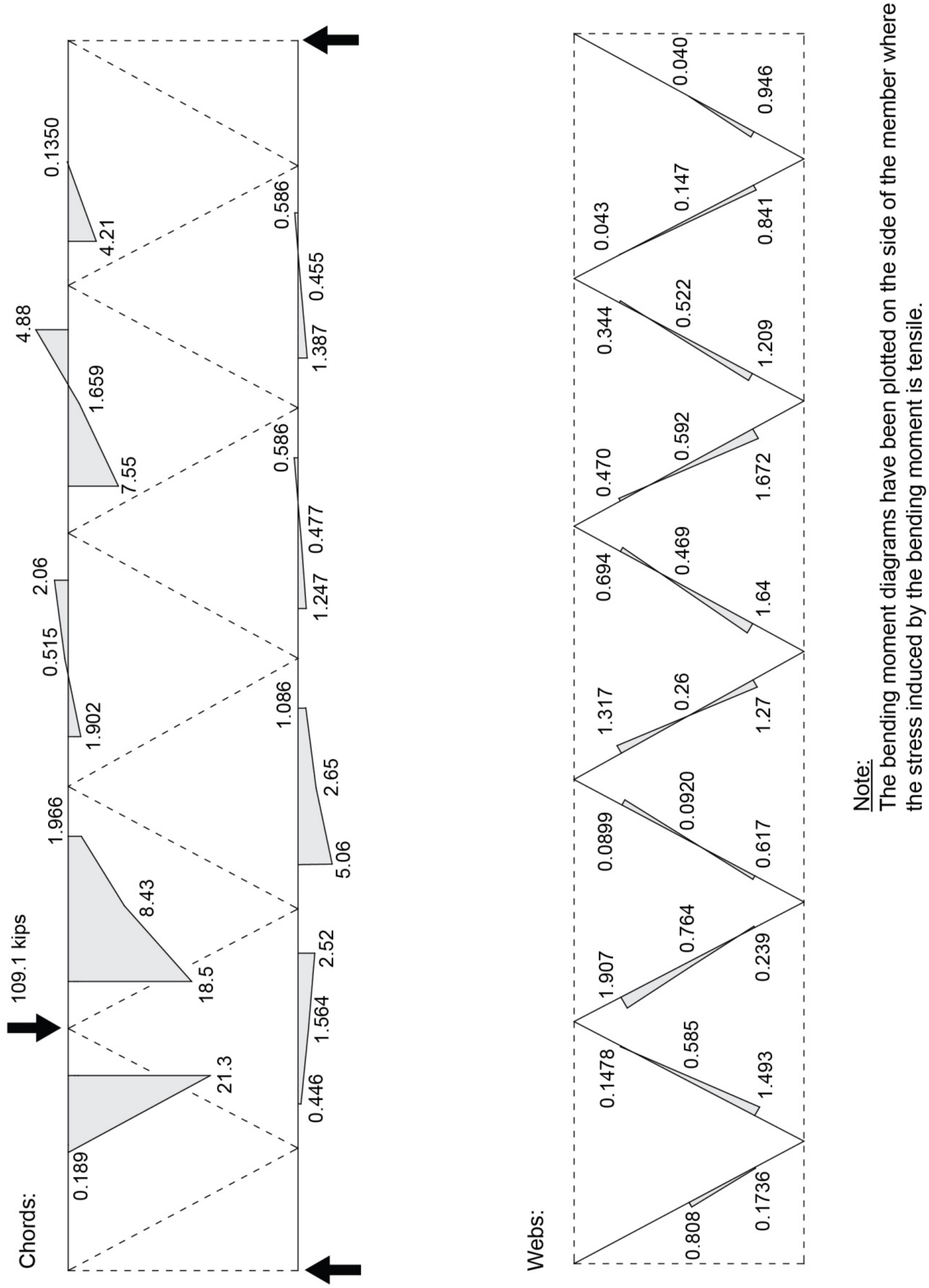

Figure 4-31 Experimental in-plane bending moment distribution (in kip-ft) for test 'Elastic 1'

Table 4-14 Experimental support settlement values for test 'Elastic 1'

Panel Point	Settlement (in.)	
	10	13
0.5 x Peak Load	0.0453	0.01701
0.8 x Peak Load	0.0636	0.0235
Peak Load (109.1 kips)	0.0823	0.0280

Table 4-15 Experimental panel point deflections for test 'Elastic 1'

Panel Point	Deflection Relative to Truss Ends (in.)				
	1	5	9	6	2
0.5 x Peak Load	0.0498	0.0972	0.0926	0.0683	0.0409
0.8 x Peak Load	0.0778	0.1490	0.1406	0.1042	0.0614
Peak Load (109.1 kips)	0.1098	0.205	0.1924	0.1421	0.0829

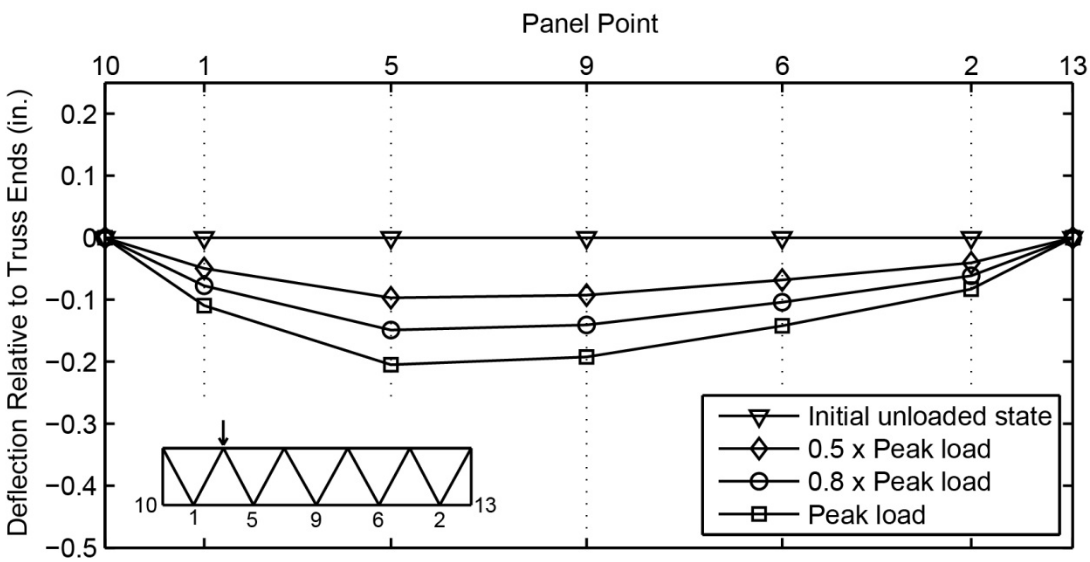

Figure 4-32 Truss bottom chord deflection profile for test 'Elastic 1'

4.5.2. Elastic 2

A modified test set up was used to perform test E2 (after the nine full-scale welded connection tests were completed). The modified test set up was designed to achieve the same effect as the original test set up but employed a 1200-kip capacity Baldwin Universal Testing Frame instead of the 600-kip capacity MTS Testing Frame. For this test, the end-plated HSS pedestals were not necessary and the load cells were located on the laboratory floor. An overall view of the assembly is shown in Figure 4-33.

Figure 4-33 Overall view of the test set up assembly for test 'Elastic 2'

The elastic component of Test E2 was recorded at a target load of 109.8 kips. The load was then increased until ultimate failure of the truss, which was governed by inelastic buckling of a compression strut (member H), and chord face rupture or "unzipping" at the connection, as a result of excessive joint rotation. Figure 4-34 shows the state of the truss at the end of the test. The inelastic buckling load was estimated to be 376 kips. This was deduced from the ratio of the load in this critical web member to the applied load, determined during the elastic tests, equal to 0.87, since axial loads in the plastic stress range are not calculable by Equation 4-4.

The measured axial force and in-plane bending moment distributions from the global elastic truss test E2 are shown in Figure 4-35 and Figure 4-36, respectively. The load of 109.8 kips is the sum of the loads measured by the two load cells at the supports. It is interesting to note the same trend as in test E1 with respect to shear lag at a distance of $2.5B_b$ from the chord face along the branch members and $1.5B$ from the heel of the branch members along the chord.

The measured deflection profile at the start of the experiment and at 50%, 80% and 100% of the weld rupture load is shown in Figure 4-37 . Measured values of the support settlement and displacement at 50%, 80% and 100% of the target load (109.8 kips) are shown in Table 4-16 and Table 4-17, respectively.

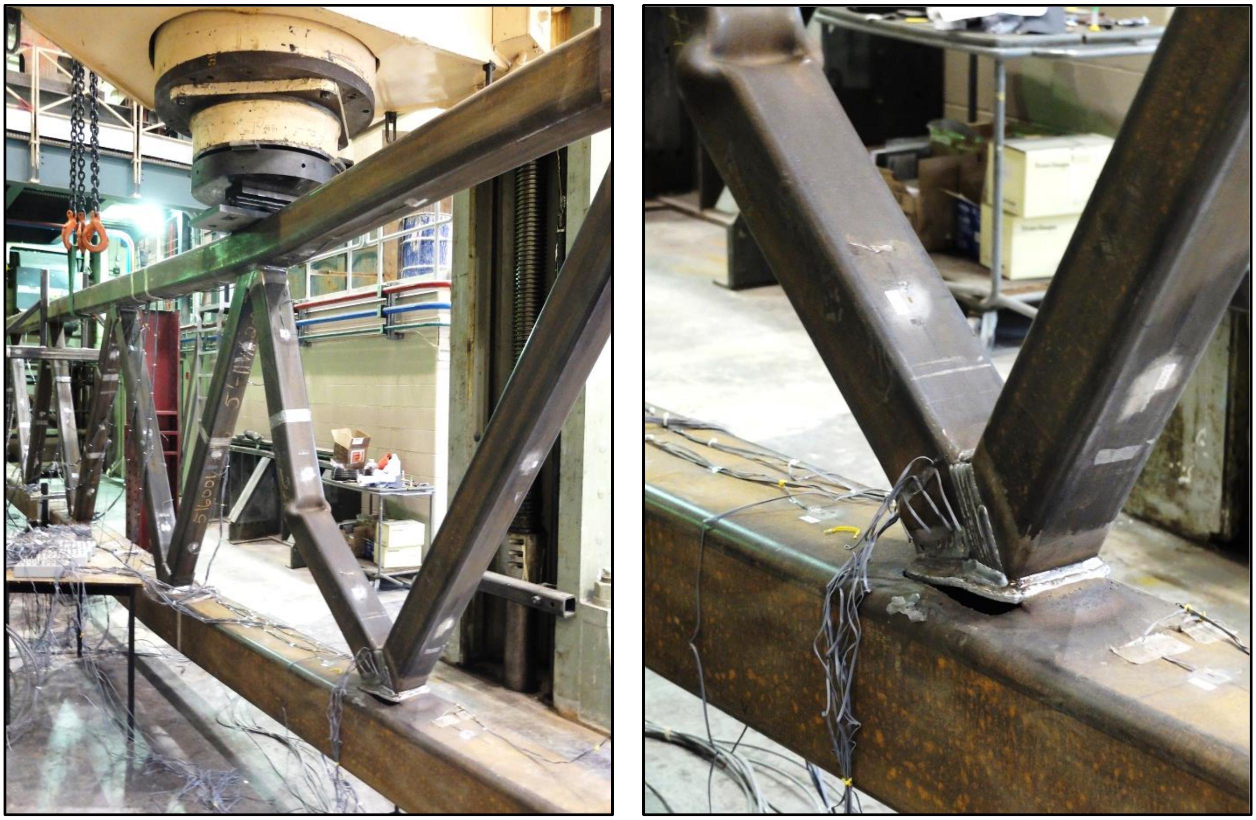

(a) Web member inelastic buckling (b) Chord face rupture

Figure 4-34 State of the truss following inelastic buckling of member H

The load-strain relationships for each of the 114 strain gages are located in Appendix I.2 and from them, spurious readings can be noted in strain gages D-7-I, O-N and O-P. The lesser number of spurious readings is because, with the experience of previous tests, many of the non-functioning strain gages were identified and replaced. The effect of the nine connections being stiffened/ strengthened as a result of over-welding and/ or plating, plus changes being made to the member alignment due to testing was minimal with respect to the change in axial force and bending moment distribution; however, upon inspection of the deflection raw data, it would appear that stiffening of the joints reduced the truss maximum deflection by 15%. This is not the case, as illustrated in Section 5.3.3 (where a detailed evaluation of the truss deflection results is conducted).

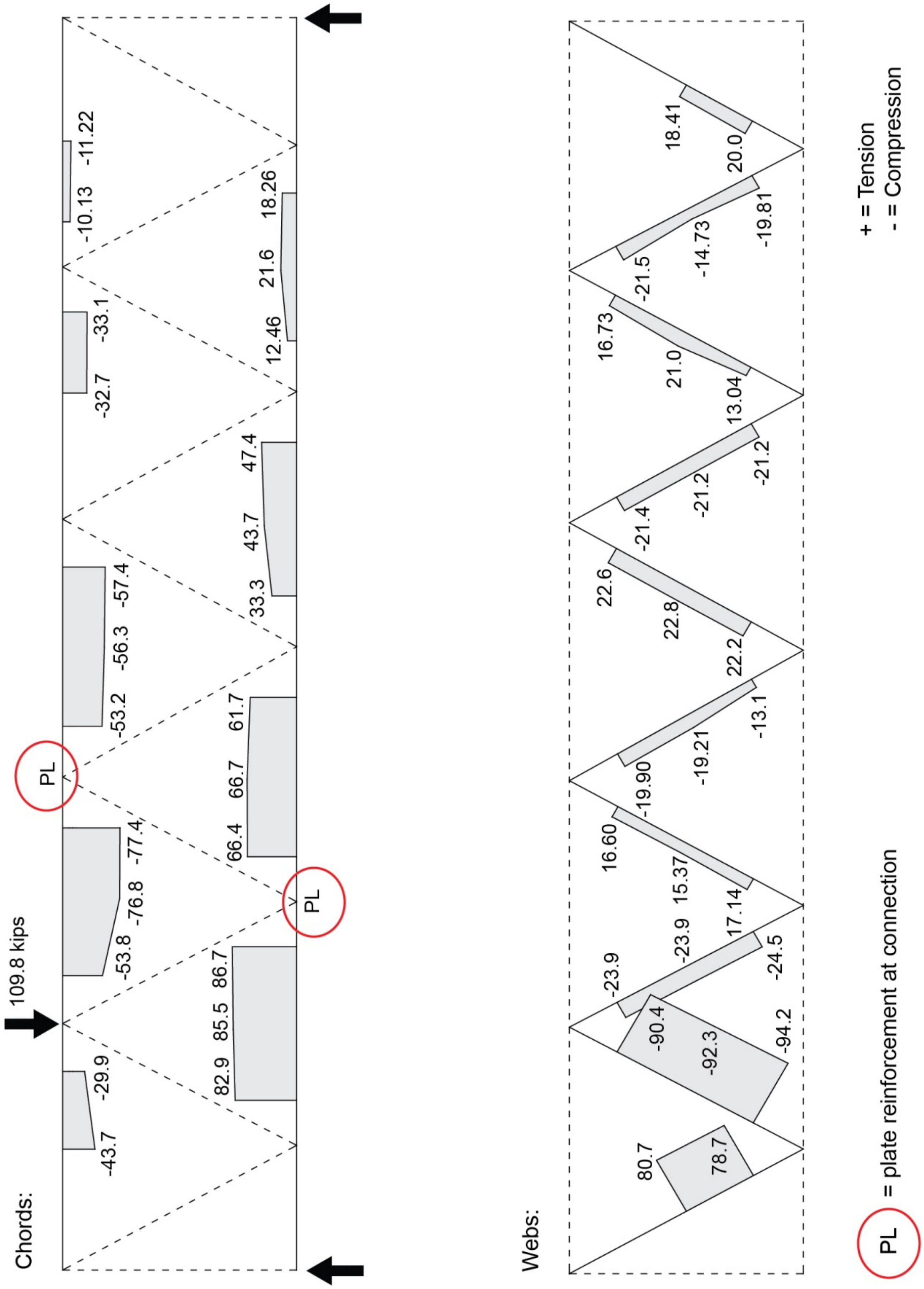

Figure 4-35 Experimental axial force distribution (in kips) for test ‘Elastic 2’

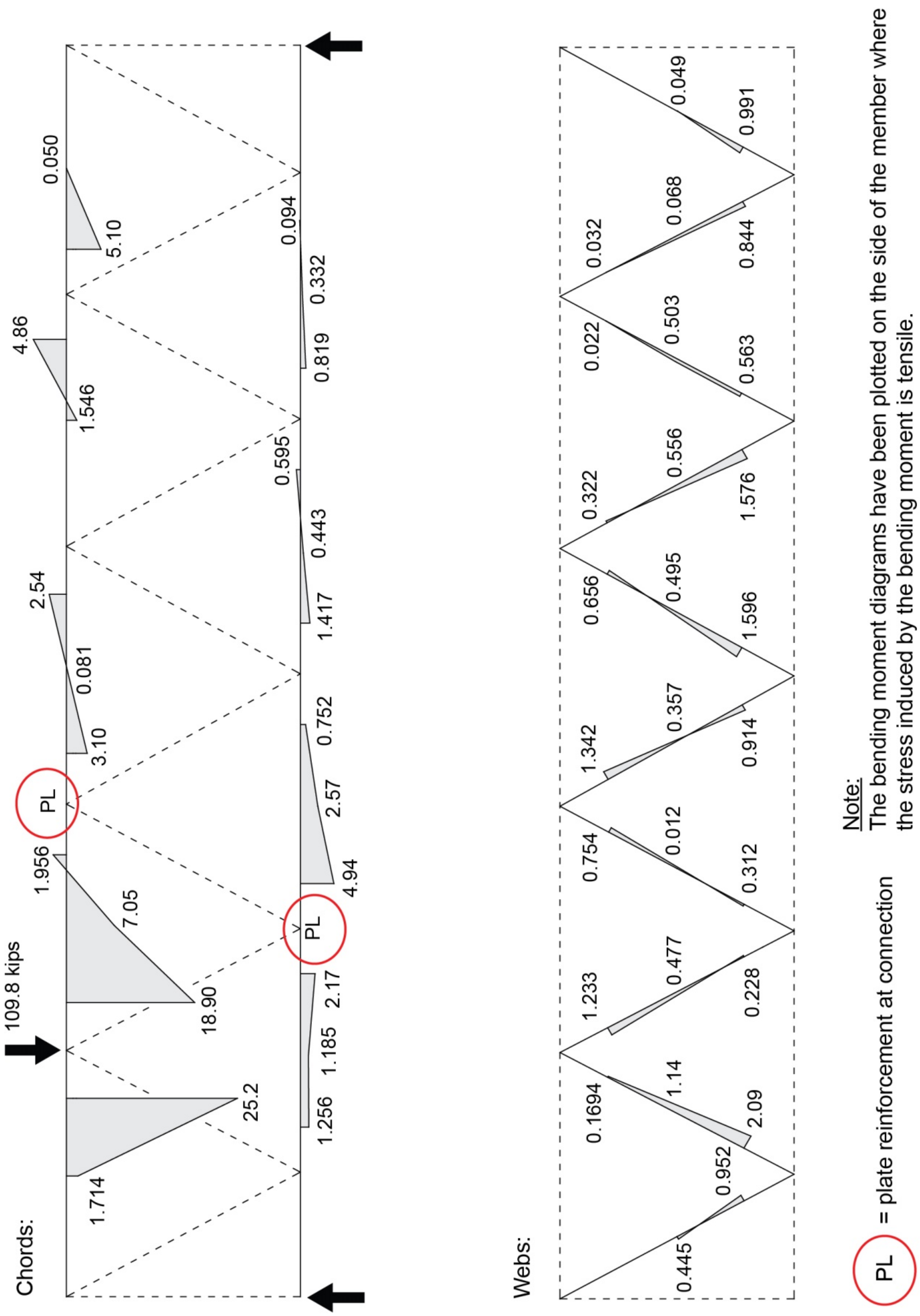

Figure 4-36 Experimental bending moment distribution (in kip-ft) for test 'Elastic 2'

Table 4-16 Experimental support settlement values for test 'Elastic 2'

Panel Point	Settlement (in.)	
	10	13
0.50 x Peak Load	0.0449	0.01004
0.80 x Peak Load	0.0613	0.01351
Peak Load (109.8 kips)	0.0732	0.01514

Table 4-17 Experimental panel point deflections for test 'Elastic 2'

Panel Point	Deflection Relative to Truss Ends (in.)				
	1	5	9	6	2
0.50 x Peak Load	0.0354	0.0879	0.0797	0.0530	0.0204
0.80 x Peak Load	0.0548	0.1330	0.1212	0.0799	0.0306
Peak Load (109.8 kips)	0.0728	0.1770	0.1620	0.1069	0.0406

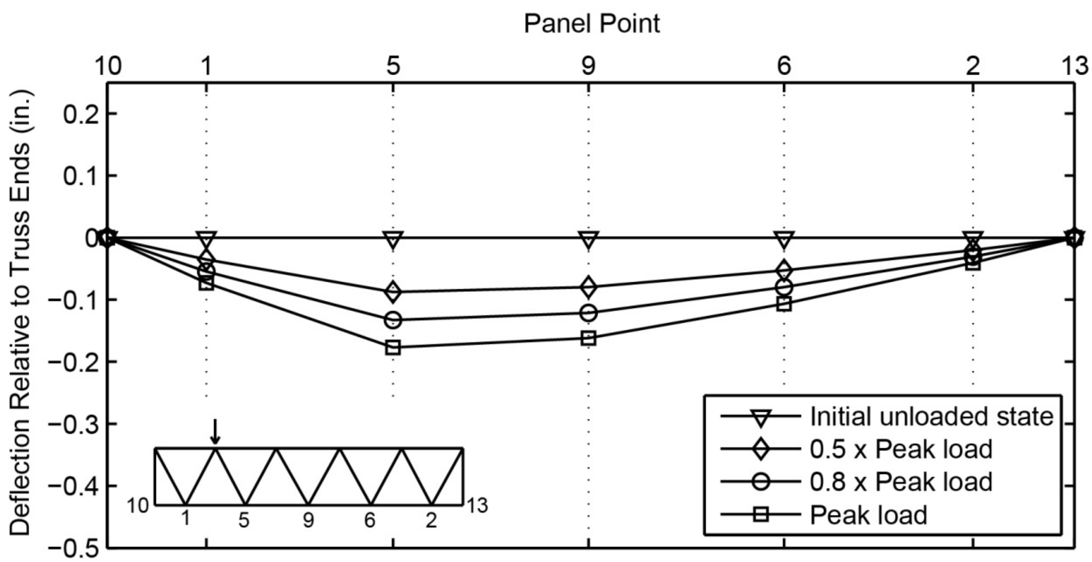

Figure 4-37 Truss bottom chord deflection profile for test 'Elastic 2'

Chapter 5: Evaluation of Results

The objective of this experimental program was to verify or adjust the current effective weld length provisions for rectangular HSS-to-HSS overlapped K-connections defined by Equations 2-19 to 2-21 and given in Table K4.1 of ANSI/AISC 360 (2010). The results for nine full-scale tests performed on weld-critical overlapped K-connections were presented in Chapter 4. In this section, correlation plots are produced using the measured ultimate weld strengths (or "rupture loads") from these tests and the results from two similar connection tests that were conducted at the University of Toronto (Frater, 1991). Using a safety index analysis, the inherent resistance factor is calculated for the following provisions:

- ANSI/AISC 360 (2010)
- ANSI/AISC 360 (2010), modified by proposal of McFadden & Packer (2013, 2014)
- ANSI/AISC 360 (2010), modified by withholding the restrictions to Equations K2-20 and K2-21 imposed by the clause "When $B_{bi}/B > 0.85$ or $\theta_i > 50°$, $b_{eoi}/2$ shall not exceed $2t$ and when $B_{bi}/B_{bj} > 0.85$ or $(180 - \theta_i - \theta_j) > 50°$, $b_{eov}/2$ shall not exceed $2t_{bj}$"

The analyses are repeated with the (1.00 + 0.50 $\sin^{1.5}\theta$) strength enhancement factor applied to fillet welds loaded at an angle of θ to their longitudinal axis. The "sin theta factor" for fillet welds is also tried in combination with the 0.6 factor on F_{EXX} for the tensile strength of PJP groove welds.

The theoretical axial forces, in-plane bending moments and deflections predicted by model P (all pinned), model R (all rigid), and model PR (continuous chord/ pin-ended webs) for loads applied to truss panel points are then compared to the results from two global elastic truss tests and deflections measured at an intermediate stage of the loading during eight of the nine weld tests.

5.1. Evaluation of Current Effective Weld Properties

The current effective weld lengths for rectangular HSS overlapped K-connections defined by Equations 2-19 to 2-21 and given in Table K4.1 of ANSI/AISC 360 (2010) are herein evaluated against the nine full-scale tests on weld-critical joints performed in this experimental program and two previous tests that achieved partial failure of the weld to the overlapping branch member (Frater, 1991). Table 4-13 (in Chapter 4) summarizes the observed (or "actual") strengths of the connections. The predicted nominal strengths are calculated using the measured geometric and mechanical properties of the HSS and weld metal. Weld sizes for the individual weld elements appear in Table 4-9. These were determined from epoxy castings (for fillet welds) and from external crown depth measurements (for PJP groove welds). Weld lengths and weld effective lengths ignore the rounded corners on all HSS branches, and use H_b and B_b, or proportions thereof. These weld lengths are given in Appendix G.1, and a summary of all the predicted strengths is located in Appendix G.2.

In order to assess whether adequate or excessive safety margins are inherent, one can check to ensure that a minimum safety index of $\beta^+ = 4.0$ (as currently adopted by ANSI/AISC 360 (2010) per Chapter B of the Specification Commentary) is achieved using a simplified reliability analysis in which the resistance factor (∅) is given by Equation 5-1 (Fisher et al., 1978; Ravindra & Galambos, 1978):

$$\emptyset = m_R \cdot exp(-\alpha \cdot \beta^+ \cdot COV) \qquad \textbf{5-1}$$

where $m_R =$ mean of the ratio : (actual element strength)/(predicted nominal element strength); $COV =$ associated coefficient of variation; and $\alpha =$ coefficient of separation taken to be 0.55 (Ravindra and Galambos, 1978).

Equation 5-1 relies solely on the so-called professional factor, a conservative approach used in the absence of reliable statistical data related to the welds. In order to evaluate the correlations discussed herein, a value of $\beta^+ = 4.0$ can be substituted into Equation 5-1, and the implied/inherent resistance factor, $\emptyset$, can be calculated. The higher of the resistance factors equal to 0.75 and 0.80 for fillet welds and PJP welds, as specified in Section K4 (AISC 360, 2010), is required.

Equation 5-1 was used to calculate an inherent resistance factor, ϕ, equal to 0.922 for the current effective weld length rules for rectangular HSS overlapped K-connections contained in Table K4.1 (AISC, 2010). The correlations to this effect are plotted in Figure 5-1. Since the implied resistance factor is larger than the resistance factors for fillet welds and PJP groove welds (0.75 and 0.80, respectively), the current equations for the effective length given in Table K4.1 (AISC, 2010) for welds in HSS overlapped K-connections can be deemed conservative.

The predicted nominal resistance of the welds was re-computed using the current effective weld length rules of AISC 360 (2010) with the 0.6 factor on F_{EXX} for the tensile strength of PJP groove welds. The correlation is given in Figure 5-2. Expectedly, the inclusion of the 0.6 factor on F_{EXX} for the tensile strength of PJP groove welds produces a very safe prediction for the nominal resistance of the welds (ϕ = 1.31). It is also shown that the inclusion of the 0.6 factor on F_{EXX} for the tensile strength of PJP groove welds provides a safe prediction for the singular connection which had uncertain root quality and was previously over- (unsafely) predicted. Thus, the arbitrary reduction merits inclusion despite its apparent excessive conservatism.

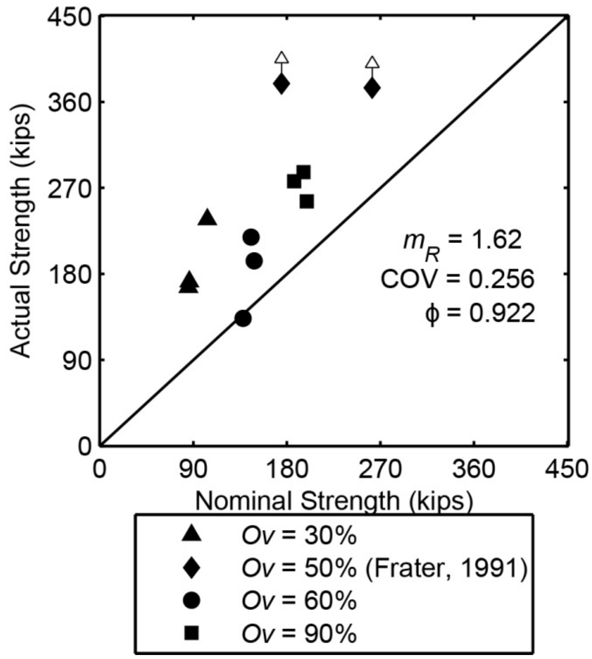

Figure 5-1 Correlation with test results for rectangular HSS-to-HSS overlapped K-connections using the current effective weld length rules of AISC 360 (2010) without the 0.6 factor on PJP welds and excluding the (1.00 + 0.50 sin$^{1.5}\theta$) term

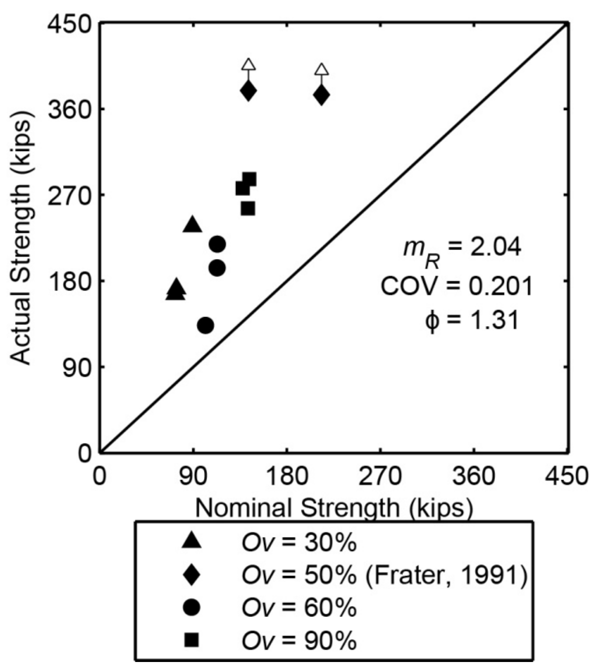

Figure 5-2 Correlation with test results for rectangular HSS-to-HSS overlapped K-connections using the current effective weld length rules of AISC 360 (2010) with the 0.6 factor on PJP welds and excluding the (1.00 + 0.50 sin$^{1.5}\theta$) term

The applicability of the (1.00 + 0.50 $\sin^{1.5}\theta$) term for fillet welds was investigated by application to the predicted nominal resistance of the welds using the current effective weld length rules of AISC 360 (2010), both with and without the 0.6 factor applied to the resistance of PJP groove welds. The (1.00 + 0.50 $\sin^{1.5}\theta$) term (or fillet weld directional strength enhancement factor) increased the predicted strength of weld elements loaded normal (θ = 90°) to the longitudinal axis of the weld (i.e. transverse elements) by a factor of 1.5, and increased the predicted strength of *fillet* welds along the height of the web member (θ = 60°) by a factor of 1.403. PJP groove welds are not covered under this factor. The correlations without the 0.6 factor on PJP groove welds, but including the (1.00 + 0.50 $\sin^{1.5}\theta$) term, are plotted in Figure 5-3 (a), and the correlations with the 0.6 factor on PJP groove welds and including the (1.00 + 0.50 $\sin^{1.5}\theta$) term are plotted in Figure 5-3 (b). The implied resistance factors, ϕ, under these provisions are 0.822 and 1.10, respectively.

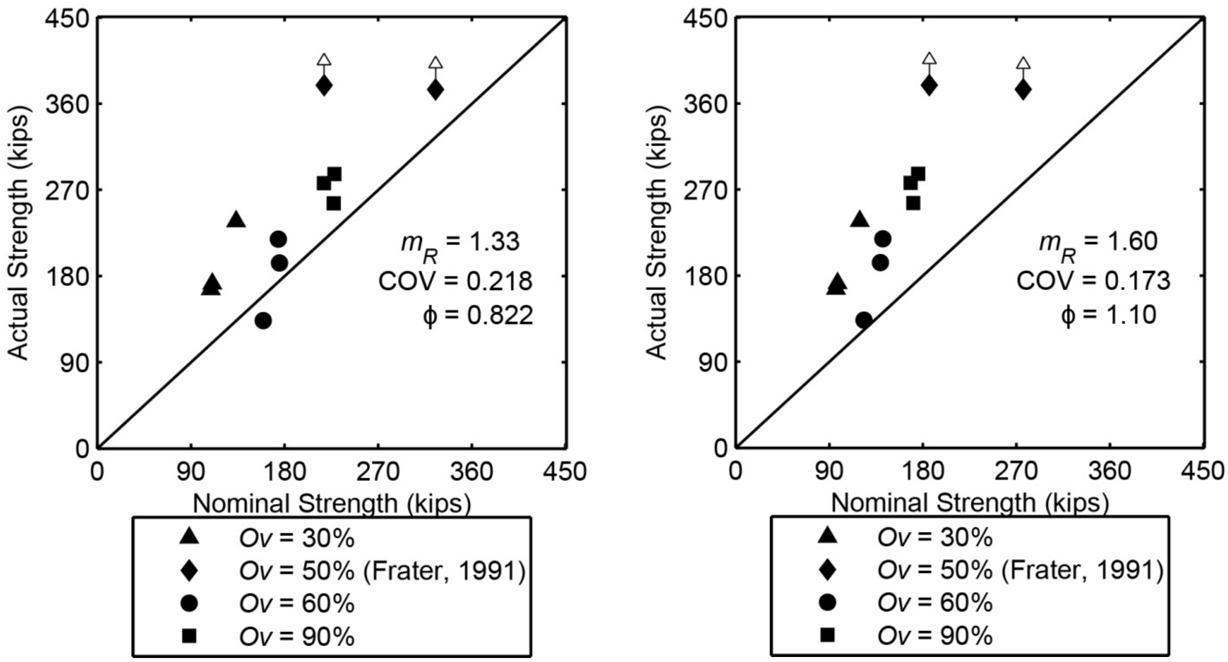

(a) Correlation without the 0.6 factor on PJP welds (b) Correlation with the 0.6 factor on PJP welds

Figure 5-3 Correlation with test results for rectangular HSS-to-HSS overlapped K-connections using the current effective weld length rules of AISC 360 (2010) including the (1.00 + 0.50 $\sin^{1.5}\theta$) term

Since $\phi \geq 0.8$, the fillet weld directional strength enhancement factor can be safely applied to the range of tested connections with the current effective weld length rules (Table K4.1) of AISC 360 (2010) for rectangular HSS overlapped K-connections. However, McFadden & Packer (2013, 2014) found that the fillet weld directional strength enhancement factor is unsafe when applied to other types of axially-loaded connections between HSS.

5.2. Evaluation of Modified Effective Weld Properties

5.2.1. Proposal by McFadden & Packer (2013, 2014)

As shown in the previous section, the current equations of AISC 360 (2010) for the effective length are quite conservative. Thus, modifying these equations to allow for a greater weld effective length can safely be done. In the Phase I Interim Report, McFadden & Packer (2013) found that the current equation for the effective elastic section modulus for in-plane bending (Equation 2-17) for rectangular HSS moment T-connections is also conservative, and proposed that the following requirement:

"When β > 0.85 or θ > 50°, $b_{eoi}/2$ shall not exceed 2t"

be modified to:

"When β > 0.85 or θ > 50°, $b_{eoi}/2$ shall not exceed $B_b/4$."

This modification increases the effective length of the transverse weld elements in many connections where the geometry is applicable, and was also valid for Equation 2-16, for axially-loaded HSS T- and X- (or Cross) connections. Thus, for consistency across Table K4.1 (AISC, 2010), a safe correlation with test results for HSS overlapped K-connections using this modified effective weld length rule (McFadden & Packer, 2013) would be favorable. Applying the modification to overlapped K-connections requires that the following clause:

"When $B_{bi}/B > 0.85$ or $\theta_i > 50°$, $b_{eoi}/2$ shall not exceed $2t$ and when $B_{bi}/B_{bj} > 0.85$ or $(180 - \theta_i - \theta_j) > 50°$, $b_{eov}/2$ shall not exceed $2t_{bj}$"

be modified to:

When $B_{bi}/B > 0.85$ or $\theta_i > 50°$, $b_{eoi}/2$ shall not exceed $B_{bi}/4$. and when $B_{bi}/B_{bj} > 0.85$ or $(180 - \theta_i - \theta_j) > 50°$, $b_{eov}/2$ shall not exceed $B_{bi}/4$."

The correlation plots from the previous section have been recalculated with the modified requirement and are shown in Figures 5-4 to 5-6. As shown, the modified requirement provides a resistance factor, ϕ, equal to 0.875 which is larger than those for fillet welds and PJP groove welds and hence, the modified requirement can be deemed adequately safe for overlapped K-connections. As in the previous section, the inclusion of the 0.6 factor to predict the strength of PJP groove welds merits inclusion to compensate for uncertain root details (see Figure 5-5); however, the use of the (1.00 + 0.50 $\sin^{1.5}\theta$) term in conjunction with the modified requirements is shown in Figure 5-6 (a) to be unsafe (ϕ = 0.756 < 0.8). Presuming that the effective length phenomenon is more closely captured by the modified equations, the result of this evaluation supports the theory that the (1.00 + 0.50 $\sin^{1.5}\theta$) term is unsafe when widely applied to all HSS connections. It is also worth noting that the (1.00 + 0.50 $\sin^{1.5}\theta$) term is only fortuitously safe when used in conjunction with the 0.6 factor on PJP groove welds (see Figure 5-6 (b)). It is thus an improvement and still conservative to predict the strength of rectangular HSS overlapped K-connections using the modified effective weld length rules of McFadden & Packer (2013, 2014).

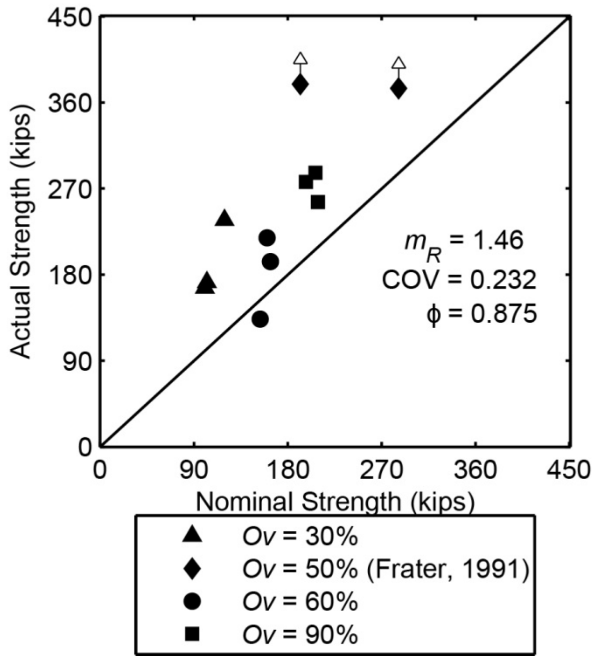

Figure 5-4 Correlation with test results for rectangular HSS-to-HSS overlapped K-connections using the modified effective weld length rules (McFadden & Packer, 2013) without the 0.6 factor on PJP welds and excluding the (1.00 + 0.50 sin$^{1.5}\theta$) term

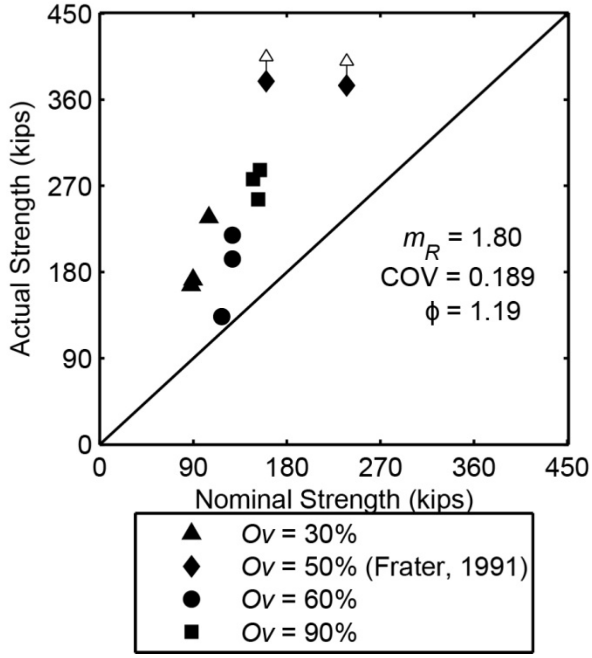

Figure 5-5 Correlation with test results for rectangular HSS-to-HSS overlapped K-connections using the modified effective weld length rules (McFadden & Packer, 2013) with the 0.6 factor on PJP welds and excluding the (1.00 + 0.50 sin$^{1.5}$*θ*) term

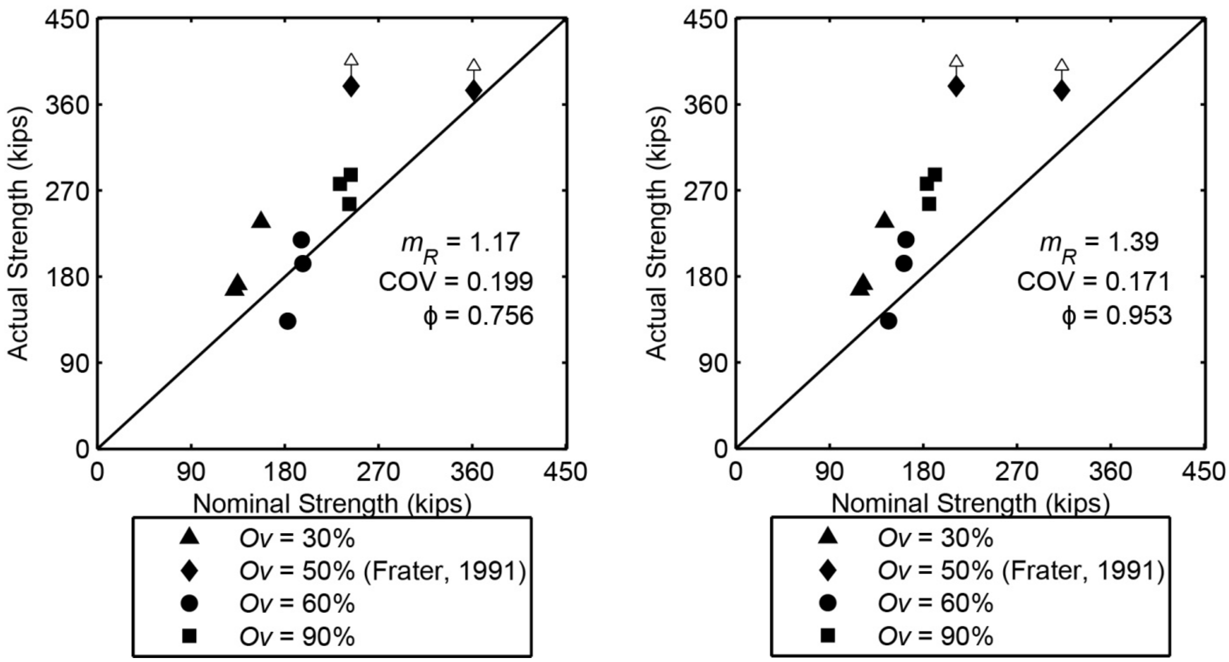

(a) Correlation without the 0.6 factor on PJP welds (b) Correlation with the 0.6 factor on PJP welds

Figure 5-6 Correlation with test results for rectangular HSS-to-HSS overlapped K-connections using the modified effective weld length rules (McFadden & Packer, 2013) including the (1.00 + 0.50 sin$^{1.5}$*θ*) term

5.2.2. Withholding the Restrictions to Equations K2-20 and K2-21

In Section 4.4, the branch strain distribution plots showed that the transverse welds were effective in resisting the applied loads beyond the limits imposed by the current requirements and the modified requirements proposed by McFadden & Packer (2013). In recognition of this, the requirements of Table K4.1 withholding the restrictions to Equations K2-20 and K2-21, akin to the Available Connection Axial Strength Equations found in Table K2.2 of AISC 360 (2010) for the overlapping branch member, were evaluated. The correlation plots are shown in Figure 5-7 and Figure 5-8.

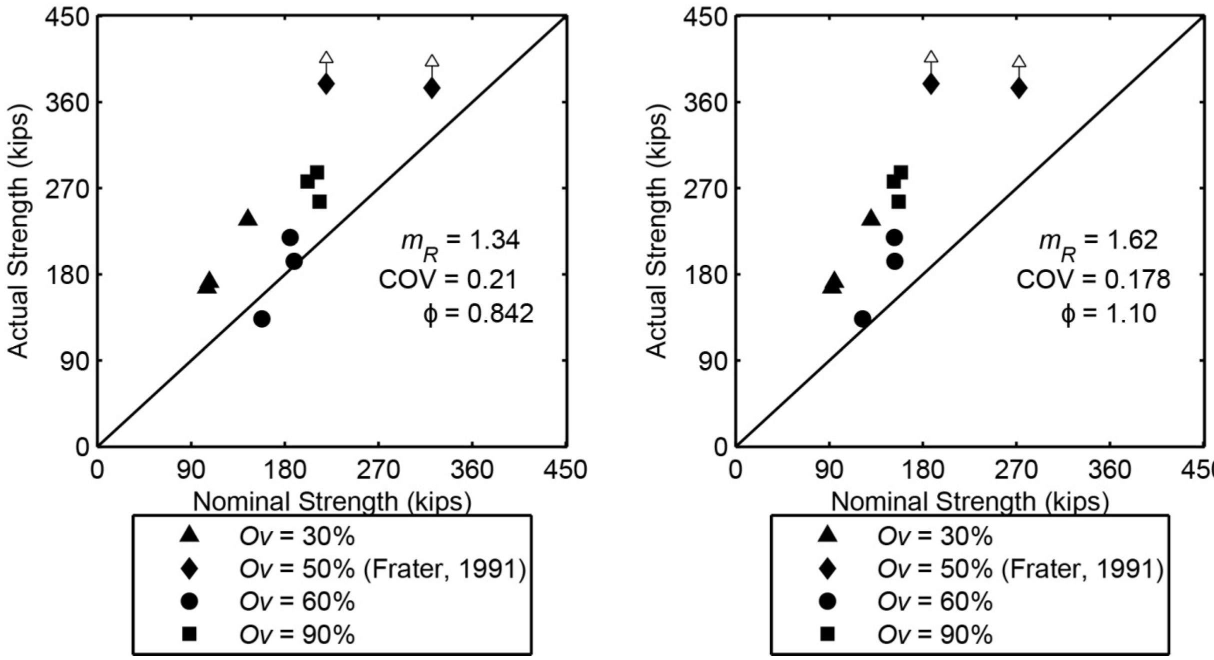

(a) Correlation without the 0.6 factor on PJP welds (b) Correlation with the 0.6 factor on PJP welds

Figure 5-7 Correlation with test results for rectangular HSS-to-HSS overlapped K-connections using the unrestricted effective weld length rules of AISC 360 (2010) excluding the (1.00 + 0.50 $\sin^{1.5}\theta$) term

As shown in Figure 5-7 (a), the limits in Table K4.1 are not necessary (ϕ = 0.842 > 0.80) and removing them alleviates excess conservatism and thereby reduces the required weld sizes for overlapped K-connections. The trends identified with respect to the 0.6 factor on PJP groove welds and for the (1.00 + 0.50 $\sin^{1.5}\theta$) term for the modified requirements of Table K4.1 proposed by McFadden & Packer (2013) persist: the inclusion of the 0.6 factor to predict the strength of PJP groove welds continues to merit inclusion to compensate for uncertain root details (see Figure 5-7 (a) versus (b)); and the (1.00 + 0.50 $\sin^{1.5}\theta$) term used in conjunction with the modified requirements (see Figure 5-8) is more unsafe (ϕ = 0.707), as expected.

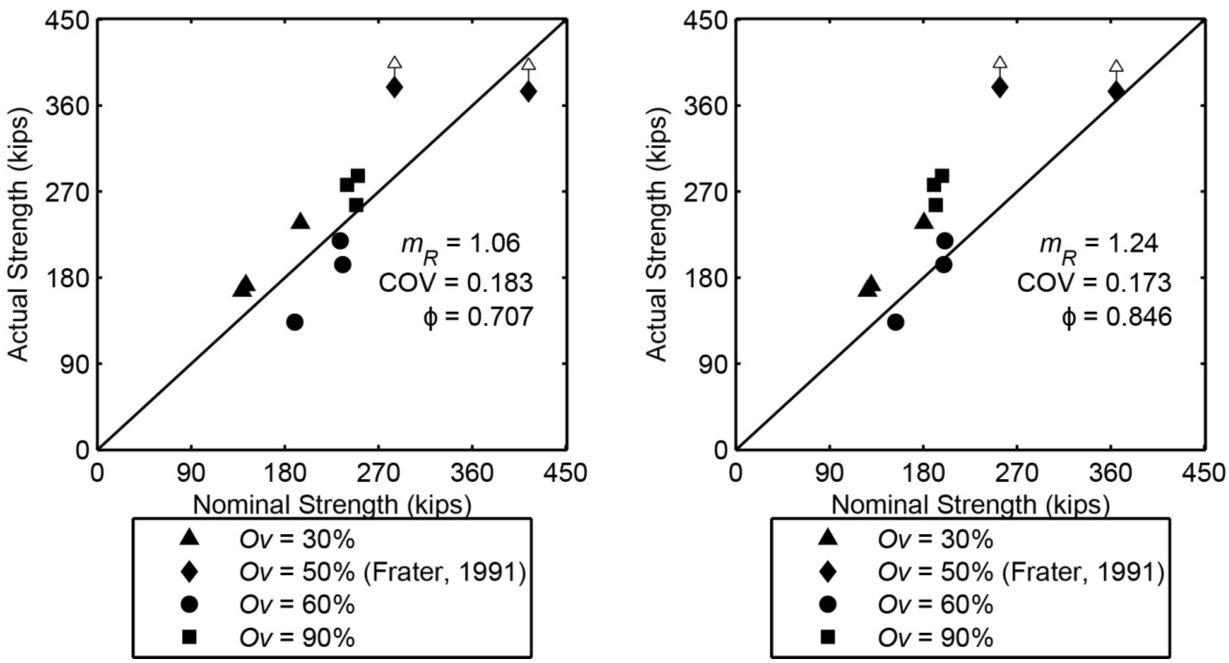

(a) Correlation without the 0.6 factor on PJP welds (b) Correlation with the 0.6 factor on PJP welds

Figure 5-8 Correlation with test results for rectangular HSS-to-HSS overlapped K-connections using the unrestricted effective weld length rules of AISC 360 (2010) including the (1.00 + 0.50 sin$^{1.5}$*θ*) term

The use of these modified provisions would not result in uniform rules across Table K4.1 for determining the resistance of welds in rectangular HSS connections. Additionally, since weld rupture can be quite sudden and without warning, it is recommended to maintain conservatism to compensate for geometric connection parameters which have not been experimentally corroborated. Therefore it is suggested that the following requirement:

"When $B_{bi}/B > 0.85$ or $\theta_i > 50°$, $b_{eoi}/2$ shall not exceed $2t$ and when $B_{bi}/B_{bj} > 0.85$ or $(180 - \theta_i - \theta_j) > 50°$, $b_{eov}/2$ shall not exceed $2t_{bj}$"

be modified to:

"When $B_{bi}/B > 0.85$ or $\theta_i > 50°$, or when $B_{bi}/B_{bj} > 0.85$ or $(180 - \theta_i - \theta_j) > 50°$, $b_{eoi}/2$ shall not exceed $B_{bi}/4$."

Table 5-1 shows a summary of the combinations that were evaluated with unsafe results ($\phi < 0.80$) in bold typeface; additional correlations, for combinations that exclude outlying data, are given in Appendix K.

Table 5-1 Summary of results from 12 reliability analyses on changes to the current Table K4.1 provisions (AISC 360-10)

	A	B	C	D
ANSI/AISC	m_R = 1.62 COV = 0.26 ϕ = 0.922	m_R = 2.04 COV = 0.20 ϕ =1.31	m_R = 1.33 COV = 0.22 ϕ = 0.822	m_R = 1.60 COV = 0.17 ϕ = 1.10
Modified AISC 360-10 per McFadden & Packer (2013)	m_R = 1.46 COV = 0.23 ϕ = 0.875	m_R = 1.80 COV = 0.19 ϕ = 1.19	**$\boldsymbol{m_R}$ = 1.17** **COV = 0.20** **ϕ = 0.756**	m_R = 1.39 COV = 0.17 ϕ = 0.953
Modified AISC 360-10 per Section 5.2.2	m_R = 1.34 COV = 0.21 ϕ = 0.842	m_R = 1.62 COV = 0.18 ϕ = 1.10	**$\boldsymbol{m_R}$ = 1.06** **COV = 0.18** **ϕ = 0.707**	m_R = 1.24 COV = 0.17 ϕ = 0.846

A – without the 0.6 factor on PJP welds and excluding the (1.00 + 0.50 $\sin^{1.5}\theta$) term
B – with the 0.6 factor on PJP welds and excluding the (1.00 + 0.50 $\sin^{1.5}\theta$) term
C – without the 0.6 factor on PJP welds and including the (1.00 + 0.50 $\sin^{1.5}\theta$) term
D – with the 0.6 factor on PJP welds and including the (1.00 + 0.50 $\sin^{1.5}\theta$) term

5.2.3. Incorporating Experimental Results

A total of 9 full-scale tests were performed on weld-critical test joints and the prior analysis has included two prior tests on welded overlapped joints, conducted by Frater (1992). In the 11 tests that constitute the data, the branch inclination angle was limited to 60°, web members were matched, and the span-to-depth ratios were similar (13.4 and 13). It was thus recommended to err on the side of safety and maintain excess conservatism to compensate for geometric connection parameters which have not been experimentally corroborated. This section discusses the observations from the trends in Table 5-1 and Section 4.4, and is thus only applicable to the range of connection parameters tested.

It was shown in Section 5.2 that limits in Table K4.1 are not necessary (ϕ = 0.842) for overlapped rectangular HSS K-connections. Furthermore, a partial safety factor included in Equations K2-20 and K2-21 (AISC, 2010; Davies & Packer, 1982) may lead to excessive conservatism. In Section 4.4, the branch strain distribution plots showed that the transverse welds were also more effective than predicted, and that the transverse weld along the toe of the branch member was fully effective regardless of overlap. (Admittedly, in these tests the toe of the overlapping branch landed on a stiff transverse HSS wall, with B_{bj}/t_{bj} = 16.3). The $O_v/50$ term that reduces the strength of the longitudinal welds in joints with 30% overlap is excessively conservative, and the strength of welds in joints with 90% overlap can be most accurately predicted by assuming a fully effective weld perimeter. Incorporating these observations into weld effective length rules, Equations 2-19, 2-20, and 2-21 are modified to Equations 5-2, 5-3, and 5-4, respectively:

When $25\% \leq O_v < 50\%$:

$$l_{e,overlapping\ branch} = 2\left[\left(1-\frac{O_v}{100}\right)\left(\frac{H_{bi}}{\sin\theta_i}\right)+\frac{O_v}{100}\left(\frac{H_{bi}}{\sin(\theta_i+\theta_j)}\right)\right]+b_{eoi}+B_{bj} \qquad \textbf{5-2}$$

When $50\% \leq O_v < 80\%$:

$$l_{e,overlapping\ branch} = 2\left[\left(1-\frac{O_v}{100}\right)\left(\frac{H_{bi}}{\sin\theta_i}\right)+\frac{O_v}{100}\left(\frac{H_{bi}}{\sin(\theta_i+\theta_j)}\right)\right]+b_{eoi}+B_{bj} \qquad \textbf{5-3}$$

When $80\% \leq O_v \leq 100\%$:

$$l_{e,overlapping\ branch} = 2\left[\left(1-\frac{O_v}{100}\right)\left(\frac{H_{bi}}{\sin\theta_i}\right)+\frac{O_v}{100}\left(\frac{H_{bi}}{\sin(\theta_i+\theta_j)}\right)\right]+B_{bi}+B_{bj} \qquad \textbf{5-4}$$

where:

$$b_{eoi} = \frac{11.7}{B/t}\left(\frac{F_y t}{F_{ybi} t_{bi}}\right) B_{bi} \leq B_{bi} \qquad \textbf{5-5}$$

Figure 5-9 (a) shows the correlation for all test data used previously and Figure 5-9 (b) shows the correlation for range of test data for which there is high confidence in workmanship and test methods, thus omitting tests that failed prematurely or by a failure mode other than weld rupture.

These modifications in Figure 5-9 produce a resistance factor, ϕ = 0.72 < 0.80 and are unsafe when the outlying tests are included. However, if the outlying data is removed, these modifications provide a resistance factor, ϕ = 0.87 and a COV equal to 0.11 which indicates a quite good fit. Note that these observations and correlations are only relevant for the range of connection parameters studied in these experiments and that further research would be required to verify if they are applicable to the full range of rectangular HSS overlapped K-connections.

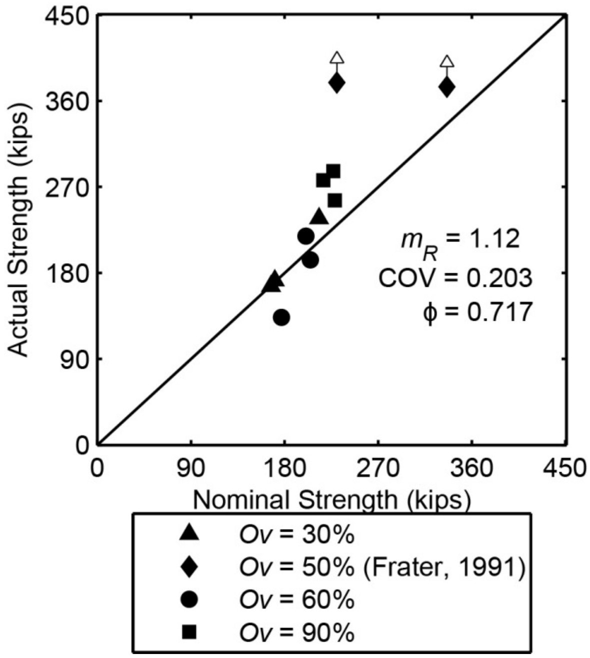

(a) Including all 11 tests on weld-critical overlapped K-connections

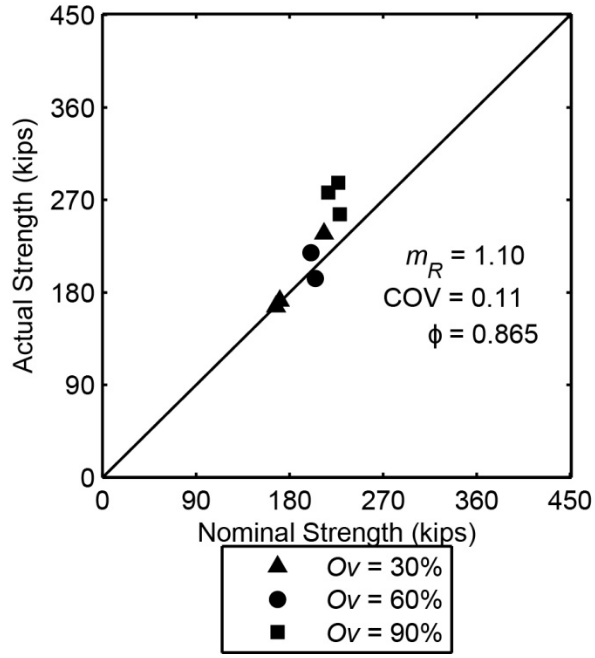

(b) omitting tests that failed prematurely or by a failure mode other than weld rupture

Figure 5-9 Correlation with test results for rectangular HSS-to-HSS overlapped K-connections based on Equations 5-2, 5-3, and 5-4.

5.3. Evaluation of Predictive Models for Axial Forces, Bending Moments and Truss Deflections

The measured elastic forces and deflections from two global truss tests undertaken at the beginning and end of the experimental program, which were presented in Section 4.5, are herein compared to three methods of elastic analysis that were applied using a SAP2000 structural model of the truss:

- A pin-jointed analysis (or “model P”)
- A rigid-jointed analysis (or “model R”)
- A combined pin- and rigid-joint model where web members are pin-connected to continuous chord members (or “model PR")

In the first two methods, the true centerline-to-centerline depth was modeled (as opposed to using the true web member inclination angle) due to a variable noding eccentricity at connections along the chords. The analysis incorporated the actual geometric and mechanical properties of the HSS sections through property modifiers, and was based on nominal truss dimensions. The sum of the load measured by the two load cells was taken as the basis for comparison and thus applied to the appropriate panel point as a single compressive point load.

5.3.1. Axial Forces

Table 5-2 gives the experimental and theoretical ratio of the web member load to the MTS load, as well as correlation factors for Models P, R, and PR from test E1.

Table 5-2 Comparison of the theoretical axial forces given by model P, model R and model PR with the experimental axial forces for test 'Elastic 1'

Member‡	Actual	Model P		Model R		Model PR	
	Load Ratio†	Load Ratio†	A/P	Load Ratio†	A/P	Load Ratio†	A/P
A	0.39	0.44	0.90	0.41	0.95	0.40	0.98
B	0.71	0.75	0.95	0.73	0.98	0.72	0.98
C	0.51	0.53	0.96	0.53	0.96	0.53	0.96
D	0.30	0.32	0.94	0.31	0.95	0.31	0.95
E	0.10	0.11	0.94	0.11	0.96	0.11	0.98
F	-	-	-	-	-	-	-
G	0.75	0.89	0.84	0.76	0.99	0.77	0.97
H	0.87	0.88	0.99	0.85	**1.02**	0.87	1.00
I	0.21	0.22	0.98	0.19	**1.10**	0.22	0.96
J	0.16	0.22	0.73	0.19	0.84	0.19	0.86
K	0.18	0.22	0.79	0.21	0.83	0.20	0.90
L	0.20	0.22	0.91	0.22	0.92	0.22	0.91
M	0.19	0.22	0.86	0.22	0.88	0.21	0.90
N	0.19	0.22	0.87	0.22	0.88	0.21	0.92
O	0.18	0.22	0.84	0.21	0.90	0.21	0.88
P	0.18	0.22	0.79	0.20	0.89	0.20	0.87
Q	-	-	-	-	-	-	-
R	-	-	-	-	-	-	-
S	0.78	0.85	0.92	0.81	0.96	0.84	0.94
T	0.60	0.64	0.94	0.63	0.95	0.63	0.96
U	0.40	0.42	0.94	0.42	0.95	0.42	0.95
V	0.20	0.21	0.94	0.21	0.95	0.21	0.95
W	-			-	-	-	-
Mean A/P Ratio			**0.90**		**0.94**		**0.94**

Note: values in bold typeface indicate unsafe predictions.
‡ Member labelling scheme corresponds to Figure 3-1.
† Load Ratio = the ratio of the axial force in any web member or section of the chords to the applied MTS load.

Experimental axial forces were derived from strain gages located at mid-length of the members. For test E1, Model R and Model PR give similar values for the axial force distribution and are generally more accurate than Model P, but model R unsafely predicts the forces for some web members. Accordingly, model R has not been suggested for conventional truss design (Packer et al., 2009). Chord axial forces were generally predicted very well (to within 5%). Erroneous strain gage readings at the mid-height of member O (see Figure 3-1) caused all models to show poor correlation with the experimentally derived axial forces at this location. Hence, in Table 5-2, the experimental axial force in member O is instead taken as the average of the two end SG readings.

Table 5-3 gives the experimental and theoretical ratio of the web member load to the MTS load, as well as correlation factors for Models P, R, and PR from test E2. The actual-to-predicted force values indicate that the analytical models better predicted the axial force distribution in test E1. This may be attributable to two things:

- repair of connections with gaps still present, thereby modifying the truss geometry; and
- stiffening/ strengthening of some joints relative to others by over-welding or the use of web plate reinforcement used to weld over the gaps.

Despite a general degradation in performance, the axial force distributions predicted by models R and PR are still better than the axial force distribution predicted by Model P, and model R still unsafely predicts the forces for some web members. The actual values of the measured and predicted member loads are given in Appendix I.3.

Table 5-3 Comparison of the theoretical axial forces given by model P, model R and model PR with the experimental axial forces for test 'Elastic 2'

Member‡	Actual	Model P		Model R		Model PR	
	Load Ratio†	Load Ratio†	A/P	Load Ratio†	A/P	Load Ratio†	A/P
A	0.39	0.44	0.88	0.42	0.93	0.40	0.97
B	0.68	0.75	0.91	0.73	0.93	0.73	0.94
C	0.50	0.54	0.93	0.53	0.94	0.54	0.93
D	0.29	0.32	0.91	0.32	0.92	0.32	0.92
E	0.10	0.11	0.89	0.11	0.91	0.11	0.93
F	-	-	-	-	-	-	-
G	0.72	0.90	0.80	0.76	0.94	0.78	0.92
H	0.82	0.89	0.92	0.86	0.95	0.88	0.93
I	0.21	0.22	0.98	0.20	**1.08**	0.23	0.94
J	0.14	0.22	0.62	0.19	0.71	0.19	0.72
K	0.17	0.22	0.76	0.21	0.80	0.20	0.86
L	0.20	0.22	0.91	0.22	0.92	0.22	0.91
M	0.19	0.22	0.84	0.22	0.86	0.21	0.88
N	0.19	0.22	0.84	0.22	0.86	0.21	0.90
O	0.13	0.22	0.59	0.21	0.61	0.21	0.62
P	0.16	0.22	0.73	0.20	0.81	0.20	0.80
Q	-	-	-	-	-	-	-
R	-	-	-	-	-	-	-
S	0.76	0.85	0.89	0.82	0.92	0.84	0.90
T	0.59	0.65	0.92	0.64	0.93	0.63	0.93
U	0.39	0.43	0.91	0.42	0.92	0.42	0.92
V	0.19	0.21	0.89	0.21	0.91	0.21	0.90
W	-	-	-	-	-	-	-
Mean A/P Ratio			**0.86**		**0.90**		**0.90**

Note: underlined values in bold typeface indicate unsafe predictions.
‡ Member labelling scheme corresponds to Figure 3-1.
† Load Ratio = the ratio of the axial force in any web member or section of the chords to the applied MTS load.

5.3.2. In-Plane Bending Moments

Figure 5-10 and Figure 5-11 show a comparison of the experimental and theoretical elastic in-plane bending moment distributions (model R and model PR) for global elastic truss tests E1 and E2, respectively. The sense of bending is often correct; however, based on these figures, the theoretical bending moments along the chords show poor numerical agreement with the experimental bending moments from both models – especially under the loading point.

In previous large-scale truss tests (Frater, 1991), it was found that large bending moments adjacent to the loading point may arise when chord rotation is restrained, either mechanically or by the loading mechanism itself. Presuming that the point load device used inadvertently prevented chord rotation at the loading point, an investigation was conducted into the applicability of applying a zero-rotation constraint to PP 4 in the SAP2000 structural model. In doing so, the axial force distributions predicted by all of the models improved marginally and the magnitude of the predicted bending moments improved marginally; however, the sense of bending predicted by all of the models diminished, especially in the web members where the models almost always wrongly predict the side of the member where the stress induced by the bending moment is tensile. The resulting axial force and in-plane bending moment distributions from Model R and Model PR, utilizing a zero-slope constraint to PP 4, are located in Appendix I.4.

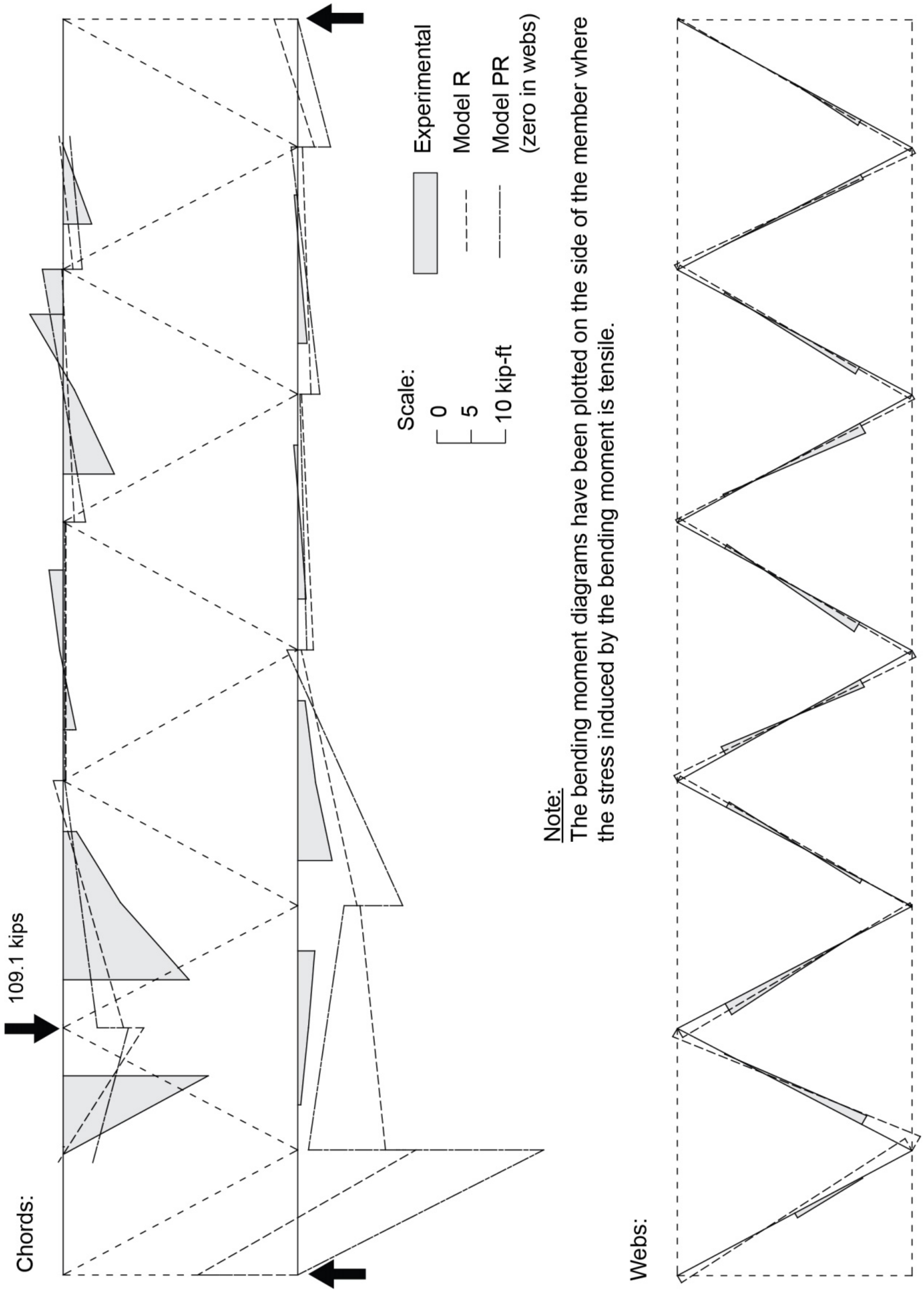

Figure 5-10 Comparison of the theoretical in-plane bending moment distribution given by model R and model PR with the experimental in-plane bending moment distribution for test 'Elastic 1'

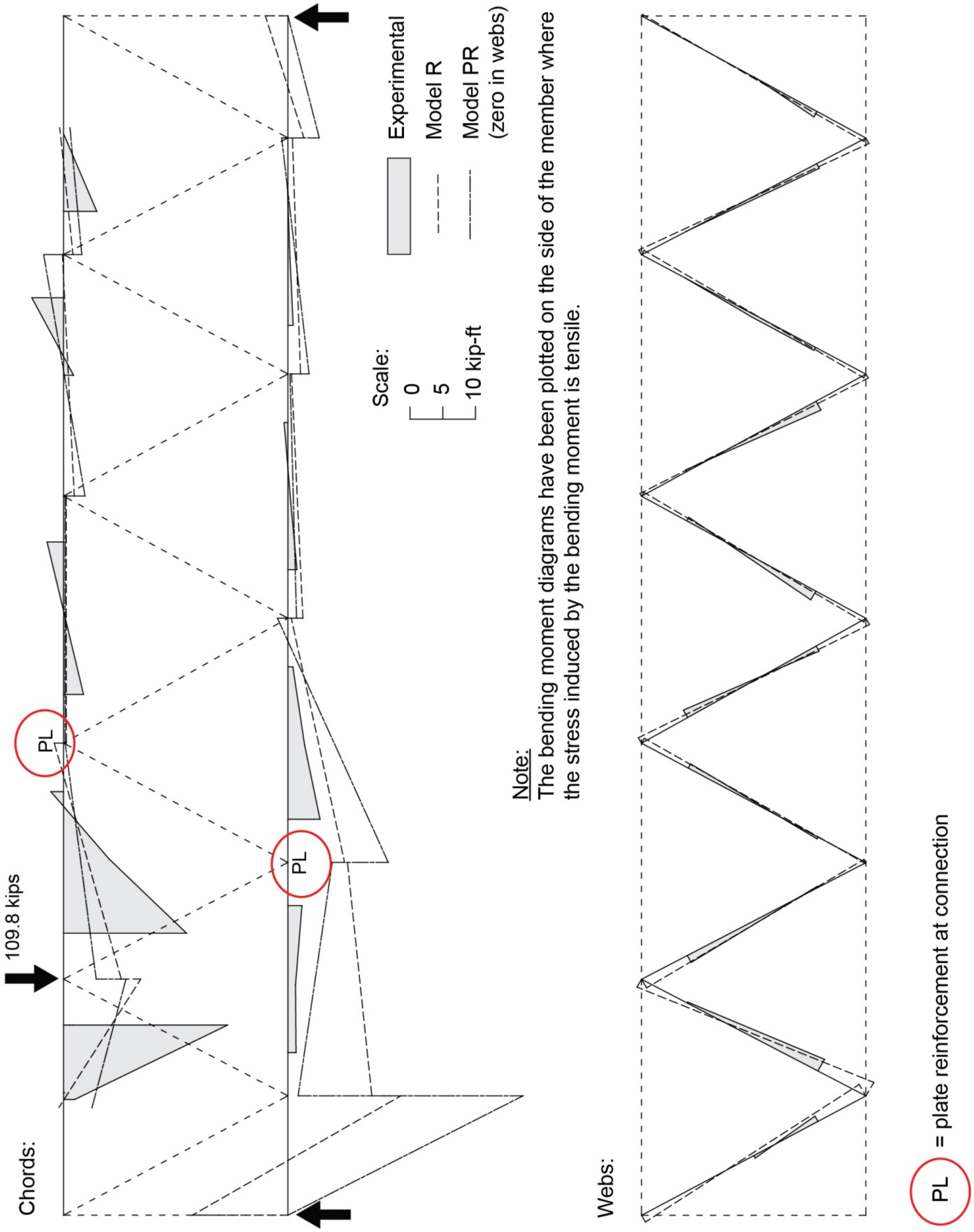

Figure 5-11 Comparison of the theoretical in-plane bending moment distribution given by model R and model PR with the experimental in-plane bending moment distribution for test 'Elastic 2'

5.3.3. Truss Deflections

A comparison of the predicted deflections by model P, model R and model PR to the experimental deflection profiles at a nominal applied panel point load of 110 kips to PP 4 is shown in Figure 5-12 (a) and Figure 5-12 (b) for test E1 and test E2, respectively. In Figure 5-12 (a), The LVDT at PP 13 appears to have been offset towards the outside of the roller support and thus the measurements obtained by it, which were intended to reflect rigid body motion, were influenced by the curvature of the bottom chord. This test has thus been deemed spurious and withheld from the comparison that follows. In lieu of two complete tests, the deflection profiles recorded during the weld tests at the initial unloaded stage and at 50%, 80% and 100% of the rupture load (located in Appendix H.6) were re-potted and compared to theoretical deflection profiles at a nominal applied panel point load of 110 kips, as shown in Figure 5-12 (c) through (k).

The mean percentage error of the maximum deflections is summarized in Table 5-4 where positive values indicate a safe (over-) prediction and negative values indicate an unsafe (under-) prediction. Tables of the deflection at each panel point under the specified load, and the deflection at each panel point from the three models, are located in Appendix I.5.

Table 5-4 Comparison of the truss theoretical maximum deflections from Model P, Model R and Model PR with the truss experimental maximum deflections

Test or Connection No.	Load (kips)	Percentage Error† (%)		
		Model P	Model R	Model PR
E2	109.8	+3.11	-2.67	-5.04
2	110.3	+8.04	+2.65	+1.32
3	111.5	-1.340	-3.08	-4.33
5	111.6	+10.13	+6.50	+3.01
6	111.8	+9.17	+5.54	+2.33
7	108.6	+6.62	+5.19	+3.12
8	108.0	+3.89	+2.41	+0.266
9	111.6	+10.58	+6.98	+3.50
Average		**+6.275**	**+2.94**	**+0.522**

†$[(Predicted - Actual)/Predicted] \times 100\%$; thus, positive values indicate safe predictions.

All three models were found to predict similar deflections for each test. The most flexible theoretical structure, represented by model P, produced predicted deflections which only slightly exceeded those given by model R and model PR. As noted by Frater & Packer (1992c), the similarity in the predicted deflections is not unexpected when trusses have a low span-to-depth (or “aspect”) ratio. When this occurs, it is the axial deformations of relatively long web members that govern the deformation response.

There does not seem to be any influence of second-order effects, due to connection deformations, since all of the analytical models still generally over-predicted truss deflections. This would be expected for relatively stiff overlapped K-connections and, as a result, large welds/stiffened joints had little effect on the accuracy of the predictions.

From the results, it is shown that model PR is most appropriate for predicting the maximum deflections of overlap-jointed rectangular HSS-to-HSS trusses, which is commensurate with the findings of Coutie et al. (1987), Philiastides (1988) and the recommendations of Packer et al. (2009).

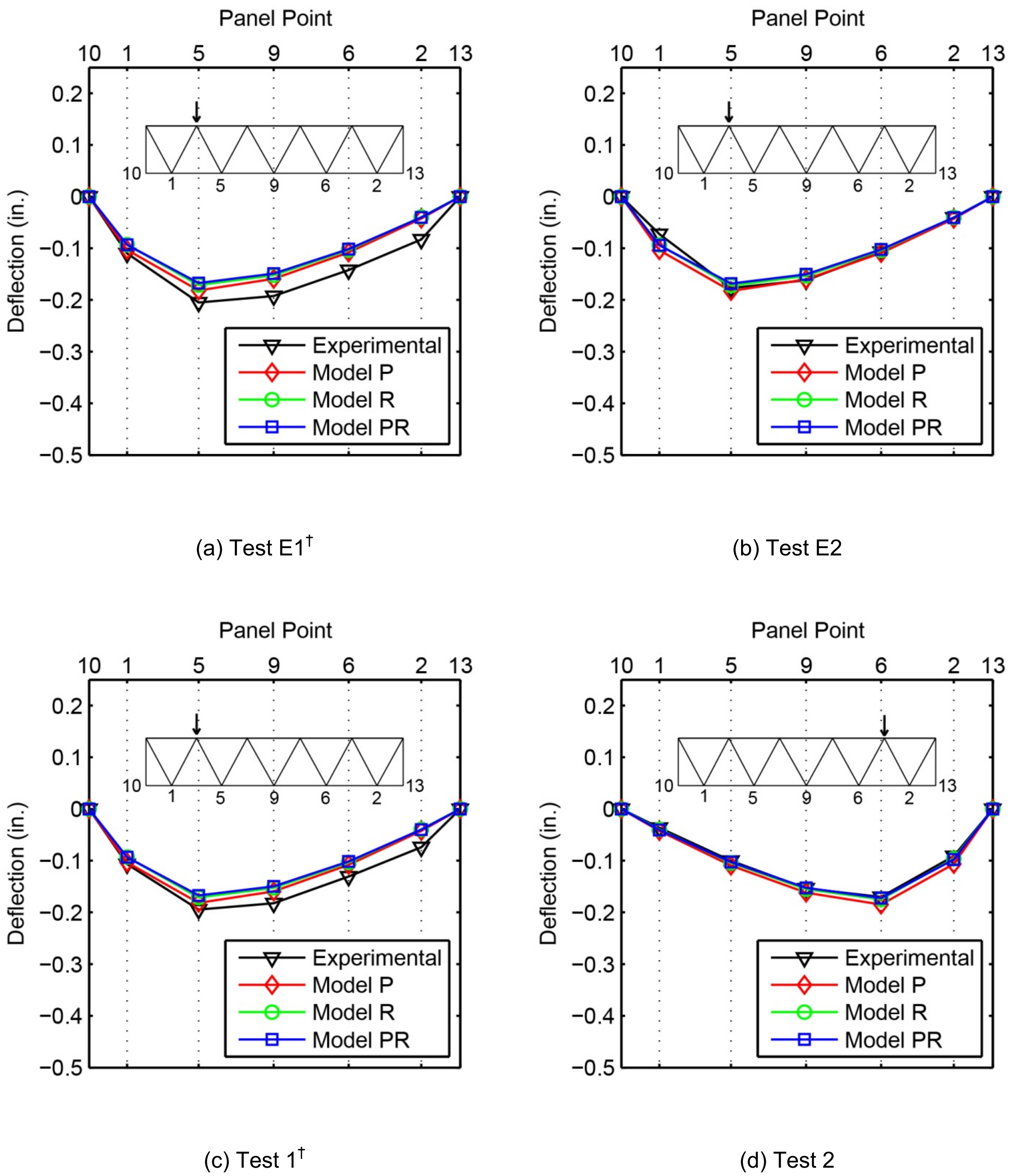

(a) Test E1†

(b) Test E2

(c) Test 1†

(d) Test 2

Figure 5-12 Comparison of theoretical truss deflections from Model P, Model R and Model PR with experimental truss deflections

†Erroneous measurements of settlement at reaction support (PP 13).

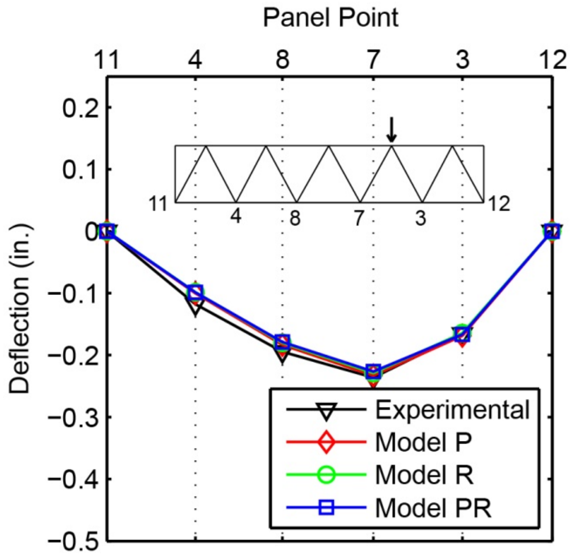

(e) Test 3

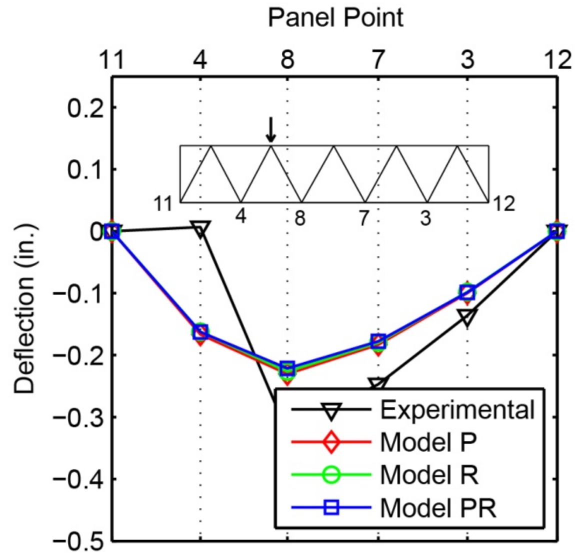

(f) Test 4‡

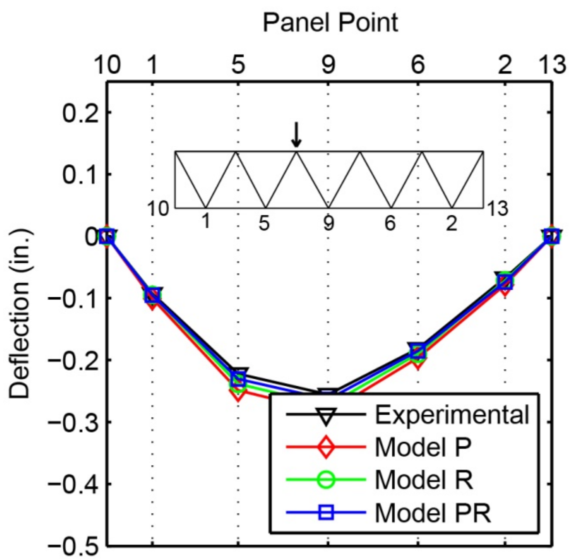

(g) Test 5

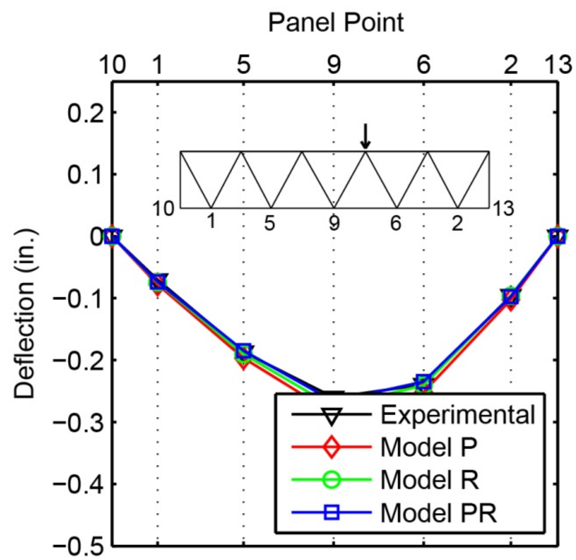

(h) Test 6

Figure 5-12 (continued) Comparison of theoretical truss deflections from Model P, Model R and Model PR with experimental truss deflections

‡Erroneous experimental readings from LVDTs.

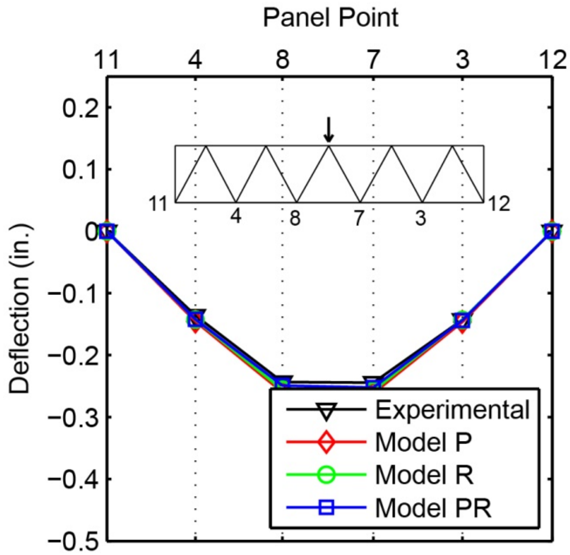

(i) Test 7

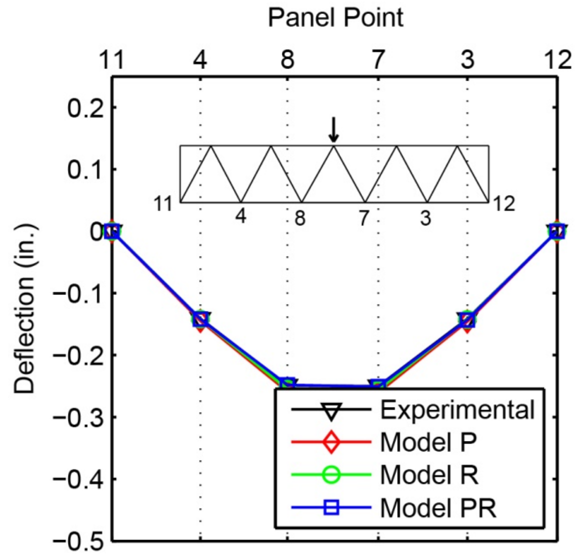

(j) Test 8

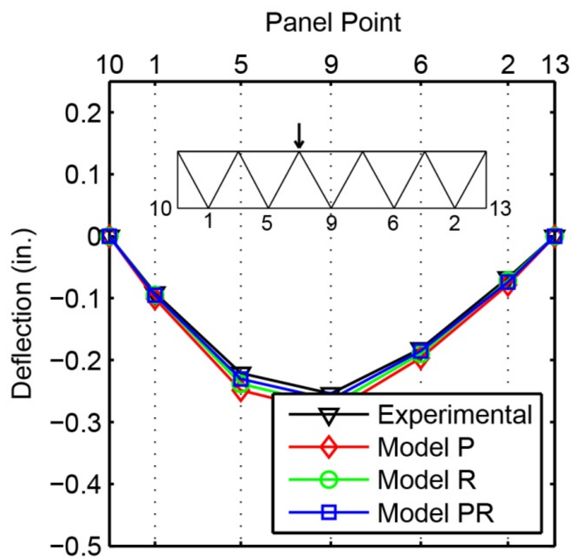

(k) Test 9

Figure 5-12 (continued) Comparison of theoretical truss deflections from Model P, Model R and Model PR with experimental truss deflections

Chapter 6: Conclusions and Recommendations

Based on the results from this experimental program, which consisted of nine full-scale tests on weld-critical rectangular HSS-to-HSS overlapped K-connections, the following conclusions and recommendations are made for weld design:

- The current effective length rules defined by Equations K4-10 to K4-12 and given in Table K4.1 of AISC 360 (2010) for welds in rectangular HSS-to-HSS overlapped K-connections are quite conservative.
- Accordingly, it is recommended to modify the requirement:

  "When $B_{bi}/B > 0.85$ or $\theta_i > 50°$, $b_{eoi}/2$ shall not exceed $2t$ and when $B_{bi}/B_{bj} > 0.85$ or $(180 - \theta_i - \theta_j) > 50°$, $b_{eov}/2$ shall not exceed $2t_{bj}$."

  to

  "When $B_{bi}/B > 0.85$ or $\theta_i > 50°$, $b_{eoi}/2$ shall not exceed $B_{bi}/4$. and when $B_{bi}/B_{bj} > 0.85$ or $(180 - \theta_i - \theta_j) > 50°$, $b_{eov}/2$ shall not exceed $B_{bi}/4$."

  to increase the predicted strength of welded joints in rectangular HSS overlapped K-connections and provide consistency across Table K4.1 (AISC, 2010). The above modification is adopted from McFadden & Packer (2013) and has been shown to still be conservative yet generally provide a more economical design approach for rectangular HSS T-, Y- and X- (or Cross-) connections subject to branch axial load or branch bending.
- The arbitrary factor of 0.6 on F_{EXX} for the tensile strength of PJP groove welds meets the intent outlined in the commentary to the Specification (AISC, 2010).
- The $(1.00 + 0.50 \sin^{1.5}\theta)$ term may be made fortuitously safe by arbitrary factors inherent in the design equations, but cannot safely be applied to all connections with or between rectangular HSS.

Based on a comparison of the predictions from three truss analysis models (all connections pin-jointed [P], all connections rigid-jointed [R], and all webs pin-jointed to continuous chords [PR]) to the measured forces and deflections from elastic truss tests, it can be concluded for trusses with rectangular HSS overlapped connections that:

- A conservative prediction of the axial forces in truss members can be obtained by using model P or model PR.
- Truss deflections can be conservatively predicted using model P, and more accurately predicted using model PR.

REFERENCES

AISC. (2010). ANSI/AISC 360-10. *Specification for Structural Steel Buildings*. Chicago, IL: American Institute of Steel Construction.

ASTM. (2006). ASTM E340-06. *Standard Test Method for Macroetching Metals and Alloys*. West Conshohocken, PA: American Society for Testing and Materials.

ASTM. (2008). E8/E8M-08. *Standard Test Methods for Tension Testing of Metallic Materials*. West Conshohocken, PA: American Society for Testing Materials.

ASTM. (2009). A370-09. *Standard Test Methods and Definitions for Mechanical Testing of Steel Products*. West Conshohocken, PA: American Society for Testing Materials.

ASTM. (2013). ASTM A1085-13. *Standard Specification for Cold-Formed Welded Carbon Steel Hollow Structural Sections (HSS)*. West Conshohcken, PA: American Society for Testing Materials.

AWS. (2010). ANSI/AWS D1.1/D1.1M:2010. *Structural Welding Code - Steel, 22*. Miami, FL: American Welding Society.

Cassidy, C. E. (1993). Effective weld length for HSS T, Y, and X connections. *Master of Applied Science Thesis*. Toronto, Canada: University of Toronto.

CEN. (2005). EN 1993-1-8. *Eurocode 3: Design of steel structures - Part 1 - 8: Design of Joints*.

Coutie, M. G., Davies, G., Philiastides, A., & Yeomans, N. (1987). Testing of Full-scale Lattice Girders Fabricated with RHS Members. *Conference on Structural Assessment Based on Full and Large-Scale Testing.* Watford, UK: Building Research Station.

CSA. (2001). CAN/CSA S16-01. *Limit States Design of Steel Structures*. Toronto, Canada: Canadian Standards Association.

CSA. (2013a). G40.20-13/G40.21-13. *General Requirements for Rolled or Welded Structural Quality Steel*. Toronto, Canada: Canadain Standards Association.

CSA. (2013b). W59. *Welded Steel Construction (Metal Arc Welding)*. Toronto, Canada: Canadian Standards Association.

CSA. (2014). CSA S16-14. *Design of Steel Structures*. Toronto, Canada: Canadian Standards Association.

Czechowski, A., Gasparski, T., Zycinski, J., & Brodka, J. (1984). IIW Doc. XV-562-84. Investigation into the Static Behaviour and Strength of Lattice Girders made of RHS. Paris, France: International Institute of Welding.

Dasgupta, A. (1970). The Behaviour of Joints in Tubular Trusses. *PhD Thesis*. Nottingham, England: University of Nottingham.

Davies, G., & Packer, J. A. (1982). Predicting the strength of branch plate - RHS connections for punching shear. *Canadian Journal of Civil Engineering, 9*(3), 458-467.

de Koning, C. H., & Wardenier, J. (1979). CIDECT Report 5Q/79/5 and 5QG-79/5. Tests on Welded Joints in Complete Girders made of Square Hollow Sections. Delft, The Netherlands: Delft University of Technology.

Fisher, J. W., Galambos, T. V., Kulak, G. L., & Ravindra, M. K. (1978). Load and resistance factor design criteria for connectors. *Journal of the Structural Division, American Society of Civil Engineers, 104*(9), 1427-1441.

Frater, G. S. (1991). Performance of Welded Rectangular Hollow Structural Section Trusses. *PhD Thesis*. Toronto, Canada: University of Toronto.

Frater, G. S., & Packer, J. A. (1992a). Weldment Design for RHS Truss Connections, I: Applications. *Journal of Structural Engineering, American Society of Civil Engineers, 118*(10), 2784 - 2803.

Frater, G. S., & Packer, J. A. (1992b). Weldment Design for RHS Truss Connections, II: Experimentation. *Journal of Structural Engineering, American Society of Civil Engineers, 118*(10), 2804 - 2820.

Frater, G. S., & Packer, J. A. (1992c). Modelling of Hollow Structural Section Trusses. *Canadian Journal of Civil Engineering, 19*(6), 947-959.

IIW. (1989). Doc. XV-701-89. Design Recommendations for Hollow Section Joints - Predominantly Statically Loaded. *2nd ed.* Paris, France: International Institute of Welding.

IIW. (2012). Doc. XV-1402-12. Static Design Procedure for Welded Hollow Section Joints - Recommendations. *3rd ed.* Paris, France: International Institute of Welding.

ISO. (2013). ISO 14346. Static Design Procedure for Welded Hollow Section Joints - Recommendations. Geneva, Switzerland: International Standards Organization.

McFadden, M. R., & Packer, J. A. (2013). Effective Weld Properties for RHS-to-RHS Moment T-connections. *Phase 1 Report to American Institute of Steel Construction*. Toronto, Canada: University of Toronto.

McFadden, M. R., & Packer, J. A. (2014). Effective Weld Properties for Hollow Structural Section T-Connections under Branch In-plane Bending. *Engineering Journal, American Institute of Steel Construction, 51*(4), 247-266.

McFadden, M. R., Sun, M., & Packer, J. A. (2013). Weld Design and Fabrication for RHS Connections. *Steel Construction, 6*(1), 5-10.

Mehrotra, B. L., & Govil, A. K. (1972). Shear lag analaysis of rectangular full-width tube connections. *Journal of the Structural Division, American Society of Civil Engineers, 98*(ST1), 287-305.

Packer, J. A., & Cassidy, C. E. (1995). Effective Weld Length for HSS T, Y, and X Connections. *Journal of Structural Engineering, American Society of Civil Engineers, 121*(10), 1402 - 1408.

Packer, J. A., & Frater, G. S. (2005). Recommended Effective Throat Sizes for Flare Groove Welds to HSS. *Engineering Journal, American Institute of Steel Construction, 42*(1), 31-44.

Packer, J. A., & Henderson, J. E. (1992). Design Guide for Hollow Structural Section Connections. *1st ed.* Toronto, Canada: Canadian Institute of Steel Construction.

Packer, J. A., & Henderson, J. E. (1997). Hollow Structural Section Connections and Trusses - A Design Guide. *2nd ed.* Toronto, Canada: Canadian Institute of Steel Construction.

Packer, J. A., Sherman, D. R., & Lecce, M. (2010). Hollow Structural Section Connections. *AISC Steel Design Guide No. 24*. Chicago, IL: American Institute of Steel Construction.

Packer, J. A., Wardenier, J., Zhao, X. L., van der Vegte, G. J., & Kurobane, Y. (2009). Design Guide for Rectangular Hollow Section (RHS) Joints under Predominantly Static Loading. *CIDECT Design Guide No. 3, 2nd ed.* Geneva, Switzerland: CIDECT.

Philiastides, A. (1988). Fully Overlapped Rolled Hollow Section Welded Joints in Trusses. *PhD Thesis*. Nottingham, UK: University of Nottingham.

Ravindra, M. K., & Galambos, T. V. (1978). Load and resistance factor design for steel. *Journal of the Structural Division, American Society of Civil Engineers, 104*(9), 1337-1353.

Salmon, C. G., & Johnson, J. E. (1980). Steel Structures, Design and Behavior. *2nd ed.* New York, NY: Harper & Row.

Seaburg, P. A., & Carter, C. J. (1997). Torsional Analysis of Structural Steel Members. Chicago, IL: American Institute of Steel Construction.

STI. (1993). Recommended Methods to Check Dimensional Tolerances on Hollow Structural Sections [HSS] Made to ASTM A500. Glenview, IL: Steel Tube Institute of North America.

STI. (2010). Brochure on Dimensions and Section Properties of HSS. Glenview, IL: Steel Tube Institute of North America.